Incorporation of organic molecules in the tunnels of the sepiolite clay mineral

Katrin Blank

Thesis submitted to the
Faculty of Graduate & Postdoctoral Studies
University of Ottawa
in partial fulfillment of the requirements for the
M.Sc. degree in the

Ottawa-Carleton Chemistry Institute

Acknowledgments

I would like to give a special thank you to Dr. Christian Detellier for giving me the opportunity to work in his research group, for his patience and encouragements.

I would also like to thank members of Dr. Detellier's research group. I am especially thankful to Sadok Letaief, Rola Mansa and Jonathan Fafard for their magnificent help and support throughout the years.

I would like to thank Dr. Glenn Facey for his help with NMR spectroscopy.

I would also like to mention Ms. Annette Campeau and Ms. Josée Rouleau for their excellent administrative work during my research years.

I would like to extend a special thanks to my mom, who is always there to support and understand me.

Table of Contests

Abbreviations and symbols

Abs	absorbance
AD	Anno Domini [Latin: In the time of our Lord]
Al	aluminum
Al^{3+}	aluminum cation with +3 oxidation state
Å	Angstrom [10 to the power of -10 meters]
α,β-unsaturated ketone	carbonyl compounds with the general structure $C_{\beta}=C_{\alpha}-(C=O)-$
BC	Before the Christian era
BET	(Brunauer, Emmett and Teller, 1938)
B^{3+}	boron cation with +3 oxidation state
Be^{2+}	beryllium cation with +2 oxidation state
C	carbon
Chemical Co.	Chemical company
C-D bond	carbon-deuterium bond
cm^3/g	centimetre cubed per gram
CP	cross polarization
CP/MAS NMR	cross polarization/magic angle spinning nuclear magnetic resonance
^{13}C	Carbon-13
°C	degrees of Celsius
DTA	Differential thermogravimetric analysis
DTG	Differential Thermogravimetric

d_6	a molecule containing six deuterium atoms
D_2O	deuterium oxide
2D	two dimensional
3D	three dimensional
EtOH	ethanol
et al.	et alii [Latin: and others]
FSLG HETCOR NMR	frequency-switched Lee-Goldburg heteronuclear correlation nuclear magnetic resonance
FTIR	Fourier transform infrared
Fe^{2+}	iron cation with +2 oxidation state
Fe^{3+}	iron cation with +3 oxidation state
g	gram
H	hydrogen
H-bond	hydrogen bond
HCl	hydrochloric acid
HDO	hydrogen deuterium oxide
HETCOR	heteronuclear correlation
HK	Horvath-Kawazoe
^1H	proton
^2H	deuterium
H_2O_{coord}	coordinated water
H_2O_{zeol}, H_2O_{zeo}	zeolitic water
I	nuclear spin quantum number
i.e.	id est, [that is; in other words]

K	Kelvin
kHz	kilohertz
M	molarity
MAS NMR	magic angle spinning nuclear magnetic resonance
MCH	3-methyl cyclohex-2-en-1-one
MeOH	methanol
Mg	magnesium
mg	milligram
MgOH	magnesium hydroxide
Mg^{2+}, Mg(II)	magnesium cation with +2 oxidation state
MHz	megahertz
min	minute
ml	millilitre
ms	millisecond
m^2/g	metre squared per gram
mm^2/g	millimetre squared per gram
mm^3/g	millimetre cubed per gram
N	nitrogen
Na	sodium
nm	nanometre
NMR	Nuclear magnetic resonance
N_2	nitrogen gas
nm^2	nanometers squered

η	asymmetry parameter
O	oxygen
-OH	hydroxyl group
ppm	parts per million
p/p^o	relative pressure
PXRD	powder X-ray diffraction
Q^2 Si	silicon atom that is attached to two other silicon atoms through oxygens
Q^3 Si	silicon atom that is attached to three other silicon atoms through oxygens
S	sulphur
SEM	Scanning electron microscope
Sep	sepiolite
Sep-MCH	sepiolite and 3-methyl cyclohex-2-en-1-one adduct
Si	silicon
SiOH	silicon hydroxide
^{29}Si NMR	silicon-29 nuclear magnetic resonance
STP	standard temperature and pressure
T	tetrahedral
TGA	Thermal Gravimetric Analysis
TGA-DTGA	Thermogravimetric Analysis-Differential Thermal Gravimetric Analysis
T-plot	t is called statistical thickness
TMS	tetramethylsilane

UV-Vis	ultraviolet visible
μs	microsecond
$\mathbf{V}_{ij}$	electric field gradient tensor
wt.%	weight percent
χ	quadrupolar coupling constant
~	Approximately

Abstract

Sepiolite is a clay mineral, a complex magnesium silicate, a typical formula for which is $(OH_2)_4(OH)_4Mg_8Si_{12}O_{30}\cdot 8H_2O$. It is formed by blocks and cavities (tunnels) growing in the direction of the fibres. The tunnels, 3.7 x 10.6 Å in cross-section, are responsible for the high specific surface area and sorptive properties of sepiolite. The co-intercalation of 3-methyl cyclohex-2-en-1-one (MCH), the Douglas-Fir beetle anti-aggregation pheromone, with methanol, ethanol, acetone, or benzene into sepiolite tunnels was studied. The resulting nanohybrid materials were characterized by means of various techniques, such as multinuclear solid-state NMR spectroscopy, porosity studies and Thermal Gravimetric Analysis (TGA). This was done in the hope of obtaining slow and controlled release of MCH from the sepiolite tunnels. It was demonstrated by ^{13}C MAS NMR (carbon-13 magic angle spinning nuclear magnetic resonance) that at room temperature there are two different MCH molecules: one MCH inside the tunnels and the other one outside the tunnels of the sepiolite. Heating nanohybrid materials at 60˚C for 20 hours removes the external MCH molecules from the sepiolite. ^{13}C MAS NMR showed that by further heating nanohybrid materials at 120˚C for 20 hours, methanol, ethanol, or acetone peaks were greatly reduced; however, the benzene peak was not reduced. To better understand how benzene acts inside sepiolite, intercalation of d_6-benzene, and co-intercalations of d_6-benzene with MCH and d_6-benzene with pyridine into sepiolite tunnels were carried out, and these samples were studied by the same techniques. Another technique was used in order to see whether the slow and controlled release of MCH from the sepiolite tunnels could be obtained: sepiolite-MCH nanohybrids were

treated with 20 ml of 0.5 M HCl solution. It was found that when 1 gram of MCH-sepiolite sample was acid treated at room temperature, about 35% of intercalated MCH was removed from the sepiolite. The role of sepiolite clay was also studied in Maya-Blue representative structure sepiolite-indigo adduct. It is known that upon heating the sepiolite and indigo mixture, the stability that is present in Maya-Blue is achieved. It is still a mystery, however, how exactly indigo and sepiolite interact with each other.

Chapter 1

Sepiolite

Clay is a naturally occurring aluminum silicate composed primarily of fine-grained minerals. Clay deposits are mostly composed of clay minerals, a subtype of phyllosilicate minerals, which impart plasticity and harden when fired or dried; they also may contain variable amounts of water trapped in the mineral structure by polar attraction (Guggenheim and Martin, 1995). Clay minerals are hydrous aluminum phyllosilicates (Meunier, 2005). Because clays are very abundant and naturally occurring, they are relatively cheap and environmentally friendly materials, which makes them very desirable materials to work with.

The tetrahedral sheet has a general composition of T_2O_5. T represents tetrahedral cation, which is usually Si^{4+}, Al^{3+}, Fe^{3+}, and rarely, Be^{2+} or B^{3+}; O represents the oxygen atom. At the centre of the tetrahedra is a silicon cation. Oxygen is at each of the four corners. Three out of the four individual oxygens connect by sharing with neighbouring tetrahedra. This results in a hexagonal pattern. The fourth oxygen is apical oxygen, and points in the direction that is perpendicular (up/down) to the sheet and forms part of the octahedral sheet. The octahedral sheet is composed of medium-sized cations at its centre, usually Al^{3+}, Mg^{2+}, Fe^{2+}, or Fe^{3+} and oxygen at the six corners. Individual octahedra share oxygens with other adjacent octahedra; individual octahedra link laterally along the edges and link vertically with the tetrahedra. Three octahedra make up the smallest unit of an octahedral sheet (Nesse, 2000). Some oxygen atoms are in the form of hydroxyl groups; this gives a negative charge to phyllosilicates. These negative charges are neutralized by various cations, water and other small molecules. Figure 1.1 shows single tetrahedron and single octahedron shapes.

Two main types of layering patterns are observed in phyllosilicates: 1:1, where one tetrahedral sheet links one octahedral sheet; and 2:1 layering, which links two tetrahedral sheets to one octahedral sheet (Figure 1.2).

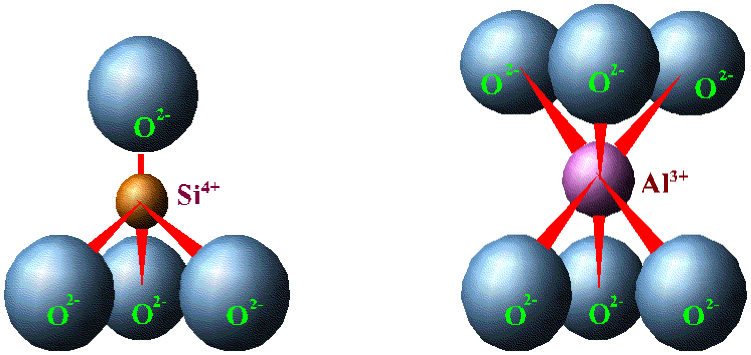

Figure 1.1 Single tetrahedron and single octahedron.

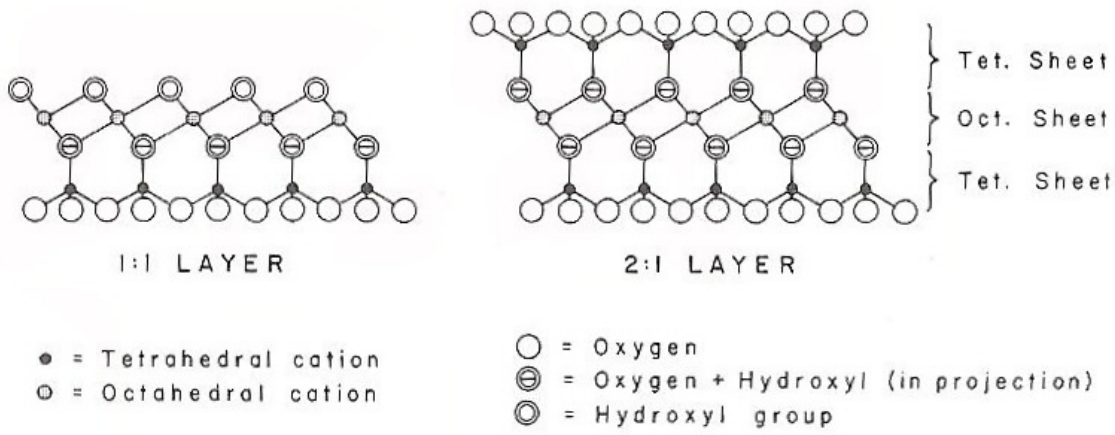

Figure 1.2 Example of layering in phyllosilicates. Obtained from Brindley and Brown (1984).

Phyllosilicates are divided into different groups: kaolin minerals, smectite minerals, illite, chlorite, and palygorskite (attapulgite) and sepiolite. The focus of this thesis is on studies of sepiolite clay due to its channel structure. A little introduction to other clays will be given before focusing fully on sepiolite.

Kaolinite, dickite, nacrite and halloysite are all clay minerals that belong to the kaolin group. The primary structural unit of this group is a layer composed of one octahedral sheet condensed with one tetrahedral sheet; it is a 1:1 layered group. Kaolinite, dickite and nacrite show very uniform chemical composition: 46.54 wt.% SiO_2, 39.50 wt.% Al_2O_3 and 13.96 wt.% H_2O, corresponding to a formula of $Al_2Si_2O_5(OH)_4$. The formula of halloysite is $Al_2Si_2O_5(OH)_4 \cdot 2H_2O$. The differences in the kaolin minerals are found in the manner in which the unit layers are stacked above one another. Kaolinite, dickite and nacrite occur as plates; halloysite, which can have a single layer of water between its sheets, occurs in a tubular form. Researchers are trying to expand the interlamellar space between the layers so that the functionalization of these clays can be studied further.

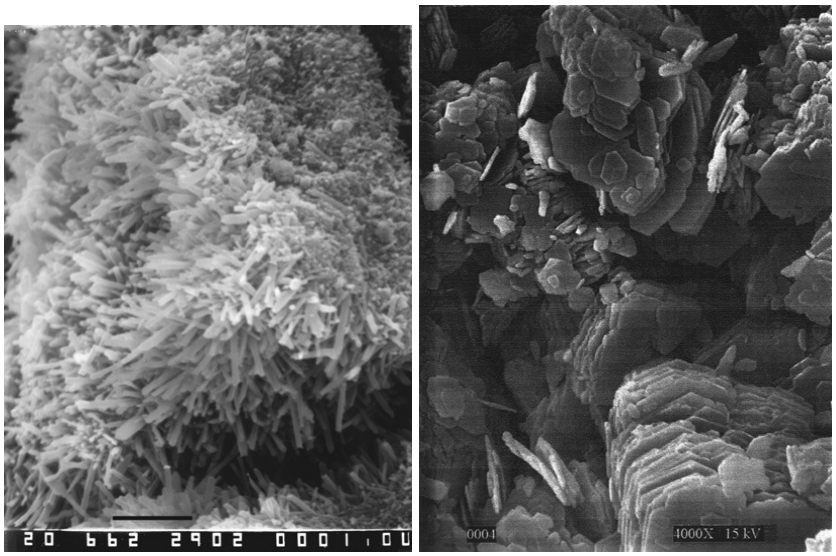

Figure 1.3 Scanning electron micrograph of halloysite (left) and kaolinite (right). Obtained from Murray (2007).

The major smectite minerals are sodium montmorillonite, calcium montmorillonite, saponite (magnesium montmorillonite), nontronite (iron montmorillonite), hectorite (lithium montmorillonite) and beidellite (aluminum montmorillonite). Smectite minerals are composed of two silica tetrahedral sheets with a central octahedral sheet and are designated as a 2:1 layer mineral. Water molecules and cations occupy the space between the 2:1 layers. The layers contain ions that are very loosely bound to one another and are easily exchangeable. The smectite family are known clay host matrices for preparations of organo-inorganic nanohybrids due to their swelling properties (Murphy and Sawyer, 2004).

Illite is a non-expanding, clay mineral mica. The structure is a 2:1 layer in which the interlayer cation is potassium; this cation is responsible for the absence of swelling. Due to the size, charge and coordination number of potassium, it fits easily in the hexagonal ring of oxygens of the adjacent silica tetrahedral sheets. This forms a strong interlocking ionic bond that is responsible for holding individual layers together and this prevents water molecules from taking up the interlayer position as they do in the smectites.

Chlorite can often be found in shales and also in underclays associated with coal seams. Clay mineral chlorites differ from well-crystallized chlorites in that there is a random stacking of the layers and also some hydration. Chlorite is a 2:1 layer mineral with an interlayer $Mg(OH)_2$. There is quite a range of cation substitutions in chlorites, most commonly Mg^{2+}, Fe^{2+}, Al^{3+} and Fe^{3+}.

Other 2:1 clay types exist, such as palygorskite (also known as attapulgite) and sepiolite. Both consist of continuous, two-dimensional talc-like tetrahedral sheets

(Hubbard *et al*., 2003). They differ, however, from the other layer silicates due to their lack of continuous octahedral sheets. The structure of both sepiolite and palygorskite contains ribbons of 2:1 phyllosilicates linked by periodic inversion of the apical oxygen of the continuous tetrahedral sheet, every six atoms of Si (three tetrahedral chains) for sepiolite and every four atoms of Si (two tetrahedral chains) for palygorskite (García-Romero and Suáres, 2010). The tetrahedral and octahedral mesh generates a series of rectangular tunnels; palygorskite tunnels measure 6.4 x 3.7 Å and sepiolite tunnels measure 10.6 x 3.7 Å. In addition to exchangeable cations, zeolitic (bound) water fills these tunnels. On the external surfaces of these clays there are channels.

The structure of sepiolite is shown in Figure 1.4. A general formula for sepiolite is $(OH_2)_4(OH)_4Mg_8Si_{12}O_{30}\cdot 8H_2O$. The crystal structure of sepiolite, a hydrous magnesium silicate mineral with a fibrous morphology, has been established by Nagy and Bradley (1955), and Brauner and Preisinger (1956). Ideal sepiolite is a pure trioctahedral mineral, and four possible octahedral positions are occupied by Mg. According to the review by Newman and Brown (1987), tetrahedral occupancy ranges from $(Si_{11.96}Al_{0.05})$ to $(Si_{11.23}Fe_{0.53}{}^{3+}Al_{0.24})$ and the total number of octahedral cations ranges from 7.01 to 8.01. Afterwards, Jones and Galan (1991) affirm that the theoretical SiO_2/MgO ratio of sepiolite is 2.23 with SiO_2 = 55.6 wt%; MgO = 24.99 wt%. But usually, SiO_2 falls in the range of 53.9 ± 1.9 wt%, and MgO between 21 and 25 wt%. Galan and Carretero (1999) evaluated composition limits for sepiolite and concluded that sepiolite is a true trioctahedral mineral, with negligible structural substitutions and eight octahedral positions filled with magnesium.

The sepiolite mineral contains two types of water molecules, one coordinated to the octahedral cations and the other loosely bound in the tunnels, which is termed 'zeolitic water.' The name sepiolite was first applied by Glocker (1847) and is derived from the Greek for "cuttlefish," the bones of which are as light and porous as the mineral. Chemically, sepiolite is a hydrous magnesium silicate whose individual particles have a needle-like morphology. The high surface area and porosity of this clay account for its outstanding absorption capacity for liquids. Sepiolite granules do not disintegrate even when saturated with liquids.

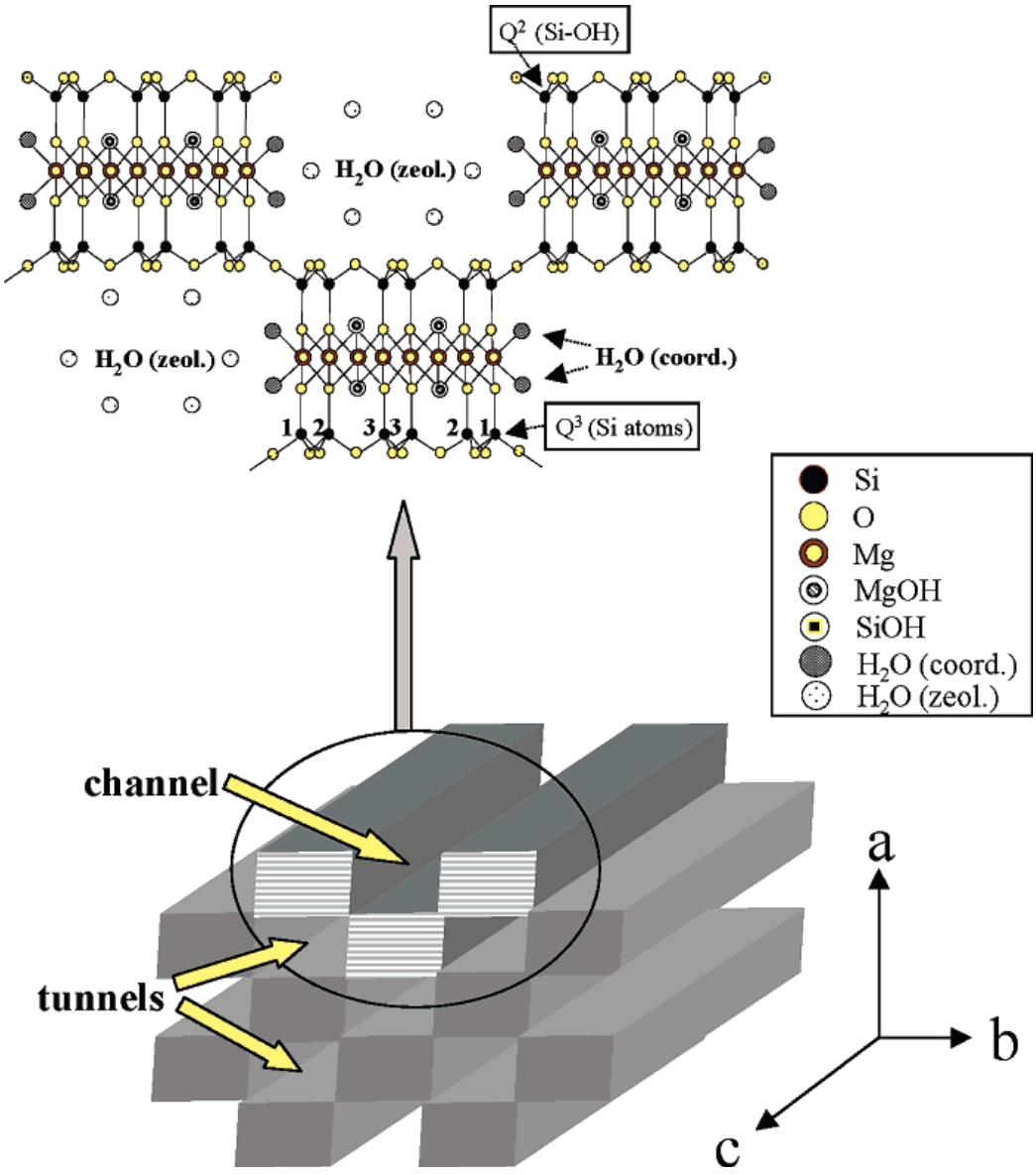

Figure 1.4 Structure of sepiolite. Figure obtained from Kuang *et al.* (2003).

Currently, a wide range of technological applications are based on the sorptive and catalytic properties of sepiolite (Galan, 1996). Sepiolite is used as a thixotropic gelling viscosity builder and suspending agent in the drilling of oil and gas wells. (Thixotropy is the property of certain gels or fluids that are thick (viscous) under normal conditions, but flow (become thin, less viscous) over time when shaken, agitated, or otherwise stressed.) Due to its high sorptive capacity sepiolite makes an excellent granular material for use as cat litter. It is also a material that is useful as a carrier for pesticides, insecticides and herbicides (of which some are liquids or sticky pastes that are very hard to use by themselves) (Maqueda *et al*., 2008). Sepiolite is often mixed with adhesives used to fill joints and cracks in drywall. Sepiolite is also used to replace more costly organic thickeners in emulsion paints: it provides film that is much less sensitive to water and offers improved colour retention upon washing because of the insolubility of the clay thickener. Sepiolite has been tested as a decolourizing agent (Demirci *et al*., 1995), as a catalyst or catalyst carrier (Damyanova *et al*., 1996), (Corma and Martin-Aranda, 1991), (d'Espinose de la Caillerie and Fripiat, 1992) and as an odorant adsorbent in environmental applications (Sugiura *et al*., 1990), (Sugiura *et al*., 1991), (Sugiura, 1993). Few field trials have evaluated the effectiveness of sepiolite in immobilizing heavy metals in soils (Zhu *et al*., 2010).

Figure 1.5 shows sepiolite structure after various thermal treatments. Purified sepiolite at room temperature is filled with water molecules (Figure 1.5a). Heating sepiolite in air at 120°C eliminates most of the zeolitic water molecules from the sepiolite channels; the structural water molecules and the Mg-OH groups are not affected by this relatively mild heating (Figure 1.5b). Coordinated structural water molecules, however,

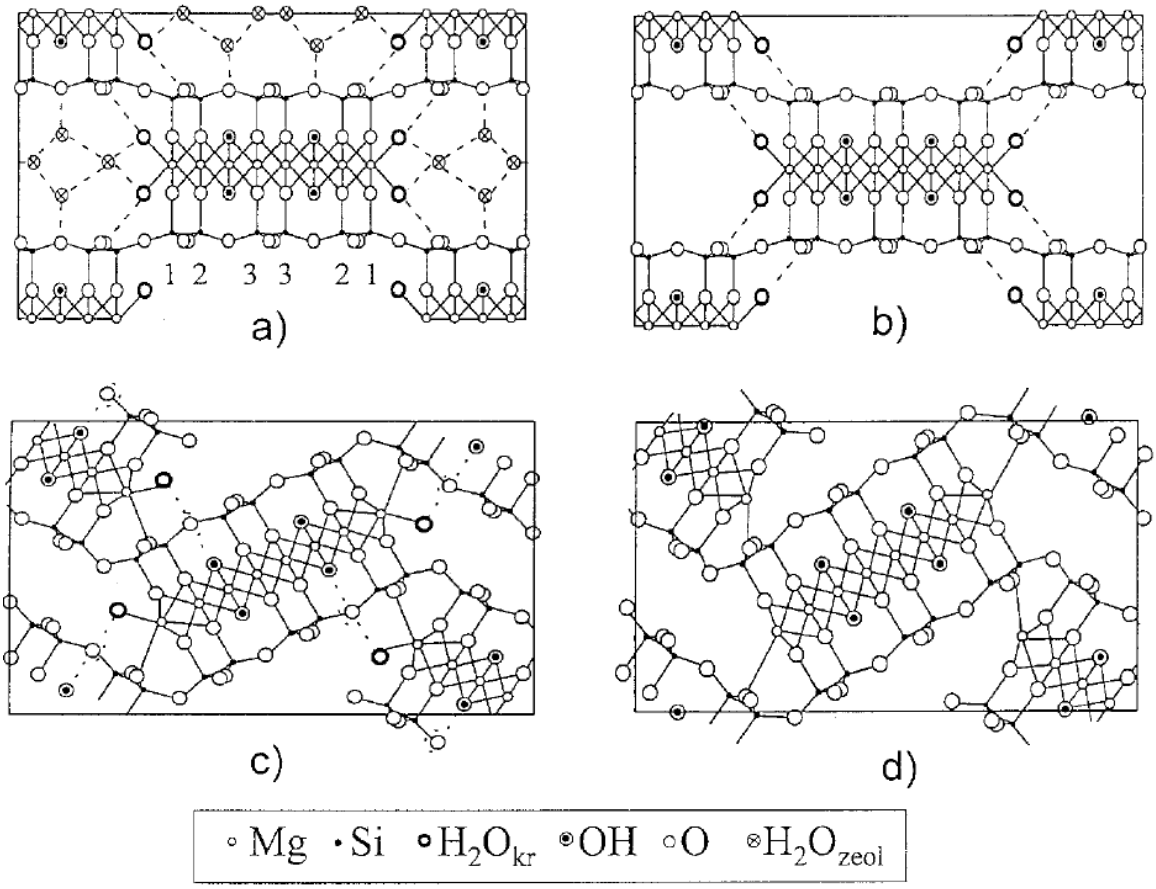

Figure 1.5 Schematic representation of the structure of sepiolite after (a) no thermal treatment, (b) heating in air to 120°C, (c) heating in air to 350°C, and (d) heating in air to 500°C. Figure adapted from Preisinger (1963). * Here $H_2O_{kr} = H_2O_{coord}$

are lost at higher temperatures. This happens in two steps: one H_2O_{coord} per Mg^{2+} is removed, first at ~286°C, and a second H_2O_{coord} is released at ~516°C (values obtained from Figure 3.4), which means that anhydride is obtained (Figure 1.5d). Those temperature values are obtained from DTG graph, which gives the middle value for each weight loss. In reality, weight losses are better represented by the TGA graph which gives the range of temperature at which certain weight losses are occurring. The first structural water is lost between 230-325°C, and second structural water is lost between 400-600°C. Folding of the sepiolite crystals occurs when approximately half of the structural water has been eliminated (Figure 1.5c), which allows the terminal Mg^{2+} to complete their coordination with the oxygen of the neighbouring silica surface (Weir *et al.*, 2002). Structural folding is nearly completely reversible provided that the treatment temperature does not exceed 250°C (Weir *et al.*, 2000), but becomes irreversible once the true anhydride is formed. Finally, the Mg-OH hydroxyl groups are released at ~780-850°C (d'Espinose de la Caillerie and Fripiat, 1994), (Pérez-Rodríguez and Galán, 1994).

Sepiolite structure has four types of silicon atoms: three Q^3 Si atoms and one Q^2 Si atom (Figures 1.4 & 1.5). Q^3 refers to a silicon atom that is attached to three other silicon atoms through oxygens; the Q^2 silicon atom is attached to two other silicon atoms through oxygens. ^{29}Si NMR for pure, unheated sepiolite shows three well-resolved resonances of approximately equal intensity for its three Q^3 silicon atoms at -92.7 (Si_2), -94.3 (Si_1) and -98.2 (Si_3) ppm (Figure 1.6a). For sepiolite that has been heated at 120°C for 20 hours, the ^{29}Si CP/MAS NMR signals of the centre and the edge Si nuclei (Si_3 and Si_1) coincide at -97.0 ppm; the near-edge Si (Si_2) is represented by a chemical shift at -93.7 ppm (Figure 1.6b). The coincided peak is much more intense than the other peak. In

the heated sepiolite sample, all the zeolitic water is evaporated and the tunnels of the sepiolite are empty. X-ray diffraction indicates that loss of zeolitic water does not result in any structural change (Nagata *et al.*, 1974). However electron diffraction studies by Rautureau and Tchoubar (1976) carried out under vacuum suggest that some minor structural changes do occur. However the changes appear to be consistent with the effects observed for interlayer water on ^{29}Si chemical shifts in layer 2:1 silicates. The presence of interlayer water induces a deshielding of ~3 ppm between talc and saponite (Barron and Frost, 1985). It appears that the resonance at -94.3 ppm has been shifted to -97.0 ppm due to loss of zeolitic water which is hydrogen bonded to the basal oxygens of this silicon. The other two resonances are only slightly shifted in contrast (Barron and Frost, 1985).

It was previously documented that upon exposure to acetone vapour, dehydrated sepiolite sequesters individual molecules of acetone in its microporous tunnels, resulting in the recovery of the original hydrated ^{29}Si CP/MAS NMR spectrum (Weir *et al*., 2000). A similar observation was reported after intercalation of pyridine (Kuang *et al*., 2002). Generally, sorption of molecules into the microporous tunnels is accomplished through hydrogen-bond interaction with the internal coordinated water of the clay mineral, after removal of zeolitic water (Serna and van Scoyoc, 1979).

On silicon NMR spectra, the Q^2 signal appears much smaller compared to the three Q^3 signals. Barron and Frost (1985) describe that this is the cross-polarization behavior of the edge SiOH resonance at -86 ppm. While this resonance is quite evident in spectra obtained with 5 ms contact, it is barely evident at contact times of 10 ms or greater (the contact time I used in my experiments was 10 ms). The three major

resonances still exhibit strong cross-polarization at greater than 20 ms. Hence, the edge Q^2 groups would appear to cross-polarize from the -OH protons which apparently exhibit much shorter ^1H-$T_{1\rho}$ (90° ^1H transmitter pulse), values than do the internal protons.

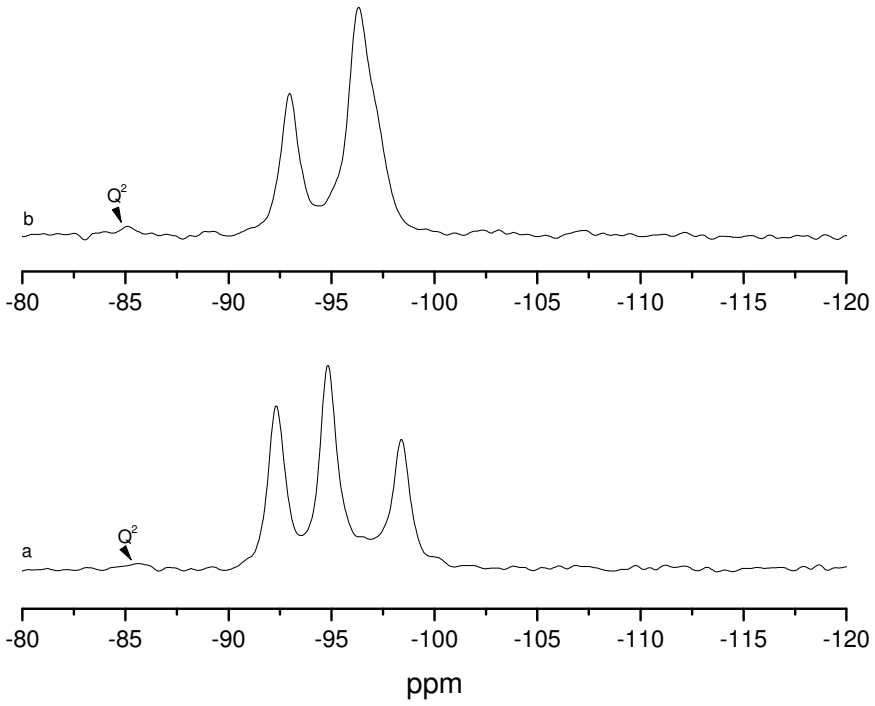

Figure 1.6 ^{29}Si CP/MAS NMR spectrum for (a) sepiolite, Q^3 signals at -92.7, -94.3 and -98.2 ppm, and (b) sepiolite heated at 120°C for 20 hours. In the heated sample, the ^{29}Si CP/MAS NMR signals of the centre and the edge Si nuclei coincide at –97.0 ppm. The near-edge Si is represented by a chemical shift at –93.7 ppm. *This is original result.

This thesis studies reactions and characterization of sepiolite clay mineral. Chapter 2 will give a small introduction to the characterization techniques used throughout the thesis. Chapter 3 studies nanostructured materials from the intercalation of semiochemical 3-methyl cyclohex-2-en-1-one (MCH) in sepiolite. Sepiolite is used in these studies because of its larger tunnel size compared to palygorskite. Chapter 4 studies potential release mechanisms of MCH from the sepiolite. This is done with the hope of potential application that sepiolite could be used as a slow and controlled release tool of the MCH. Chapter 5 studies Maya-Blue representative structure indigo-sepiolite adduct in order to understand how indigo interacts with sepiolite. Chapter 6 is a general conclusion for this thesis.

References

Barron, P.F. and Frost, R.L. (1985) Solid state ^{29}Si NMR examination of the 2:1 ribbon magnesium silicates, sepiolite and palygorskite. *American Mineralogist*, **70**, 758-766.

Brauner, K. and Preisinger, A. (1956) Struktur und Entstehung des Sepioliths. *Tschermaks Miner. Petr. Mitt*. **6**, 120-140.

Brindley, G.W. and Brown, G. (1984) Crystal Structures of Clay Minerals. *Mineralogical Society*, Spottiswoode Ballantyne ltd.

Corma, A. and Martin-Aranda, R.M. (1991) Alkaline-substituted sepiolites as a new type of strong base catalyst. *J. Catal*., **130**, 130-137.

Damyanova, S., Daza, L. and Fierro, J.L.G. (1996) Surface and catalytic properties of lanthanum-promoted Ni/sepiolite catalysts for styrene hydrogenation. *J. Catal*., **159**, 150-161.

Demirci, S., Erdogan, B. and Akay, Y. (1995) Removal of turbidity and color of sugar juices by using some Turkish bentonites and sepiolite. *EUROCALY*, Leuven, 158-159.

d'Espinose de la Caillerie, J.-B. and Fripiat, J.J. (1992) Al modified sepiolite as catalyst or catalyst support. *Catal.*, Today, **14**, 125-140.

d'Espinose de la Caillerie, J.-B. and Fripiat, J.J. (1994) A reassessment of the ^{29}Si MAS-NMR spectra of sepiolite and aluminated sepiolite. *Clay Minerals,* **29**, 313-318.

Galan, E. (1996) Properties and applications of palygorskite-sepiolite clays. *Clay Minerals,* **31**, 443-453.

Galan, E. and Carretero, I. (1999) A new approach to composition limits for sepiolite and palygorskite. *Clays Clay Miner*. **47**(4), 399-409.

García-Romero, E. and Suáres, M. (2010) On the chemical composition of sepiolite and palygorskite. *Clays and Clay Minerals*, **58**(1), 1-20.

Glocker, E.F. (1847) Generum et specierum mineralium secundum ordines naturales digestorium synopsis. *Halle*, 348.

Guggenheim, S. and Matrin, R.T. (1995) Definition of clay and clay mineral: joint report of the AIPEA nomenclature and CMS nomenclature committees. *Clay and Clay minerals*, **43**, 255-256 and *Clay Minerals*, **30**, 257-259.

Hubbard, B., Kuang, W., Moser, A., Facey, G.A. and Detellier, C. (2003) Structural study of Maya Blue: textural, thermal and solid-state multinuclear magnetic resonance

characterization of the palygorskite-indigo and sepiolite-indigo adducts. *Clay and Clay minerals*, **51**(3), 318-326.

Jones, B.F. and Galan, E. (1991) Palygorskite-sepiolite. In: Bailey, S.W. (Ed.) Chapter 16 in Hydrous Phyllosilicates (Exclusive on Micas). *Review in Mineralogy*, **19**, BookCrafters, Inc., Chelsea, Michigan, pp.631-674.

Kuang, W., Hubbard, B., Moser, A., Facey, G.A. and Detellier, C. (2002) Organo-sepiolite and palygorskite nanocomposites. *Proceedings of the 5th International Conference on Solid State Chemistry*, Bratislava, Slovak Republic.

Kuang, W., Facey, G.A., Detellier, C., Casal, B., Serratosa, J.M. and Ruiz-Hitzky, E. (2003) Nanostructured hybrid materials formed by sequestration of pyridine molecules in the tunnels of sepiolite. *Chemistry of Materials*, **15**(26), 4956-4967.

Maqueda, C., Villaverde, J., Sopeňa, F., Undabeytia, T. and Morillo, E. (2008) Novel system for reducing leaching of the herbicide metribuzin using clay-gel-based formulations. *J. Agric. Food Chem.*, **56**, 11941-11946.

Meunier, A. (2005) *Clays*, Springer-Verlag Berlin Heidelerg, Germany, 472 p.

Murphy, T.B. and Sawyer, A.J (2004) Advancement of Natural and Synthetic Clays in Personal Care Applications. *Süd-Chemie Inc.*, Germany, 5 p.
Obtained: http://www.touchbriefings.com/pdf/846/SudChemie_Tech.pdf

Murray, H.H. (2007) Applied Clay Mineralogy: Occurrences, processing and application of kaolins, bentonites, palygorskite-sepiolite, and common clays. Elsevier publications, chapter 2, p. 11.

Nagata, H., Shimoda, S. and Sudo, T. (1974) On dehydration of bound water of sepiolite. *Clays and Clay Minerals*, **22**, 285-293.

Nagy, B. and Bradley, W.F. (1955) The structural scheme of sepiolite. *Amer. Miner.* **40**, 885-892.

Nesse, W. (2000) *Introduction to Mineralogy*, Oxford University Press, Inc., NY, NY, 442 p.

Newman, A.C.D. and Brown, G. (1987) The chemical constitution of clays. In: Chemistry of Clays and Clay Minerals (A.C.D Newman, editor). Monograph 6, Mineralogical Society, London, pp. 1–128.

Pérez-Rodríguez, J.L. and Galán, E. (1994) Determination of impurity in sepiolite by thermal analysis. *Journal of Thermal Analysis*, **42**, 131-141.

Preisinger, A. (1963) Sepiolite and related compounds: its stability and application. *Clays and Clay Minerals*, **10**, 365-371.

Rautureau, M. and Tchoubar, (1976) Structural analysis of sepiolites by selected area electron diffraction-relations with physico-cherrical properties. *Clays and Clay Minerals*, **24**, 43-49.

Serna, C. and van Scoyoc, G.E. (1979) Infrared study of sepiolite and palygorskite surfaces. 197-206 in: *Proceedings of the International Clay Conference, Oxford, 1978* (M.M. Mortland and V.C. Farmer, editors). Elsevier, Amsterdam.

Sugiura, M. (1993) Removal of methanethiol by sepiolite and various sepiolite-metal compound complexes in ambient air. *Clay Science*, **9**, 33-41.

Sugiura, M., Fukumoto, K. and Inagaki, S. (1991) Adsorption of odorous vapors by sepiolite in ambient air. *Clay Science*, **8**, 129-145.

Sugiura, M., Horii, M., Hayashi, H., Suzuki, T., Kamigaito, O., Nogawa, S. and Oishi, S. (1990) Deodorizing paper using β-sepiolite. 91-100 in: *Proceedings of the 9th International Clay Conference*, Strasbourg, France.

Weir, M.R., Facey, G.A. and Detellier, C. (2000) ^{1}H, ^{2}H, and ^{29}Si solid state NMR study of guest acetone molecules occupying the zeolitic channels of partially dehydrated sepiolite clay. *Studies in Surface Science and Catalysis* (A. Sayari *et al.*, editors), **129**, 551-558.

Weir, M.R., Kuang, W., Facey, G.A. and Detellier, C. (2002) Solid state nuclear magnetic resonance study of sepiolite and partially dehydrated sepiolite. *Clay and Clay Minerals*, **50**(2), 240-247.

Zhu, Q.-H., Huang, D.-Y., Zhu, G.-X., Ge, T.-D., Liu, G.-S., Zhu, H.-H., Liu, S.-L., Zhang, X.-N. (2010) Sepiolite is recommended for the remediation of Cd-contaminated paddy soil. *Acta Agriculturae Scandinavica Section B: Soil and Plant Science*. **60**(2), 110-116.

Chapter 2

Characterization techniques used to study organo-clay composites

Thermal Analysis

Thermal analysis is used as a complementary technique to analytical methods such as x-ray diffraction for the study of clay materials. Thermal analysis techniques monitor the changes in physical properties and/or reaction products when a substance is heated under controlled conditions. The principal types of thermal analysis are differential thermal analysis and thermal gravimetric analysis; other less commonly used techniques include evolved gas detection/analysis (Paterson and Swaffield, 1987), (Stucki *et al.*, 1990). In addition to helping to characterize clay materials thermal analysis is also useful for the study of various reaction processes under varying temperature and pressure regimes, such as dehydration/hydration, interactions of clays with organic and inorganic compounds, oxidation and reduction processes (Stucki *et al.*, 1990).

Thermal Gravimetric Analysis (TGA) measures the amount and rate of change in the weight of a material as a function of temperature or time in a controlled atmosphere. Measurements are used primarily to determine the composition of materials and to predict their thermal stability at temperatures up to 1000°C. The technique can characterize materials that exhibit weight loss or gain due to decomposition, oxidation, or dehydration. The following features could be investigated by the TGA instrument: composition of multicomponent systems, thermal stability of materials, oxidative stability of materials, estimated lifetime of a product, and decomposition kinetics of materials, the effect of reactive or corrosive atmospheres on materials, and moisture and volatiles content of materials.

Thermogravimetric analysis produces integral weight loss data curves that can be difficult to interpret. Consequently interpretations of the TGA data are better made using the first derivative of the weight loss curve. This is derivative thermogravimetric (DTG) analysis.

Differential thermal analysis (DTA) monitors changes in thermal properties by measuring differences in temperature between the sample and a thermally inert reference standard over a controlled temperature range. This type of analysis allows exothermic or endothermic thermal reactions that occur over this temperature range to be differentiated. An exothermic reaction in the sample produces heat and an increase in temperature of the sample relative to the standard and the reverse for an endothermic reaction in the sample in which heat is absorbed (Reeves *et al.*, 2006). Water loss reactions are generally endothermic whilst recrystallization reactions are usually exothermic, for example.

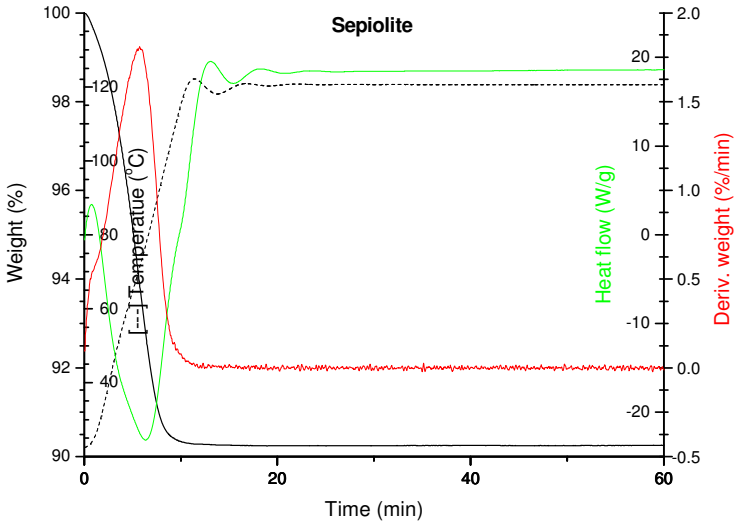

Figure 2.1 Thermal analyses (TGA, DTG, DTA) of pure sepiolite. Sample was ramped to 120°C and heated at this temperature for 2 hours (only the first hour is shown); the temperature curve is illustrated with a broken line.

Figure 2.1 is TGA, DTG and DTA analyses for pure sepiolite that was ramped to 120°C and heated at this temperature for two hours (only first hour is shown in the figure). TGA curve shows a weight loss of about 9.8% in first 10 minutes (loss of zeolitic water), DTG confirms this weight loss. DTA tells that the weight loss that is occurring is endothermic.

Porosimetry

Porosimetry is an analytical technique used to determine various quantifiable aspects of a material's porous nature, such as pore diameter, total pore volume, surface area, and bulk and absolute densities.

Surface area helps determine such things as how solids burn, dissolve, and react with other materials. To determine the surface area, solid samples are pretreated by applying some combination of heat, vacuum and/or flowing gas to remove absorbed contaminants acquired from atmospheric exposure. The solid is then cooled, under vacuum, usually to cryogenic temperature. (Cryogenics is the study of the production of very low temperature (below -150 °C) and the behavior of materials at those temperatures.) An adsorptive (typically nitrogen) is admitted to the solid in controlled increments. After each dose of adsorptive, the pressure is allowed to equilibrate and the quantity of gas adsorbed is calculated. The gas volume adsorbed at each pressure (at one constant temperature) defines an adsorption isotherm, from which the quantity of gas required to form a monolayer over the external surface of the solid and its pores is

determined. With the area covered by each adsorbed gas molecule known, the surface area can be calculated (Schuth *et al.*, 2002).

Surface area determinations involve creating the conditions required to adsorb an average monolayer of gas molecules onto a sample. By extending this process so that gas is allowed to condense in the pores, the sample's fine pore structure can be evaluated. As pressure increases, the gas condenses first in the pores with the smallest dimensions. The pressure is increased until saturation is reached, at which time all pores are filled with liquid. The adsorptive gas pressure then is reduced incrementally, evaporating the condensed gas from the system. Evaluation of the adsorption and desorption branches of theses isotherms and the hysteresis between them reveals information about the pore size, pore volume, pore area, and pore shape.

Micropore dimensions ranging from 3.5 to 20 Angstroms are important to researchers and to manufacturers using materials such as carbons, zeolites, silicas and aluminas in their processes. For analysis of pores in this range, the ability to reach and measure very low pressures is required. Factors such as temperature stability, vacuum capability, and transducer sensitivity are crucial in micropore analysis and these factors are precisely what Micrometrics' instrumentation provides. Micrometrics has pioneered instruments designed to collect data in the low pressure regions required to gain meaningful information about the microporosity of samples.

The method of Brunauer, Emmet and teller is employed to determine surface area on a model of adsorption which incorporates multilayer coverage.

The t-Plot method most commonly used to determine the external surface area and micropore volume of microporous materials. It is based on standard isotherms and

thickness curves which describe the statistical thickness of the film of adsorptive on a non-porous reference surface.

(Including cylindrical and spherical pore models) The method of Horvath and Kawazoe (H-K) provides a means by which the micropore volume distribution by size is extracted from the experimental isotherm. The original H-K method is based on slit-shaped pores; however additions by Saito-Foley and Cheng-Yang extend the method to apply to cylindrical and spherical pores, respectively.

The nitrogen adsorption-desorption isotherm of purified sepiolite is shown in Figure 2.2. The curve may be classified as a general Type IV isotherm characteristic of a microporous material, with some inherent inter-particle mesoporosity (Lao and Detellier, 1996). The main characteristic feature of a type IV isotherm is the presence of a hysteresis loop, associated with capillary condensation, in which the adsorption and desorption branches do not coincide (Gregg and Sing, 1982). During the desorption process, the desorption rate is not identical to the adsorption rate, since the processes of condensation and evaporation do not necessarily take place as exact reverses of each other. Evaporation of the liquid phase can occur spontaneously from the meniscus as soon as the pressure is low enough.

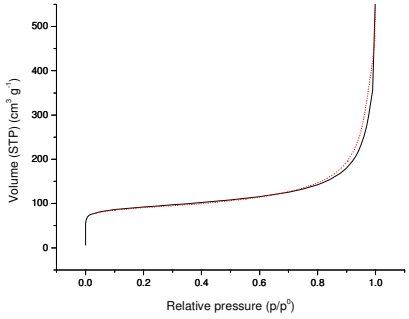

Figure 2.2 Adsorption-desorption isotherm of sepiolite.

Nuclear magnetic resonance for solids

Solid state nuclear magnetic spectroscopy is a kind of NMR spectroscopy, characterized by the presence of anisotropic (directionally dependent) interactions. In solid state NMR, the sample analyzed is first grinded with a mortar and pestle to a fine powder and then packed tightly to NMR rotor shown in the figure 2.3:

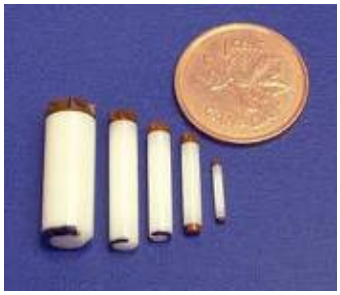

Figure 2.3 Solid NMR rotors. *Most of the samples in this thesis where packed into 7mm (in diameter) rotor.

In solution NMR, spectra consist of a series of very sharp transitions, due to averaging of anisotropic NMR interactions by rapid random tumbling. By contrast, solid-state NMR spectra are very broad, as the full effects of anisotropic or orientation-dependent interactions are observed in the spectrum. High-resolution NMR spectra can provide the same type of information that is available from corresponding solution NMR spectra, but a number of special techniques/equipment are needed, including magic angle spinning, cross polarization, special 2D experiments, enhanced probe electronics, etc. (Schurko, 2009).

Anisotropic dipolar interactions could be suppressed by introducing artificial motions on the solid - this technique involved rotating the sample about an axis oriented at 54.74° with respect to the external magnetic field. This became known as magic angle spinning (MAS). By spinning the sample at the magic angle with respect to the direction

of the magnetic field, the normally broad lines become narrower, increasing the resolution for better identification and analysis of the spectrum.

Cross polarization is one of the most important techniques in solid state NMR. In this technique, polarization from abundant spins such as ^{1}H or ^{19}F is transferred to dilute spins such as ^{13}C or ^{15}N. In example in figure 2.4, the abundant nucleus was chosen to be ^{1}H and the observed nucleus is ^{13}C. (This also works with other combinations of nuclei.) The abundant nucleus is excited, and its energy is then transferred to the observed nucleus by using a long low power pulse on both channels. The radio frequency (RF) power ratio of these pulses needs to be tuned so that the transition energy for both nuclei is the same. So that for instance for the polarization transfer from a ^{1}H to a ^{13}C, the rotating field B_1 must be 4 times weaker for the proton channel than for the carbon channel. This method often gives a much stronger signal than direct excitation, allow faster repetition rate. The major limitation of CP method is the requirement of high power irradiation that could deteriorate the sample or the probe.

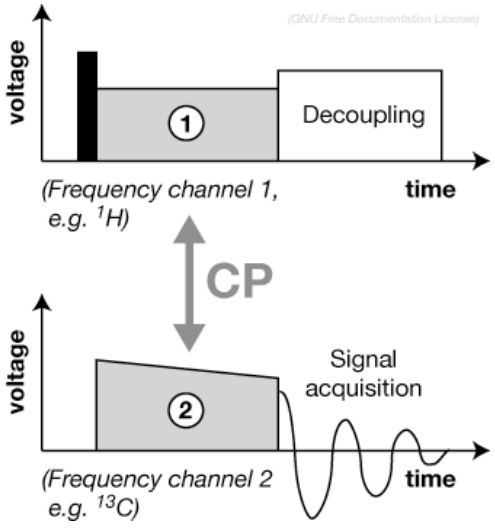

Figure 2.4 CP pulse sequence.

When CP is combined with MAS, polarization from abundant nuclei like ^{1}H, ^{19}F and ^{31}P can be transferred to dilute or rare nuclei like ^{13}C, ^{15}N, ^{29}Si in order to enhance signal-to-noise and reduce waiting time between successive experiments.

A ramped CP pulse consists in a gradual increase of the proton or carbon spin-lock field in the rotating frame during the CP time, so that several Hartmann-Hahn (HH) conditions are satisfied. This allows an improvement in the signal-to-noise ratio for some of the carbon resonances and a suppression of HH condition mismatches. The key to obtaining efficient cross polarization is setting the Hartmann-Hahn match properly. In this case, the radio frequency (RF) fields of the dilute spin (e.g., $\omega_{1C\text{-}13}$) is set equal to that of the abundant spin (e.g., $\omega_{1H\text{-}1}$) by adjusting the power on each of the channels: $\gamma_{C\text{-}13} B_{C\text{-}13} = \gamma_{H\text{-}1} B_{H\text{-}1}$, where B is magnetic field and γ is gyromagnetic ratio (the gyromagnetic ratio of a particle or system is the ratio of its magnetic dipole moment to its angular momentum). If these are set properly, the proton and carbon magnetization process in the rotating frame at the same rate, allowing for transfer of the abundant spin polarization to carbon (Le Guerneve and Auger, 1995).

References

Gregg, S.J. and Sing, K.S.W. (1982) Adsorption, Surface Area and Porosity. 2nd edn. Academic Press.

Lao, H. and Detellier, C. (1996) "Microporosimetry" in physical methods in supramolecular chemistry, Volume **8** of "Comprehensive Supramolecular Chemistry", *J. Ripmeester*, Ed., Pergamon, Elsevier Sc. Ltd., Oxford, ch. 6, 277-305.

Le Guerneve, C. and Auger, M. (1995). New Approach to Study Fast and Slow Motions in Lipid Bilayers: Application to Dimyristoylphosphatidylcholine-Cholesterol Interactions. *Biophysical Journal*, **68**, 1952-1959.

Paterson, E. and Swaffield, R (1987) Thermal analysis. In: Wilson, M.J. (ed.) *A Handbook of Determinative Methods in Clay Mineralogy*, Blackie, Glasgow, 99-132.

Reeves, G.M., Sims, I. and Cripps, J.C. (ed.) (2006) Clay materials used in construction. Geological Society Engineering Geology Special Publication No. 21. London. Chapter 8. pp. 207-208.

Schurko, R. (2009) Introductory Solid State NMR Notes.
Obtained form http://mutuslab.cs.uwindsor.ca/schurko/ssnmr/ssnmr_schurko.pdf

Schuth, F., Sing, K.S.W. and Weitkamp, J. (2002) *Handbook of Porous Solids*.

Stucki, J.W., Bish, D.L. and Mumpton, F.A. (ed.) (1990) *Thermal Analysis in Clay Science: CMS Workshop Lectures*, 3, Clay Minerals Society.

Chapter 3

MCH intercalation into sepiolite

Introduction

This chapter studies the intercalation of the 3-methyl cyclohex-2-en-1-one (MCH) molecule into sepiolite tunnels. MCH is a simple organic compound with the chemical formula $C_7H_{10}O$ (Figure 3.1), belonging to a class of α,β-unsaturated ketones, which has proven useful in naturally controlling Douglas-Fir beetle populations/infestations (Ross *et al*., 2002). MCH is the Douglas-Fir beetle's anti-aggregation pheromone. Beetles and other insects communicate using pheromones. MCH replicates the beetle pheromone that tells other beetles the tree is full and that the food supply is insufficient for additional beetles. Arriving beetles receive the "message" that they should look elsewhere for a suitable host.

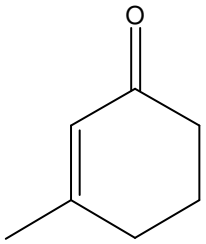

Figure 3.1 Structure of 3-methyl cyclohex-2-en-1-one.

It has been previously shown that small molecules like acetone and pyridine can be intercalated into previously dehydrated sepiolite (Weir *et al*., 2000), (Kuang *et al*., 2002). It was hoped that sepiolite could be used as an effective carrier and potential release tool for MCH molecules to control Douglas-Fir beetle infestations in North American forests. This kind of application has the potential to be commercially feasible.

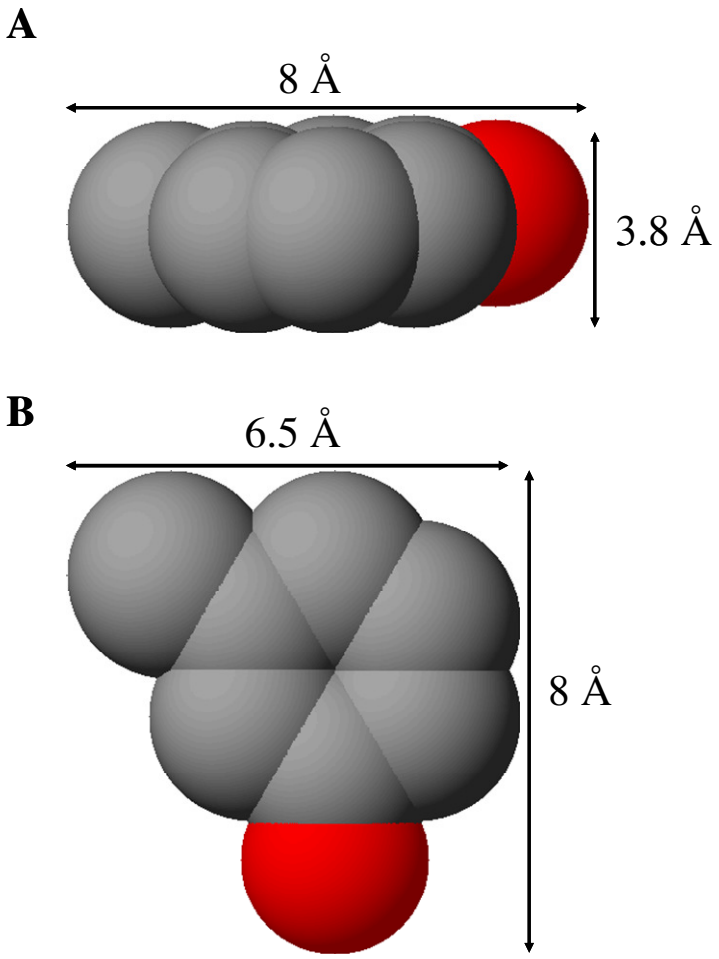

Figure 3.2 3D Space filling models of MCH created using ACD ChemSketch 5.0 of a) the XY plane, and b) the YZ plane. Corresponding dimensions were estimated using Chem CS 3Dpro.

Douglas-Fir beetles are found naturally in most Douglas-Fir stands, but when populations are at low numbers they typically kill only a few trees a year. However, in the right environmental conditions, like after a forest fire, for example, their populations can grow explosively. This happens because wildfire does not completely kill all the trees, and the trees that are left are fire-weakened and stressed, which are perfect hosts for a variety of insects including the Douglas-fir bark beetle. The favourite targets of the Douglas-Fir beetles are trees that are over 50% Douglas-Fir, trees that are over 120 years old and greater than 14 inches in diameter. The mature trees are not as strong and healthy as younger trees. Douglas-Fir beetles normally infest felled trees, mature damaged trees, logging debris and trees stressed by drought. However, when sufficient host material is unavailable, they will attack and kill vigorous trees, causing broader damage.

Douglas-Fir beetles typically lay one generation of eggs per year. They begin emerging for flight in late April to early June once daytime temperatures start reaching 15°C, searching for fresh trees in which they can reproduce. After finding the target trees, females lay their eggs in long galleries constructed parallel to the grain of inner bark. After hatching, beetle larvae feed perpendicular to the original parent gallery on the phloem (Ross and Daterman, 1997). If the larvae population is large enough, the inner bark becomes "girdled," preventing the flow of water up from the roots and nutrients down from the needles. This leads to the death of the tree.

MCH has been used widely to protect high-value, high-risk trees from Douglas-Fir beetle infestation. MCH is dispersed via aerial and ground applications. Labour is a major proportion of the cost of MCH treatments; this is related to the time applicators have to spend walking through an area and dispersing the formulated pheromone. The application of fewer MCH dispensers eluting at a higher rate than those currently

registered for operational use could potentially reduce treatment costs (Ross *et al*., 2002). Also, hand dispensers do not give homogeneous distribution in the application fields; this might leave certain areas untreated. It is hoped that the more homogeneous distribution of MCH pheromone there will be, the more time beetles will be spending searching for a host, they presumably will have a greater chance of dying as a result of longer exposure to natural enemies and other mortality factors.

Chemical pesticides have been used to protect forest and agriculture from a great variety of pest infestation. Some of these pesticides are quite toxic and have caused severe environmental and ecological problems. Facing this challenge, numerous efforts have been made to develop low toxicity or even toxicity-free pesticides.

To solve some of the encountered problems, the microencapsulation of insect sex pheromone has been proposed (Campion 1976), (Eng *et al*., 2003): i.e., techniques that employ polymer microcapsules. In work done by Gu *et al.* (2010), dodecanol ($C_{12}OH$) (as a model molecule of insect sex pheromone) encapsulation was carried out through simple coacervation of gelatin, and complex coacervation of gelatin and acacia gum.

Another example is encapsulations of herbicide. Metribuzin is an herbicide widely used for weed control that has been identified as a groundwater pollutant. It contaminates the environment even when it is used according to the manufacturer's instructions. To reduce herbicide leaching and promote weed control, new controlled-release formulations were developed by entrapping metribuzin within a sepiolite-gel-based matrix (Maqueda *et al*., 2008).

MCH is considered environmentally friendly and non-toxic to humans, animals, and even the beetles themselves. Nevertheless, anything that would be exposed in large amounts into environment could have potential harmful effects. MSDS sheet lists MCH

as harmful and says that the toxicological properties of this material have not been fully investigated. The main problem with the MCH at this point is that a lot of money is spent on the MCH application process onto the trees, as mentioned earlier. It is thus very desirable to obtain MCH protection with fewer applications of MCH pheromone and applications that would last longer. It would be very desirable: (1) if with fewer applications of MCH, the cost of the application of MCH could be decreased, (2) if the MCH could be released at the slower rate for longer periods of time, then less MCH would be released into environment at any specific time compared to now. It was hoped that sepiolite could be used as a potential tool for slow and controlled release of MCH. The first step in investigating this possibility is the MCH intercalation into sepiolite, which is the focus of this chapter. Chapter 4 will be investigating potential releasing possibilities of the MCH from the sepiolite clay.

Experimental

Materials and methods

Crude sepiolite was obtained from the University of Missouri's Source Clay Mineral Repository. It was then purified according to already established procedures involving crushing, centrifuging and weak acid treatment to eliminate carbonates (Weir *et al*., 2001). Synthetic 3-methyl cyclohexen-1-one (MCH) was obtained from Lancaster Synthesis Inc., and was used as received.

Preparation of samples

Before the intercalation of MCH, 500 mg of pure sepiolite was placed in a small ceramic crucible and heated at 120˚C for 20 hours by means of a Thermoline 48000 furnace. Heating was necessary to evaporate the zeolitic water and the surface water from the nanotunnels of sepiolite; the elimination of the zeolitic water and the surface water was confirmed by ^{29}Si CP/MAS MNR (Figure 1.6). Once dry, the ceramic crucible was quickly placed in a large glass bottle already containing 1 ml of MCH. (The amount of 1 ml was determined by trial; after one week of intercalation there was still quite a bit of MCH at the bottom of the bottle. MCH was even observed in the bottle, after two weeks of MCH intercalation. Also, in chapter 4, there will be calculation shown telling how much of MCH was absorbed into sepiolite, which is about 111 mg of MCH in 1 g of MCH-sepiolite sample.) The transfer of the crucible from oven to glass bottle was done in the air environment. It is possible that some water got absorbed into sepiolite in that time frame, however, the transferring process was very quick and the clay was still very hot, which would make the absorbed amount of water quite negligible. The bottle was then topped with a rubber stopper. Ten minute daily doses of N_2 were introduced to the apparatus to eliminate any air/moisture. The apparatus was maintained in the same state for 1 week, after which characterization experiments were conducted. Using the same apparatus and method, another sepiolite sample was introduced and left untouched, purging with N_2 gas daily for 10 minutes, for 2 weeks.

Thermal analysis

Differential thermal analysis (DTA) and thermal gravimetric analysis (TGA-DTGA) were accomplished using a SDT 2960 Simultaneous DSC-TGA instrument. For each analysis, samples of about 12 mg were placed in ceramic crucibles and analyzed. The furnace chamber was flooded with nitrogen gas flow (100 ml/min), with a heating rate of 10˚C min^{-1} up to 1100°C.

Textural analysis

BET surface area and micropore measurements were taken using a Micromeritics ASAP-2010 instrument, with N_2 used as an adsorbent gas at 77K. Samples were degassed according to thermal gravimetric results (120˚C) to eliminate surface and zeolitic water; degassing was done at 10^{-2} Torr. The molecular cross-section of nitrogen used in the data analysis was of 0.1620 nm^2. T-plot measurements were made using a standard thickness range of 3.5-5 Å.

Nuclear Magnetic Resonance spectroscopy

Solid state ^{29}Si and ^{13}C cross-polarization magic-angle spinning nuclear magnetic resonance (CP/MAS NMR) and ^{13}C MAS NMR were used to characterize and detect MCH signals and sepiolite structure changes at various temperatures. Samples were run on a Bruker AVANCE 200 solids spectrometer. ^{29}Si spectra were acquired at 39.75 MHz, whereas ^{13}C spectra were acquired at 50.31 MHz. A ramped CP pulse was used in all ^{29}Si and ^{13}C cross-polarization experiments. Recycle delay time was set to 2 seconds and the proton 90° pulse was 3.75 μs for ^{29}Si and 4 μs for ^{13}C. The contact time to allow

magnetization transfer between proton and ^{13}C nuclei was 2 ms, whereas for ^{29}Si it was 10 ms. Recycle delay time was set to 10 seconds for magic angle spinning ^{13}C, the proton 90° pulse was 3.9 μs, and the contact time to allow magnetization transfer between proton and ^{13}C nuclei was 2 ms. Spinning rates were 4.5 kHz and 4.0 kHz for ^{13}C nuclei and ^{29}Si nuclei respectively. The ^{29}Si NMR signals were externally referenced to the -$Si(CH_3)_3$ group, the resonance of tetrakis trimethylsilylsilane at -9.9 ppm, corresponding to tetramethylsilane (TMS) at 0 ppm. ^{13}C signals were externally referenced to the high frequency signal of glycine at 176.41 ppm.

Liquid NMR samples were run on an AVANCE 400 automated spectrometer with D_2O as a source of deuterium.

Results and discussion

As already discussed in Chapter 1, sepiolite is a fibrous hydrated magnesium silicate. It has two different types of water molecules in its structure: water molecules that are free to move inside the sepiolite tunnels and water molecules that are found on the external surface of the sepiolite; these are referred to as zeolitic water ($[H_2O]_{zeo}$). Other water molecules are coordinated to the magnesium cations found at the edge of the nanotunnels deeper within the sepiolite structure. These coordinated water molecules are abbreviated as $[H_2O]_{coord}$. The zeolitic water was completely removed by simple heating at 120˚C for 20 hours. The complete elimination of the zeolitic water and the surface water was confirmed by ^{29}Si CP/MAS MNR (Figure 1.6). The two coordinated water molecules may also be removed by heating to approximately 260˚C and 510˚C

respectively (Kuang *et al.*, 2003). As expected, the two $[H_2O]_{coord}$ molecules are not removed at the same temperature: as one $[H_2O]_{coord}$ molecule is eliminated, the coordination between the magnesium host and the remaining $[H_2O]_{coord}$ molecules becomes stronger. Before of the elimination of the second structural water, there is some structural folding occurring (Figure 1.5c). Thus, when the crystal folds, the remaining water molecules enter a new environment, that of the hexagonal holes of the neighbouring silica surface (Serna *et al.*, 1975) This makes the second structural water harder to eliminate than the first structural water.

Figure 3.3 shows an SEM image of purified sepiolite fibres. Sepiolite's structure is derived from talc-like tetrahedral-octahedral-tetrahedral (T-O-T) ribbons expanding infinitely along the c direction (Figure 1.4), giving sepiolite a fibrous morphology (Figure 3.3).

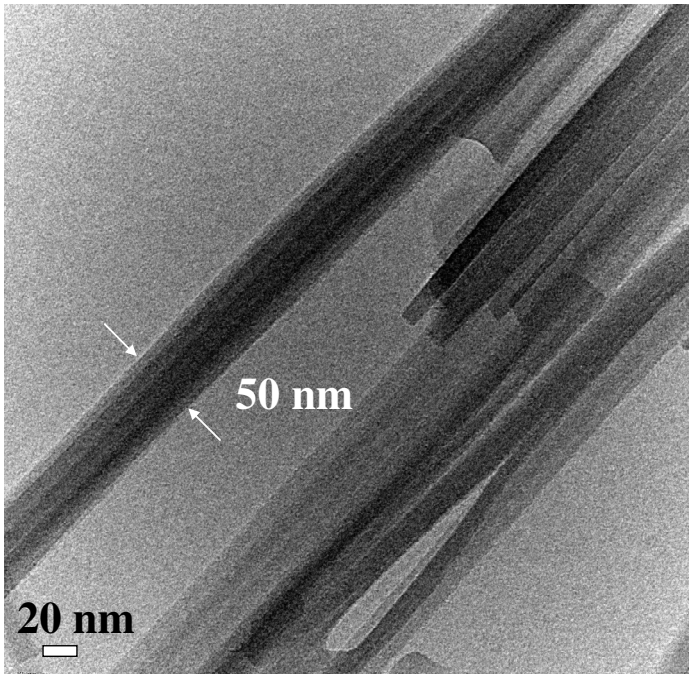

Figure 3.3 SEM of sepiolite fibres.

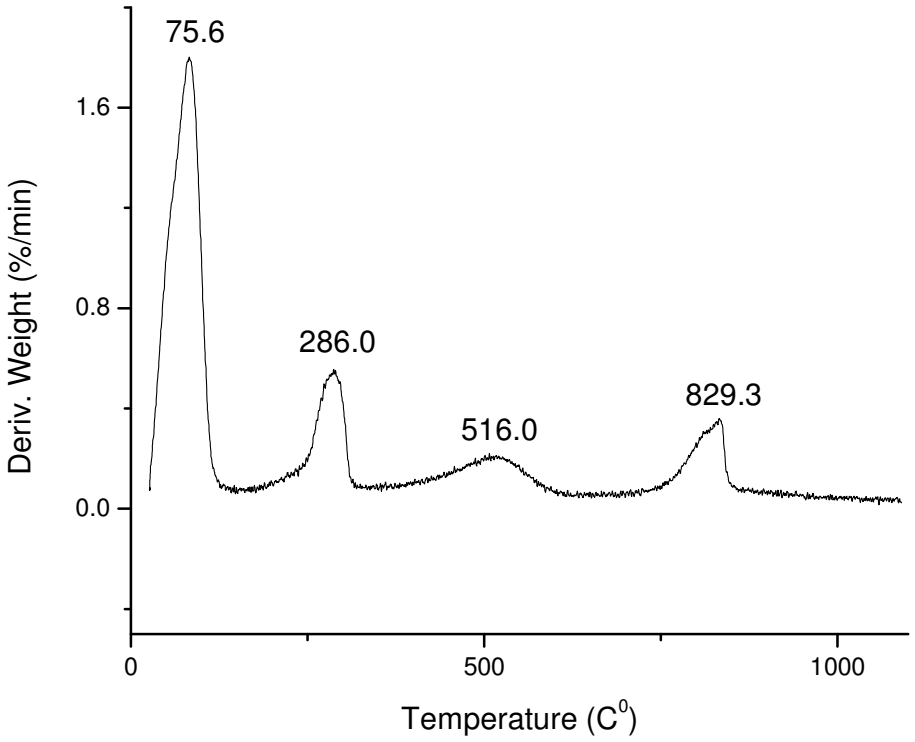

Figure 3.4 DTG of pure sepiolite. Experiment was done under nitrogen gas.

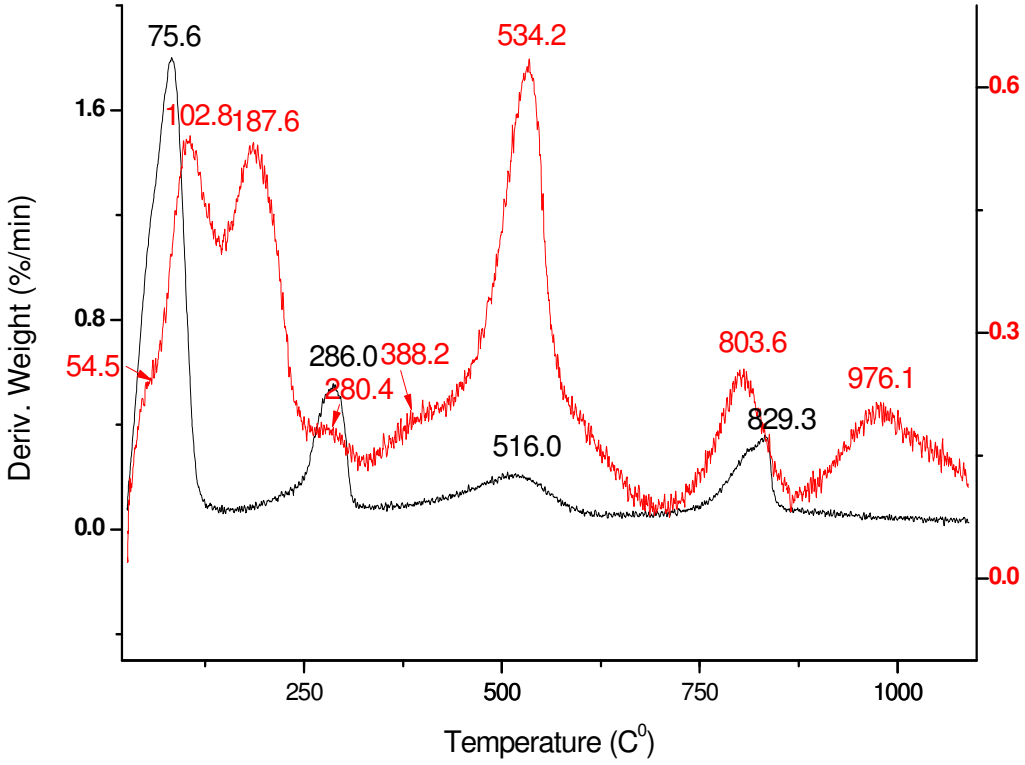

Figure 3.5 DTG traces of (black) pure sepiolite and (red) sepiolite intercalated with MCH vapours for 1 week. Experiments were done under nitrogen gas.

The DTG spectrum confirms four weight loss instances due to elimination of water molecules from sepiolite (Figure 3.4). The first weight loss, occurring at 75.6˚C, corresponds to the zeolitic water elimination as well as to surface water elimination. The second weight loss at 286.0˚C corresponds to the elimination of the first structural $[H_2O]_{coord}$ molecule; the third weight loss at 516.0˚C corresponds to the elimination of the second structural $[H_2O]_{coord}$ molecule. Lastly, the fourth weight loss at 829.3˚C indicates the dehydroxylation of the internal Mg-OH bonds (Kuang *et al*., 2003), (Hubbard *et al*., 2003).

Figure 3.5 illustrates a DTG comparison between the pure sepiolite material and the nanohybrid material Sep-MCH obtained by intercalation of MCH vapours into 500 mg of pure sepiolite, which had been pre-heated at 120˚C for 20 hours. The intercalation was permitted for one week. By heating the host inorganic material at 120˚C, it was expected that all of the zeolitic water would be eliminated, permitting MCH molecules to enter the sepiolite tunnels freely and possibly displace the coordinated water molecules, as previously shown with pyridine and acetone (Kuang *et al.*, 2003), (Kuang *et al.*, 2006). The obtained results follow a very similar pattern to the previously reported data pertaining to organic molecule intercalation in sepiolite. With the intercalation of pyridine or acetone into sepiolite, simultaneous mass spectroscopy was run during DTG analysis, which confirmed the losses due to water molecules and due to pyridine or acetone in intercalated samples. Mass spectroscopy was not run on the MCH intercalated samples due to its unavailability. The MCH intercalated sample DTG peak assignments were done strongly referring to pyridine and acetone intercalated samples.

The obtained results seem to demonstrate that MCH did displace some of the coordinated water molecules. In figure 3.5, the first two peaks of the red graph, at 54.5˚C and 102.8˚C, correspond to the elimination of surface MCH molecules and free MCH molecules within the nanotunnels, as well as MCH bonded to water molecules through hydrogen bonds. Free MCH molecules are eliminated at a lower temperature than $[H_2O]_{zeo}$ molecules (75.6˚C). This is thought to be due to the possible hydrogen bonds. H-bonds can be formed between water molecules; however, MCH molecules cannot form equally strong stabilizing H-bonds between themselves. The two peaks at 187.6˚C and 280.4˚C correspond to the elimination of the MCH linked to the sepiolite through coordination with the magnesium atoms found at the end of the zeolitic tunnels and the first coordination water molecule, respectively. The presence of these two distinctly different peaks indicates that the MCH has displaced the water molecules that were coordinated with the magnesium. These results mimic those which were obtained for the intercalation of acetone (Kuang *et al.*, 2006). The Mg-MCH coordination bonds appear to be weaker than the Mg-$[H_2O]_{coord}$ bonds.

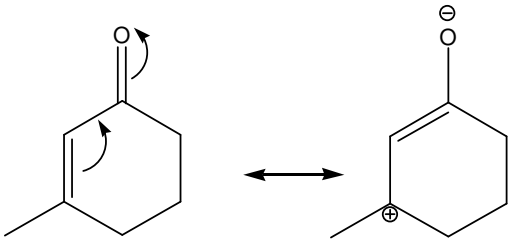

Scheme 3.1 Resonance structure of 3-methyl cyclohex-2-en-1-one (MCH). Scheme was created using ChemDraw Ultra 7.0.

The MCH molecule has two different resonance structures and it is believed to bind to Mg through the oxygen atom. Perhaps, this kind of bonding displaces the bonding between water and Mg. The coordinated water molecules seem to be much more stable

than those of the MCH; this is indicated by the large difference between elimination temperatures. The coordinated water molecules may interact with one another through hydrogen bonds, causing stabilization within the sepiolite structure. The MCH coordinated molecules are eliminated almost 100˚C earlier than the coordinated water molecules. The smaller number of stabilization bonds (H-bonds) could be an explanation for this. In Figure 3.5, the two peaks, at 534.2˚C (red spectrum) and 516.0˚C (black spectrum), are fairly similar in temperature. Like in the case of the loss of the first structural water, the loss of the second structural water is accompanied by a loss of the MCH; MCH is eliminated (small peak at 388.2°C is an indication for that) as well as any structural water still present in the structure. The peak at 803.6˚C indicates the dehydroxylation of the internal Mg-OH bonds. Finally, pyrolysis (thermochemical decomposition of organic material at elevated temperatures in the absence of oxygen) can be observed at 976.1˚C.

Sepiolite is microporous mineral. It was interesting to observe how different conditions affect the porosity of this material. For that following samples were prepared: (A) pure sepiolite; (B) pure sepiolite heated to 120˚C over 20 hours; (C) pure sepiolite heated to 350˚C over 20 hours and (D-E) pure sepiolite heated to 120˚C over 20 hours, then intercalated with MCH vapour over 1 week (D) and 2 weeks (E). These samples were analyzed by porosimeter and data is shown in table 3.1.

Table 3.1 Textural properties obtained from the analysis of nitrogen adsorption-desorption isotherms of (A) pure sepiolite; (B-C) pure sepiolite heated to 120˚C and 350˚C over 20 hours; and (D-E) pure sepiolite heated to 120˚C over 20 hours, then intercalated with MCH vapour over 1 week and 2 weeks.

Sample	BET surface Area (m^2/g)	T-Plot		Horvath-Kawazoe	
		Micropore Area (m^2/g)	Micropore Volume (cm^3/g)	Maximum Pore Volume (cm^3/g)	Median Pore Diameter (Å)
A	244	105	0.054	0.113	6.4
B	267	158	0.081	0.128	6.1
C	129	8.03	0.0028	0.054	8.2
D	149	6.32	0.0017	0.062	9.3
E	104	-	-	0.042	9.5

Once sepiolite was heated to 120˚C, the BET surface area was found to be 267 m^2/g. The increase in temperature results in the elimination of zeolitic and surface water molecules. This in turn results in greater surface area for adsorbtion of N_2 and thus concurs with previously reported results for pure heated sepiolite (Kuang *et al*., 2003), (Hubbard *et al*., 2003). The t-plot analysis of the isotherm for the same sample produced a micropore area of 158 m^2/g and a micropore volume of 81 mm^3/g. The increase in values in comparison to pure, unheated sepiolite can be explained as it was done for the BET surface area above. These values also concur with previously reported data. Finally, the Horvath-Kawazoe analysis produced a value of 6.1 Å, which also resembles previous data, for the same reason stated above (Grillet *et al*., 1988), (Facey *et al*., 2005), (Kuang *et al*., 2006). After heating to 350˚C, however, a drastic decrease in parameters occurs. This is due to a structural change caused by the loss of the first $[H_2O]_{coord}$ molecule and perhaps a little of the second $[H_2O]_{coord}$. The elimination of the first structural water molecule causes a change in sepiolite structure that is reversible; however, once the second molecule is eliminated, the structure change becomes permanent (Kuang *et al*., 2006). For the Sep-MCH, which underwent both 1 week and 2 weeks of intercalation (samples D and E), the results follow expectations, as the intercalated MCH vapour

reduces the amount of available space for N_2 gas to accumulate in the pores. This explains the BET and t-plot analyses results as well as the maximum pore volume obtained. However, the median pore area remains the same for 1 week or 2 weeks of MCH intercalation. This might be possible due to saturation: the maximum amount of intercalated MCH possible was attained after one week of intercalation. For samples C, D and E, the median pore diameter values are inaccurate as the micropore areas for these samples are too small to be detected (very often negative values were obtained for those samples); thus, pore diameters of 8.2, 9.3 and 9.5 Å are not possible. If the overall pore area and volume are decreased drastically in sepiolite (samples C, D and E), pore diameter cannot increase.

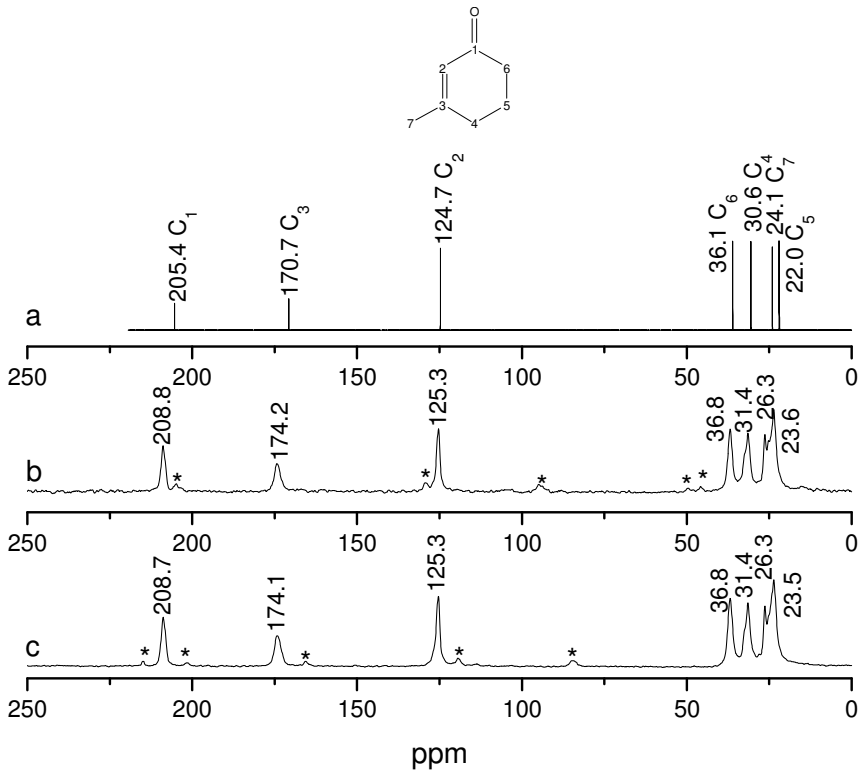

Figure 3.6 ^{13}C CP/MAS spectra of: (a) pure MCH (liquid NMR); (b) sepiolite intercalated with MCH for 1 week; and (c) sepiolite intercalated with MCH for 2 weeks. The * mark all visible spinning sidebands of the peaks. The reason why the spinning sidebands of spectra (b) and (c) are in different positions is because spectrum (b) was run at 4.0 kHz and spectrum (c) at 4.5 kHz.

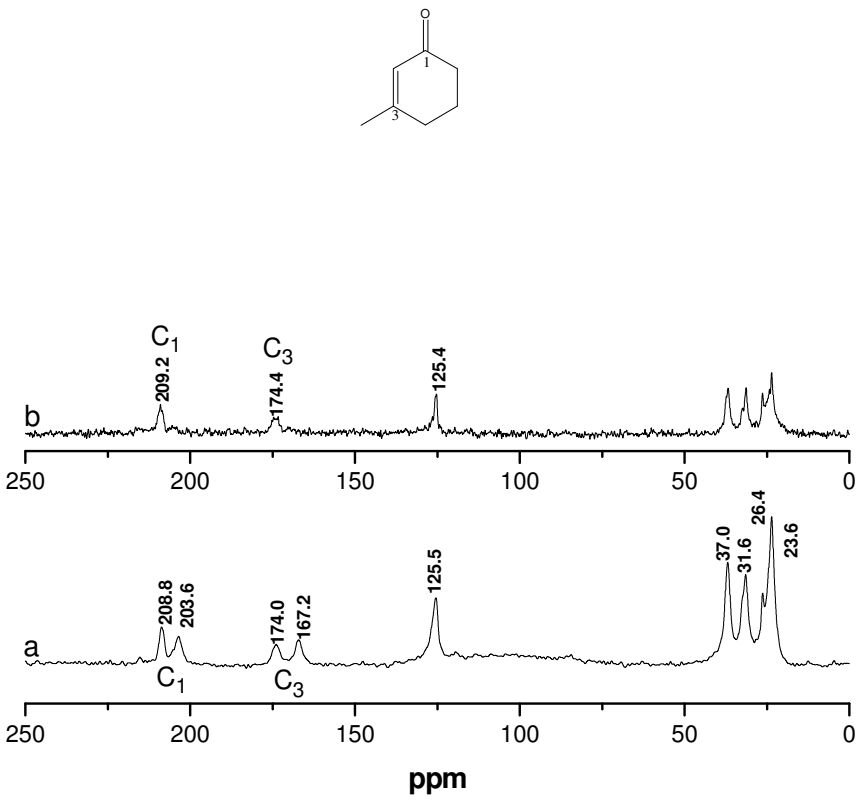

Figure 3.7 ^{13}C MAS NMR spectra of: (a) sepiolite intercalated with MCH for 1 week and (b) sample (a) heated at 60°C for 20 hours.

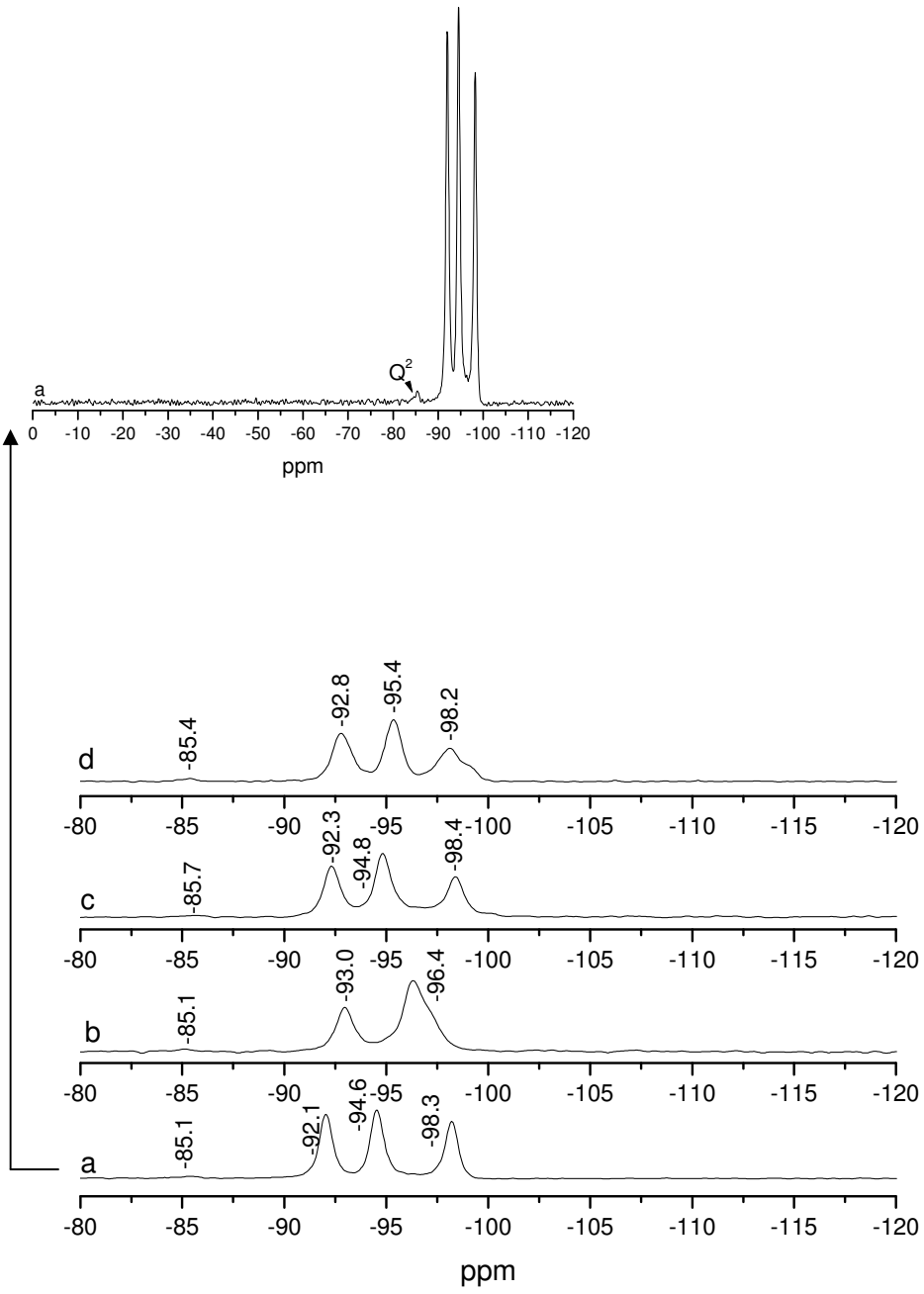

Figure 3.8 ^{29}Si CP/MAS NMR spectra of (a) pure sepiolite; (b) sepiolite previously heated at 120ºC for 20 hours; (c) sample (b) after standing in open air for 1 hour; and (d) nanohybrid MCH-sepiolite obtained by intercalation of 3-methyl cyclohexen-1-one during 1 week.

Figure 3.6 displays the carbon spectra for pure MCH (liquid state NMR), the carbon spectra for sepiolite intercalated with MCH for one week and sepiolite intercalated with MCH for two weeks (both solid state NMR). Based on the spectrum of pure 3-methyl cyclohexen-1-one, C_1 can be identified at 205.4 ppm, C_3 at 170.7 ppm and C_2 at 124.7 ppm. These numbered carbon assignments are based are estimation with ChemDraw Ultra 7.0. C_6 is believed to be at 36.1 ppm, C_4 at 30.6 ppm and C_5 at 22.0 ppm. These carbon positions were determined according to their proximity to the carbonyl electron-attracting group. Finally, the methyl group C_7 appears at 24.1 ppm.

Figure 3.6 shows ^{13}C CP/MAS NMR spectra for the solid samples (b and c). When comparing the chemical shifts observed in pure MCH and MCH adsorbed in sepiolite, we note that in the case of the sep-MCH nanohybrid a slight displacement of peak values (ppm) pertaining to C_1 and C_3 has occurred. Figure 3.7 shows ^{13}C MAS NMR spectra for sep-MCH hybrid at room temperature and a sample that has been heated at 60°C for 20 hours. There are two peaks for C_1 and C_3 carbons at room temperature. By the analogy done with pyridine studies (Kuang *et al.*, 2003), the following interpretation was made: it is believed that there are two different types of MCH molecules present in the sample: ones that are inside the sepiolite tunnels and others that are outside the sepiolite tunnels. When the sep-MCH hybrid material is heated, all the external MCH is evaporated. In Figure 3.7b, the peaks at 209.2 and 174.4 ppm are representative of the MCH molecule that is inside the tunnels of sepiolite.

^{29}Si NMR spectra are very useful for the characterization of various nanohybrid sepiolite materials (Kuang and Detellier, 2005), (Hubbard *et al*., 2003). The pure sepiolite ^{29}Si NMR spectra contains three main signals, which are known as Q^3 signals at -92.1,

-94.6 and -98.3 ppm, and one minor Q^2 signal at -85.1 ppm (Figure 3.8a) (see pages 22 and 23 for the explanation of the small size of Q^2 peak). The Q^2 signal corresponds to the inner silicon atoms deep within the sepiolite structure (Weir *et al*., 2000). Upon heating sepiolite at 120˚C for 20 hours, the two peaks at -94.6 and -98.3 ppm collapse in a higher intensity signal at -96.4 ppm, while the third signal shifts slightly from -92.1 to -93.0 ppm. This ^{29}Si NMR spectrum is characteristic of dehydrated (the tunnels are "empty") sepiolite (Figure 3.8b). Figure 3.8c is the ^{29}Si CP/MAS NMR spectrum for a dehydrated sepiolite sample that was exposed to air for one hour after heating; the three characteristic Q^3 signals are observed again. This is an indication that sepiolite is a very absorbent material and that water molecules can be removed and absorbed back into sepiolite quite freely. The characteristic three peaks of the ^{29}Si CP/MAS NMR spectrum of sepiolite are almost completely recovered in less than a minute at room temperature (Kuang and Detellier, 2005). If the dehydrated state of sepiolite is desired, it is necessary to keep dehydrated sepiolite in an air-free environment, under nitrogen in a glove container, for example.

The dehydrated sepiolite sample was allowed to intercalate with MCH vapours for one week. After that, the ^{29}Si CP/MAS NMR spectrum was obtained (Figure 3.8d). In this spectrum, three Q^3 signals are observed again, indicating that the tunnels of sepiolite are filled, this time with MCH and some water molecules. (All the samples where analyzed in the air environment, so some water might have found its way back to sepiolite as it is very absorbent material.)

Conclusion

This study sheds light on the characteristics of the incorporation of an organic molecule, MCH, within the nanotunnels of an inorganic molecule, sepiolite. There are additional peaks due to MCH molecule on the DTG spectrum compared to pure sepiolite, the porosity studies show that MCH molecules fill the pores of sepiolite, also ^{29}Si NMR shows the characteristic three peaks for the Q^3 silicon atoms after MCH intercalation indicating that the sepiolite tunnels are not empty. The newly formed nanohybrid composite is great starting material for the investigation for insect and pest control in North American Douglas-Fir forests. This study suggests possibilities for developing environmentally friendly pest-control methods and may serve as a basis for future attempts to do so.

References

Campion, D.G. (1976) Sex pheromones for the control of lepidopteran pests using microencapsulated and dispenser techniques. *Pesticide Sci.*, **7**, 636-639.

Eng, J.A., Holmes, E., Larsen, T., Stadlmann, S. and Ketner, K. (2003) Effects of sunlight on encapsulated sprayable codling moth pheromone. *Proceedings 77th Western Orchard Pest and Disease Management Conference*, 15-17 January, Portland, OR. p9.

Facey, G.A., Kuang, W. and Detellier, C. (2005) Multinuclear Spectroscopy studies of the structuration of the tunnels of sepiolite in the presence of intracrystalline pyridine molecules. *J. of Phys. Chem.*, **109**, 22359-22365.

Grillet, Y., Cases, J.M., Francois, M., Rouquerol, J. and Poirier, J.E. (1988) Modification of the porous structure and surface area of sepiolite under vacuum thermal treatment. *Clays and Clay Minerals*, **36**(3), 233-242.

Gu, X.-L., Zhu, X., Kong, X.-Z. and Tan, Y. (2010) Comparisons of simple and complex coacervations for preparation of sprayable insect sex pheromone microcapsules and release control of the encapsulated pheromone molecule. *Journal of Microencapsulation*, **27**(4), 355-364.

Hubbard, B., Kuang, W., Moser, A., Facey, G.A. and Detellier, C. (2003) Structural study of Maya Blue: textural, thermal and solid-state multinuclear magnetic resonance characterization of the palygorskite-indigo and sepiolite-indigo adducts. *Clay and Clay minerals*, **51**(3), 318-326.

Kuang, W. and Detellier, C. (2005) Structuration of organo-minerals: Nanohybrid materials resulting from the incorporation of alcohols in the tunnels of palygorskite. *Studies in Surface Science and Catalysis*, **156**, 451-456.

Kuang, W., Facey, G.A. and Detellier, C., (2006) Organo-mineral nanohybrids. Incorporation, coordination and structuration role of acetone molecules in the tunnels of sepiolite. *Journal of Materials Chemistry*, **16**(2), 179-185.

Kuang, W., Facey, G.A., Detellier, C., Casal, B., Serratosa, J.M. and Ruiz-Hitzky, E. (2003) Nanostructured hybrid materials formed by sequestration of pyridine molecules in the tunnels of sepiolite. *Chemistry of Materials*, **15**(26), 4956-4967.

Kuang, W., Hubbard, B., Moser, A., Facey, G.A. and Detellier, C. (2002) Organo-sepiolite and palygorskite nanocomposites. *Proceedings of the 5th International Conference on Solid State Chemistry*, Bratislava, Slovak Republic.

Maqueda, C., Villaverde, J., Sopeňa, F., Undabeytia, T. and Morillo, E. (2008) Novel system for reducing leaching of the herbicide metribuzin using clay-gel-based formulations. *J. Agric. Food Chem.*, **56**, 11941-11946.

Ross, D.W. and Daterman, G.E. (1997) Using pheromone baited traps to control the amount and distribution of tree mortality during outbreaks of the Douglas-Fir beetle. *Forest Science*, **43**(1), 65-70.

Ross, D., Daterman, G. and Gibson, K. (2002) Elution rate and spacing of anti-aggregation pheromone dispensers for protecting live trees from dendroctonus pseudotsugae (Coleoptera Scolytidae). *J. Econ. Entomology*, **5**(4) 778-781.

Serna, C., Ahlrichs, J.L. and Serratosa, J.M. (1975) Folding in sepiolite crystals. *Clays and Clay Miner*. **23**(6), 452-457

Weir, M.R., Facey, G.A. and Detellier, C. (2000) ^{1}H, ^{2}H, and ^{29}Si solid state NMR study of guest acetone molecules occupying the zeolitic channels of partially dehydrated sepiolite clay. *Studies in Surface Science and Catalysis* (A. Sayari *et al.*, editors), **129**, 551-558.

Weir, M.R., Rutinduka, E., Detellier, C., Feng, C.Y., Wang, Q., Matsuura, T. and Le Van Mao, R. (2001) Fabrication, characterization and preliminary testing of all-inorganic ultrafiltration membranes composed entirely of a naturally occurring sepiolite clay mineral. *Journal of Membrane Sci.*, **182**, 41-50.

Chapter 4

Release studies of MCH from the sepiolite

Introduction

A pheromone is a secreted or excreted chemical factor that triggers a social response in members of the same species. Pheromones are chemicals capable of acting outside the body of the secreting individual to impact the behaviour of the receiving individual. There are sex pheromones, alarm pheromones, food trail pheromones and many others that affect physiology or behaviour. Pheromone use among insects has been especially well documented. In addition, some vertebrates and plants communicate by using pheromones (Wyatt, 2003).

Aggregation pheromones act as signals for alarm and defence, territory and trail-marking, and social regulation and recognition. Pheromones are now being used in insect control, for example, as bait to attract males to field traps or, in very high concentrations, to disorient insects and prevent mating.

MCH is the Douglas-Fir beetle's anti-aggregation pheromone. MCH replicates the beetle pheromone that tells other beetles the tree is full and that the food supply is insufficient for additional beetles. Arriving beetles receive the "message" that they should look elsewhere for a suitable host.

The previous chapter featured a comprehensive study of a newly formed sepiolite-MCH nanohybrid material resulting from the intercalation process of pure sepiolite with MCH molecules. The purpose of this chapter is to study the possibilities of obtaining the slow and controlled release of MCH from the sepiolite tunnels. The Sep-MCH compound is a very stable compound resistant to heat as it was observed that MCH molecules were in the tunnels of sepiolite even after heating nanohybrid materials at 300 ˚C for 20 hours.

This chapter investigates other possibilities obtaining slow and controlled release of MCH from sepiolite other than heating Sep-MCH nanohybrids. (1) Co-intercalations of MCH with organic solvents into sepiolite tunnels were carried out. It was hoped that organic solvent molecules could fill the tunnels of sepiolite clay, allowing the slow release of MCH from the sepiolite tunnels. (2) Sep-MCH samples were acid treated. Acid would start attacking magnesium atoms of the sepiolite making the tunnel size of sepiolite hopefully larger. So, that MCH would have more room to escape the sepiolite.

Experimental

Materials and methods

Crude sepiolite was obtained from the University of Missouri's Source Clay Mineral Repository. It was then purified according to already established procedures involving crushing, centrifuging and weak acid treatment to eliminate carbonates (Weir *et al*., 2001). Synthetic 3-methyl cyclohexen-1-one (MCH) was obtained from Lancaster Synthesis Inc., and was used as received. All organic solvents (methanol, ethanol, acetone, benzene, pyridine, deuterated benzene) were received from the Aldrich Chemical Co., and were used as received. Concentrated HCl (36.5-38.0% assay) was received from Fisher Scientific and was used in a 0.5 M concentration.

Preparation of samples

Before the co-intercalation of MCH with organic solvents, ~500 mg of pure sepiolite was placed in a small ceramic crucible and heated at 120˚C for 20 hours by means of a Thermoline 48000 furnace. Heating was necessary to evaporate the zeolitic water and the surface water from the nanotunnels of sepiolite. Once dry, the ceramic crucible was quickly placed in a large glass bottle already containing 50:50 by weight of MCH and some organic solvent (1 gram of each), or 2 grams of deuterated benzene, or 50:50 by weight of pyridine and deuterated benzene (1 gram of each); the bottle was then topped with a rubber stopper. Ten minute daily doses of N_2 were introduced to the apparatus to eliminate any air/moisture. The apparatus was maintained in the same state for 1 week, after which characterization experiments were conducted.

0.5 M HCl was prepared and used in acidic treatments of sepiolite-MCH nanohybrides. Samples were treated with 20 ml of 0.5 M HCl for various times in beakers with magnetic stir bars on stir plates. Then, solutions were filtered and filtrates analyzed with a UV-Vis spectrophotometer.

Thermal analysis

Differential thermal analysis (DTA) and thermal gravimetric analysis (TGA-DTGA) were accomplished using a SDT 2960 Simultaneous DSC-TGA instrument. For each analysis, samples of about 12 mg were placed in ceramic crucibles and analyzed. The furnace chamber was flooded with nitrogen gas flow (100 ml/min) with a heating rate of 10˚C min^{-1} up to 1100°C.

In the release studies, samples of MeOH:MCH sepiolite and EtOH:MCH sepiolite were heated to 100°C in 5 minutes and allowed to stay at that temperature for a day.

Textural analysis

BET surface area and micropore measurements were taken using a Micromeritics ASAP-2010 instrument, with N_2 used as an adsorbent gas at 77K. Samples were degassed according to thermal gravimetric results (120˚C) to eliminate surface and zeolitic water; degassing was done at 10^{-2} Torr. The molecular cross-section of nitrogen used in the data analysis was 0.1620 nm^2. T-plot measurements were made using a standard thickness range of 3.5-5 Å.

Nuclear Magnetic Resonance spectroscopy

Solid state ^{29}Si cross-polarization magic-angle spinning nuclear magnetic resonance (CP/MAS-NMR), ^{13}C MAS NMR and ^{2}H NMR were used to characterize and detect MCH and organic solvent signals, and sepiolite structure changes at various temperatures. Samples were run on a Bruker AVANCE 200 spectrometer. ^{29}Si spectra were acquired at 39.75 MHz, whereas ^{13}C spectra were acquired at 50.31 MHz. A ramped CP pulse was used in all ^{29}Si cross-polarization experiments. Recycle delay time was set to 2 seconds and the proton 90° pulse was 3.75 μs for ^{29}Si. The contact time to allow magnetization transfer between proton and ^{29}Si nuclei was 10 ms. Recycle delay time was set to 10 seconds for Magic Angle Spinning ^{13}C, the proton 90° pulse was 3.9 μs, and the contact time to allow magnetization transfer between proton and ^{13}C nuclei was 2 ms. Spinning rates were 4.5 kHz and 4.0 kHz for ^{13}C nuclei and ^{29}Si nuclei, respectively. The ^{29}Si NMR signals were externally referenced to the $-Si(CH_3)_3$ group, the resonance of

tetrakis trimethylsilylsilane at -9.9 ppm, corresponding to tetramethylsilane (TMS) at 0 ppm. ^{13}C signals were externally referenced to the high frequency signal of glycine at 176.41 ppm. The ^{2}H broadline NMR experiments were measured at room temperature on a Bruker AVANCE 200 spectrometer, operating at 0.72 MHz, using the quadrupolar echo pulse technique (Facey *et al*., 2005), with ^{2}H 90° pulses of 2.7 μs and an interpulse delay of 35μs. Typically, 1500 scans were collected with a 2 s recycle time.

Liquid NMR samples were run on an AVANCE 400 automated spectrometer with D_2O as a source of deuterium.

UV-Vis spectroscopy

Absorption spectra were recorded at room temperature with 1 nm resolution using a Varian Cary-1 Dual Beam UV-Vis spectrophotometer.

Results and discussion

Co-intercalation of MCH with organic solvents into sepiolite

As already established in the previous chapter, when MCH is intercalated into sepiolite, the ^{13}C NMR spectrum shows that at room temperature, there are two different MCH molecules present in the sample: ones inside the sepiolite tunnels and others outside the sepiolite tunnels. When the sep-MCH hybrid material is heated, all of the external MCH is slowly evaporated. However, the internal MCH was found to be very

resistant to heat as it was observed that MCH molecules were in the tunnels of sepiolite even after heating nanohybrid materials at 300 ˚C for 20 hours. It was interesting to find out if the slow and controlled release of the internal MCH could be obtained. For that purpose, co-intercalations of MCH with organic solvents into sepiolite tunnels were carried out. It was hoped that organic solvent molecules could fill the tunnels of sepiolite clay, allowing the slow release of MCH from the sepiolite tunnels.

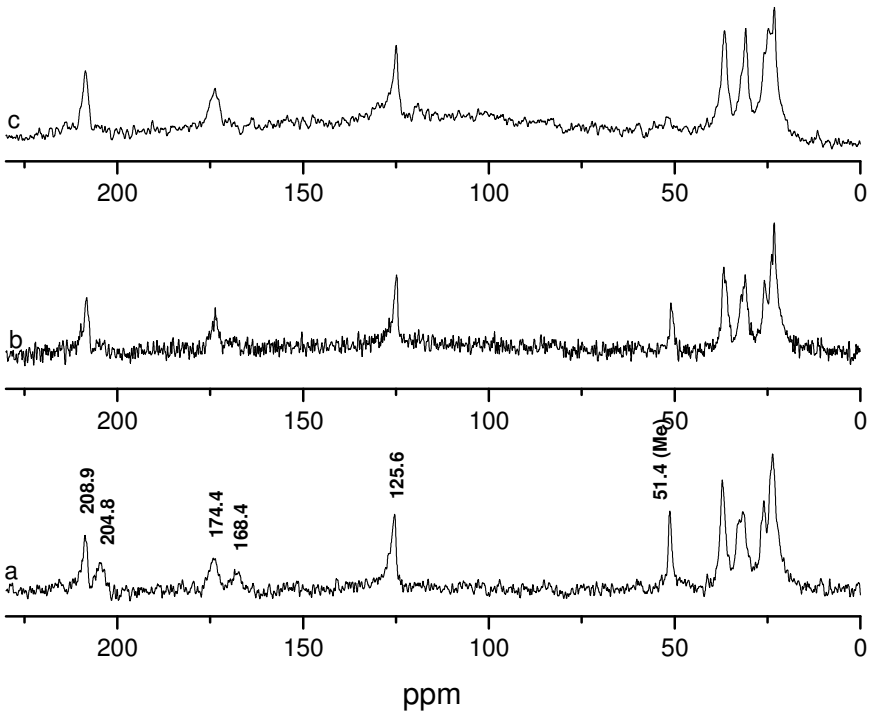

Figure 4.1 Preheated sepiolite was co-intercalated with methanol:MCH 50:50 by mass mixture and then analyzed. ^{13}C MAS NMR spectra of: (a) sample at room temperature; (b) sample (a) heated at 60°C for 20 hours; and (c) sample (b) heated at 120°C for 20 hours.

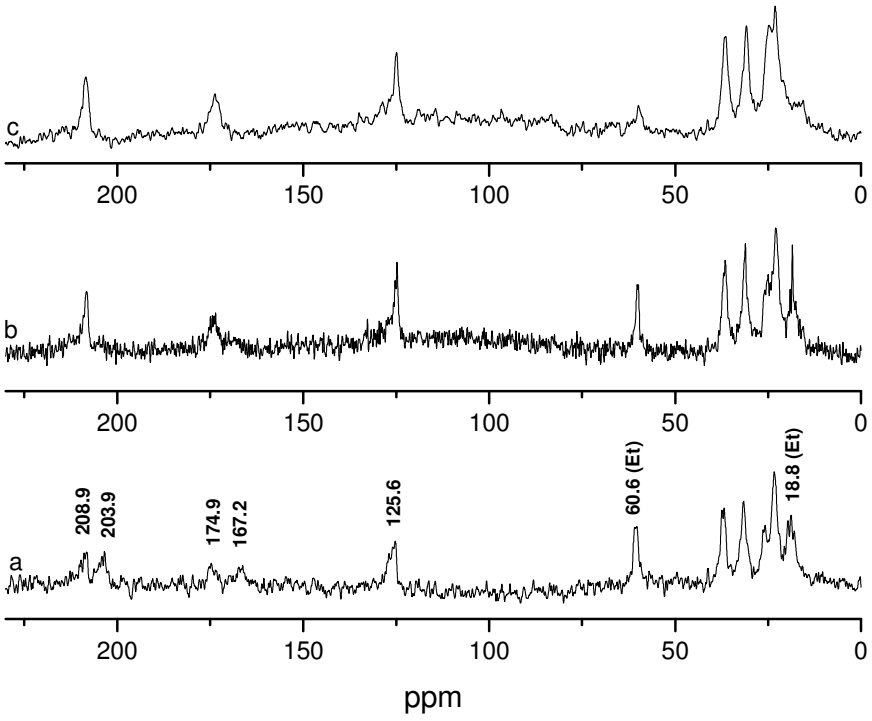

Figure 4.2 Preheated sepiolite was co-intercalated with ethanol:MCH 50:50 by mass mixture and then analyzed. ^{13}C MAS NMR spectra of: (a) sample at room temperature; (b) sample (a) heated at 60°C for 20 hours; and (c) sample (b) heated at 120°C for 20 hours.

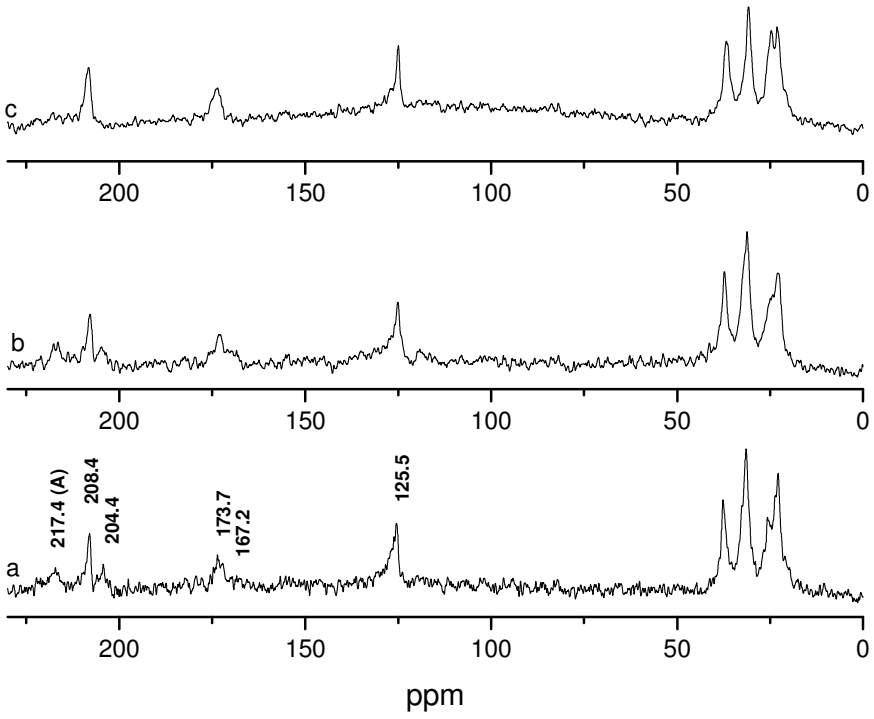

Figure 4.3 Preheated sepiolite was co-intercalated with acetone:MCH 50:50 by mass mixture and then analyzed. ^{13}C MAS NMR spectra of: (a) sample at room temperature; (b) sample (a) heated at 60°C for 20 hours; and (c) sample (b) heated at 120°C for 20 hours.

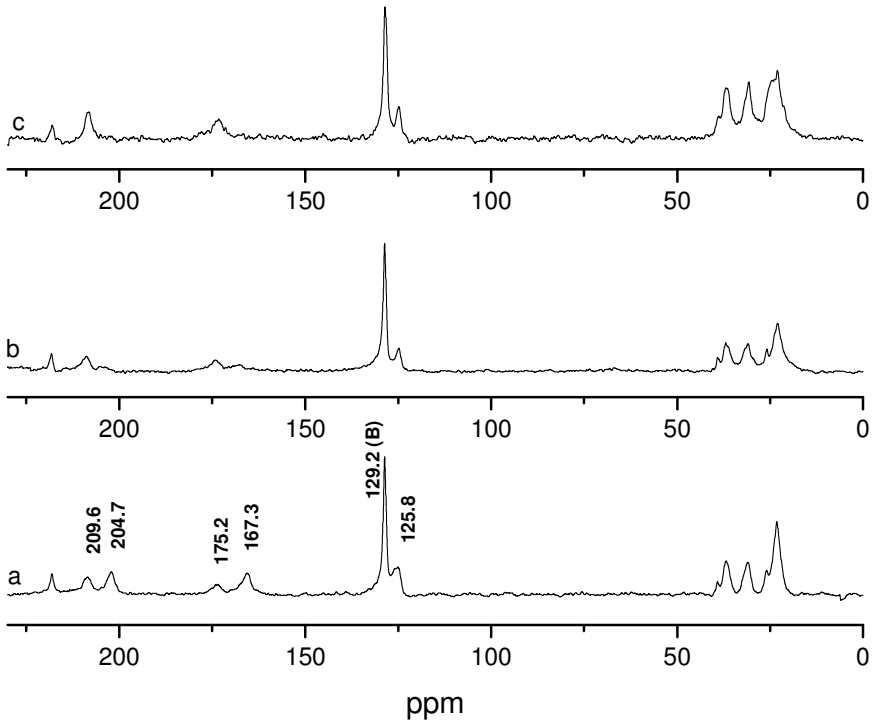

Figure 4.4 Preheated sepiolite was co-intercalated with benzene:MCH 50:50 by mass mixture and then analyzed. ^{13}C MAS NMR spectra of: (a) sample at room temperature; (b) sample (a) heated at 60°C for 20 hours; and (c) sample (b) heated at 120°C for 20 hours.

Figure 4.1 shows the ^{13}C MAS NMR spectra for methanol and MCH co-intercalation into sepiolite. At room temperature (Figure 4.1a) there are two peaks for C_1 (208.9 and 204.8 ppm) and C_3 (174.4 and 168.4 ppm) carbons of MCH. This means that there are two different types of MCH molecules present in the sample: ones inside the sepiolite tunnels and others outside the sepiolite tunnels. The peak at 125.6 ppm is representative of the C_2 of the MCH molecule and four aliphatic peaks of MCH are found in the higher magnetic field of the ^{13}C NMR spectrum. The peak at 51.4 ppm is a methanol peak. Figure 4.1b is the ^{13}C MAS NMR spectrum for a methanol:MCH sepiolite sample that has been heated for 20 hours at 60°C in the Thermoline 48000 furnace. It could be noticed that peaks at 204.8 and 168.4 ppm for the C_1 and C_3 of the MCH are very much reduced, which means that most of the external MCH is evaporated from the sample. The methanol peak looks a bit reduced as well when compared to the spectrum at room temperature. Then methanol:MCH sepiolite sample is further heated at 120°C for another 20 hours in the Thermoline 48000 furnace; Figure 4.1c shows the ^{13}C MAS NMR spectrum after this heating. It might be noted in the end that most of the methanol and external MCH are evaporated from the sample, and mostly only internal MCH is left in the sepiolite tunnels.

Figure 4.2 shows the ^{13}C MAS NMR spectra for ethanol and MCH co-intercalation into sepiolite. At room temperature (Figure 4.2a) there are two peaks for the C_1 (208.9 and 203.9 ppm) and C_3 (174.9 and 167.2 ppm) carbons of the MCH. This means that there are two different types of MCH molecules present in the sample: ones inside the sepiolite tunnels and others outside the sepiolite tunnels. The peak at 125.6 ppm is representative of the C_2 of the MCH molecule and four aliphatic peaks of MCH

are found in the higher magnetic field of the ^{13}C NMR spectrum. Peaks at 60.6 and 18.8 ppm are ethanol peaks. Figure 4.2b is the ^{13}C MAS NMR spectrum for an ethanol:MCH sepiolite sample that has been heated for 20 hours at 60°C in the Thermoline 48000 furnace. It might be noted that peaks at 203.9 and 167.2 ppm for the C_1 and C_3 of the MCH are very much reduced, which means that most of the external MCH is evaporated from the sample. Ethanol peaks look quite the same when compared to the spectrum at room temperature. Then, the ethanol:MCH sepiolite sample is further heated at 120°C for another 20 hours in the Thermoline 48000 furnace; Figure 4.2c shows the ^{13}C MAS NMR spectrum after this heating. It might be noted in the end that most of the ethanol and external MCH are evaporated from the sample, and mostly only internal MCH is left in the sepiolite tunnels.

Figure 4.3 shows the ^{13}C MAS NMR spectra for acetone and MCH co-intercalation into sepiolite. At room temperature (Figure 4.3a) there are two peaks for the C_1 (208.4 and 204.4 ppm) and C_3 (173.7 and 167.2 ppm) carbons of the MCH. This means that there are two different types of MCH molecules present in the sample: ones inside the sepiolite tunnels and others outside the sepiolite tunnels. The peak at 125.5 ppm is representative of the C_2 of the MCH molecule and four aliphatic peaks of MCH are found in the higher magnetic field of the ^{13}C NMR spectrum. The peak at 217.4 ppm is an acetone peak. Figure 4.3b is the ^{13}C MAS NMR spectrum for an acetone:MCH sepiolite sample that has been heated for 20 hours at 60°C in the Thermoline 48000 furnace. It could be noticed that peaks at 204.4 and 167.2 ppm for the C_1 and C_3 of MCH are very much reduced, which means that most of the external MCH is evaporated from the sample. The acetone peak looks a bit reduced as well when compared to the spectrum

at room temperature. Then, the acetone:MCH sepiolite sample is further heated at 120°C for another 20 hours in the Thermoline 48000 furnace; Figure 4.3c shows the ^{13}C MAS NMR spectrum after this heating. It might be noted in the end that most of the acetone and external MCH are evaporated from the sample, and mostly only internal MCH is left in the sepiolite tunnels.

Figure 4.4 shows the ^{13}C MAS NMR spectra for benzene and MCH co-intercalation into sepiolite. At room temperature (Figure 4.4a) there are two peaks for the C_1 (209.6 and 204.7 ppm) and C_3 (175.2 and 167.3 ppm) carbons of the MCH. This means that there are two different types of MCH molecules present in the sample: ones inside the sepiolite tunnels and others outside the sepiolite tunnels. The peak at 125.8 ppm is representative of the C_2 of the MCH molecule and four aliphatic peaks of MCH are found in the higher magnetic field of the ^{13}C NMR spectrum. The peak at 129.2 ppm is a benzene peak. The small peak that is in the lowest magnetic field in Figure 4.4 is a repeating side band for the benzene peak. Figure 4.4b is the ^{13}C MAS NMR spectrum for a benzene:MCH sepiolite sample that has been heated for 20 hours at 60°C in the Thermoline 48000 furnace. It could be noticed that peaks at 204.7 and 167.3 ppm for the C_1 and C_3 of MCH are very much reduced, which means that most of the external MCH is evaporated from the sample. The benzene peak looks quite the same way when compared to the spectrum at room temperature. Then, the benzene:MCH sepiolite sample is further heated at 120°C for another 20 hours in the Thermoline 48000 furnace; Figure 4.4c shows the ^{13}C MAS NMR spectrum after this heating. It might be noted in the end that most of the external MCH is evaporated from the sample, and benzene and internal MCH molecules are left in the sepiolite tunnels.

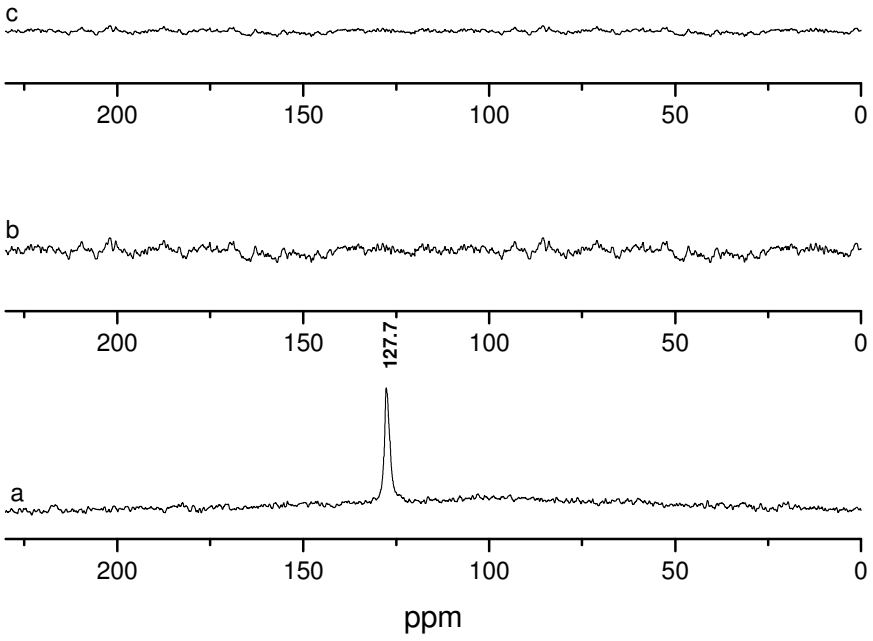

Figure 4.5 Preheated sepiolite was intercalated with d_6-benzene and then analyzed. ^{13}C MAS NMR spectra of: (a) sample at room temperature; (b) sample (a) heated at 60°C for 20 hours; and (c) sample (b) heated at 120°C for 20 hours.

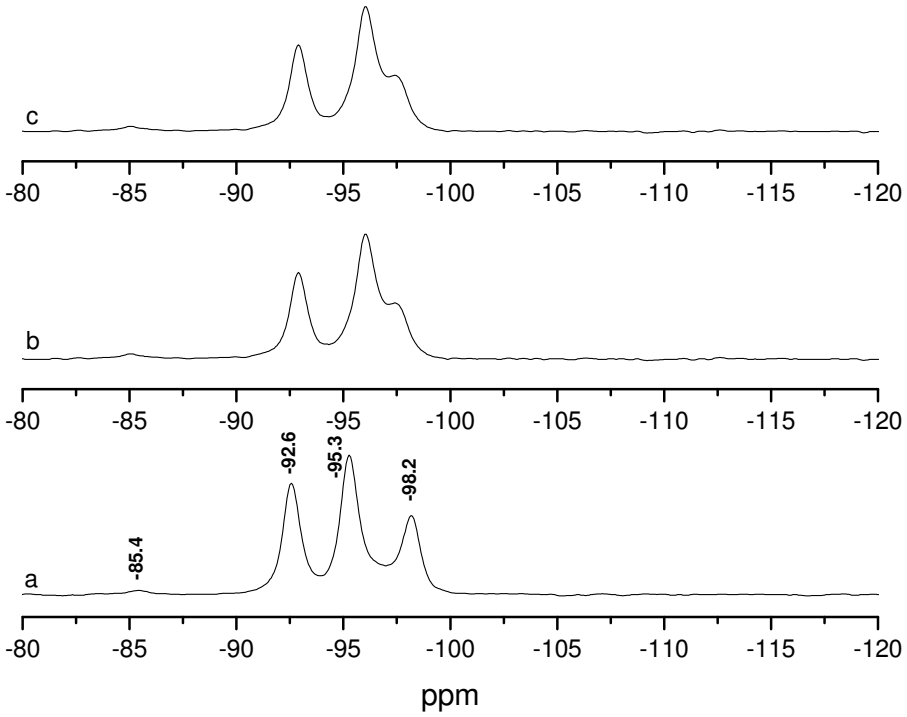

Figure 4.6 Preheated sepiolite was intercalated with d_6-benzene and then analyzed. ^{29}Si CP/MAS NMR spectra of: (a) sample at room temperature; (b) sample (a) heated at 60°C for 20 hours; and (c) sample (b) heated at 120°C for 20 hours.

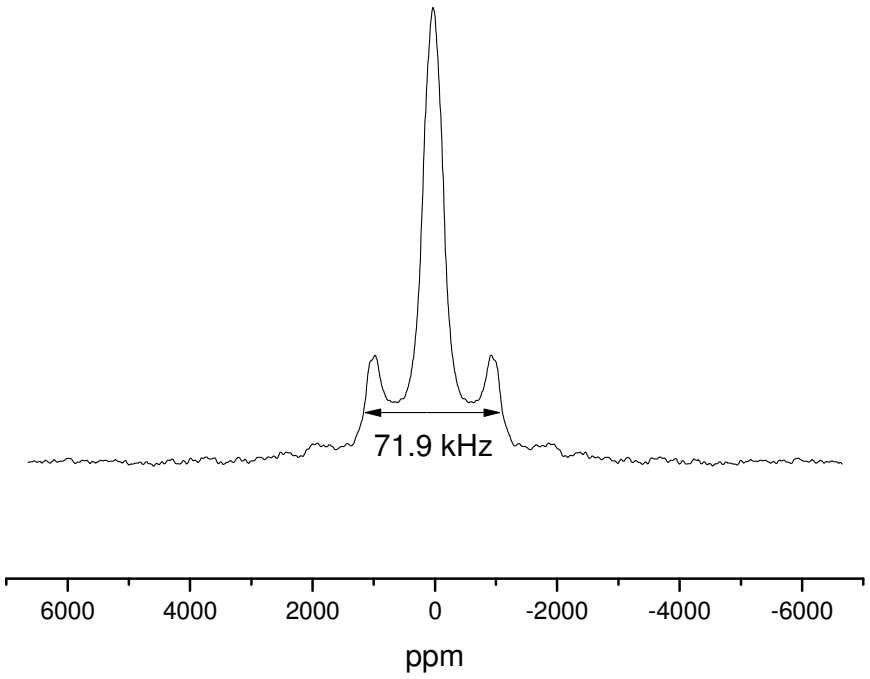

Figure 4.7 Preheated sepiolite was intercalated with d_6-benzene and then analyzed. ^{2}H NMR spectrum of sample at room temperature.

It was interesting that all other solvents except the benzene were evaporated almost completely with heating from the co-intercalated samples. Accordingly, further studies were prompted to find out how the benzene molecule that is not evaporated by heating the benzene:MCH nanohybrids is positioned in the sepiolite tunnels. The intercalation of deuterated benzene as well as co-intercalations of deuterated benzene with pyridine or MCH into sepiolite were carried out. Temperature dependence of the samples was studied again.

Figure 4.5 shows the ^{13}C MAS NMR spectra for d_6-benzene intercalation into sepiolite. At room temperature (Figure 4.5a) there is one peak at 127.7 ppm; this is the benzene peak. As the d_6-benzene sepiolite sample is heated, d_6-benzene is completely evaporated from the sepiolite already after heating the sample at 60°C for 20 hours. Figure 4.6 shows the ^{29}Si CP/MAS NMR spectra for d_6-benzene intercalation into sepiolite and it confirms the emptying of sepiolite tunnels with heating.

Also, ^{2}H NMR was performed on samples with deuterated benzene; ^{2}H NMR is highly useful for the study of molecular dynamics in solids. ^{2}H is a spin $I = 1$ nucleus with three Zeeman states. The pure Zeeman states are perturbed by the interaction of the nuclear quadrupole moment with the electric field gradients that surround the nucleus, thus producing two resonance frequencies for each crystallographically unique deuteron. The difference in frequency between the two resonances is determined by the quadrupolar coupling constant, χ, and the orientation of the electric field gradient tensor at the nuclear site with respect to the static magnetic field vector (Facey *et al*., 1995). The electric field gradient tensor, V_{ij}, is usually very close to being axially symmetric with the C-D bonds of organic molecules, with its largest component, $V_{zz} = eq$, parallel to the

bond. In powder samples, all orientations of the C-D bonds with respect to the magnetic field are possible. This results in a powder pattern with three pairs of features that are given by (Facey *et al*., 2005):

- $\Delta\nu_{zz} = \nu_q = 3\chi/2$
- $\Delta\nu_{yy} = \frac{1}{2}\nu_q(1 + \eta)$
- $\Delta\nu_{xx} = \frac{1}{2}\nu_q(1 - \eta)$
- η = *asymmetry parameter*

$[\eta = (\Delta\nu_{yy} - \Delta\nu_{xx}) / \Delta\nu_{zz}]$

$0 \leq \eta \leq 1$

- $\Delta\nu_{xx} \leq \Delta\nu_{yy} \leq \Delta\nu_{zz}$

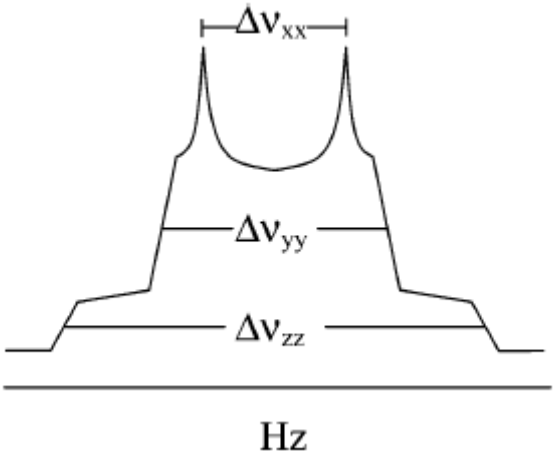

Figure 4.8 Calculated general ^{2}H NMR powder pattern with an asymmetry parameter of 0.2. This figure is obtained from Facey *et al*., (2005), Figure 2.

Also, since V_{ij} is a traceless tensor, $\Delta\nu_{xx} + \Delta\nu_{yy} = \Delta\nu_{zz}$, when molecular motions occur on a time scale quickly with respect to the quadrupolar interaction, components of the electric field gradient tensor are averaged, thereby reducing the values of $\Delta\nu_{xx}$, $\Delta\nu_{yy}$, and $\Delta\nu_{zz}$. Isotropic motion will reduce all of the splittings to zero and yield an isotropic

line, whereas anisotropic motions will unequally average particular components of V_{ij} and may even leave one of the frequency separations unchanged with respect to the static spectrum (Facey *et al*., 2005).

In Figure 4.7, the spectrum consists of an intense Lorentzian central line superposed on a much broader powder pattern at the base. The intense central peak is attributed to benzene molecules adsorbed on the external surfaces undergoing rapid isotropic motion, while the broad powder pattern is predominantly attributed to benzene molecules trapped inside the tunnels as well as some rigid structural HDO molecules from any isotopic exchange that may have occurred.

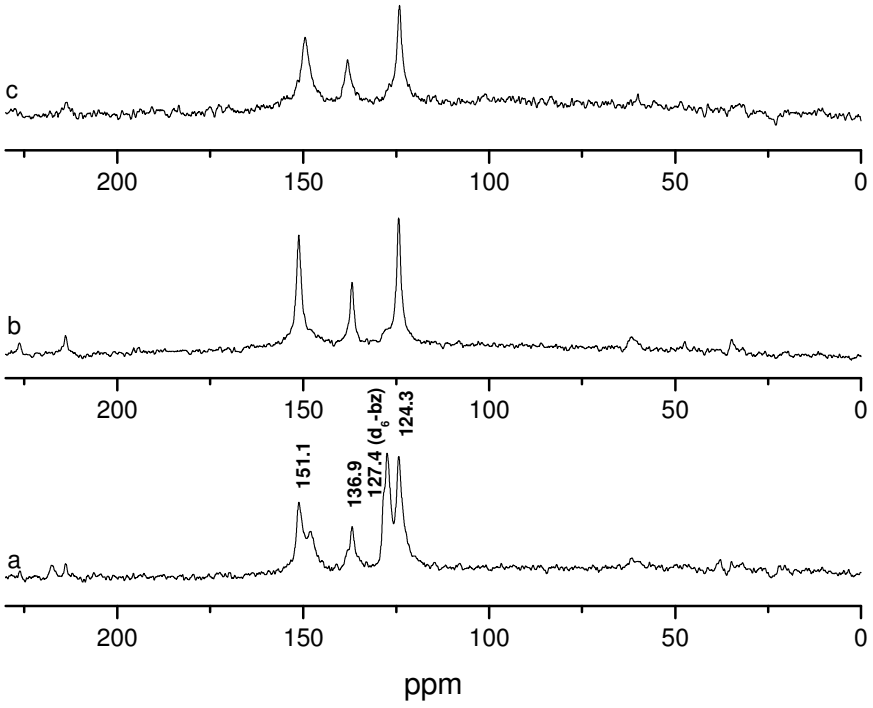

Figure 4.9 Preheated sepiolite was co-intercalated with d_6-benzene:pyridine 50:50 by mass mixture and then analyzed. ^{13}C MAS NMR spectra of: (a) sample at room temperature; (b) sample (a) heated at 60°C for 20 hours; and (c) sample (b) heated at 120°C for 20 hours.

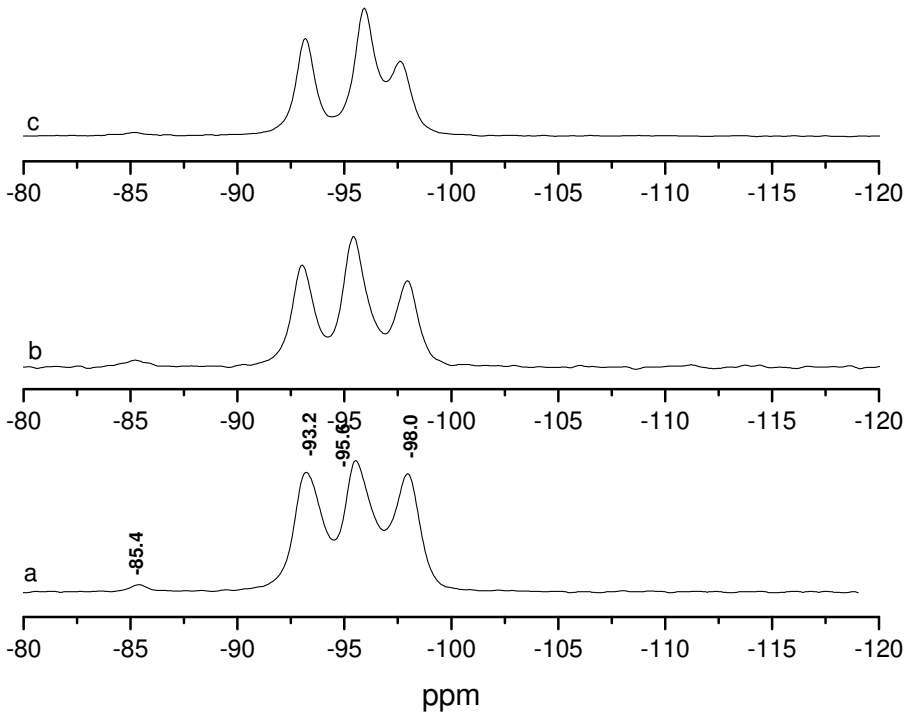

Figure 4.10 Preheated sepiolite was co-intercalated with d_6-benzene:pyridine 50:50 by mass mixture and then analyzed. ^{29}Si CP/MAS NMR spectra of: (a) sample at room temperature; (b) sample (a) heated at 60°C for 20 hours; and (c) sample (b) heated at 120°C for 20 hours.

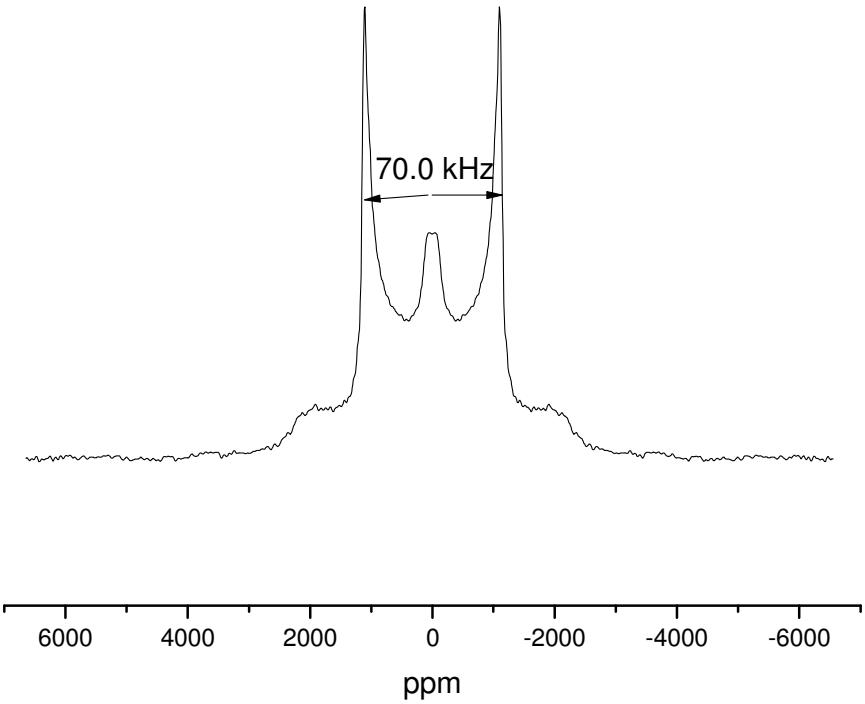

Figure 4.11 Preheated sepiolite was co-intercalated with d_6-benzene:pyridine 50:50 by mass mixture and then analyzed. ^{2}H NMR spectrum of sample at room temperature.

Previous studies have been done on the intercalation of pyridine molecules into sepiolite (Kuang *et al*., 2003), (Facey *et al*., 2005). In the first step of the formation of Sep-pyridine, the pyridine molecules were incorporated at room temperature into the tunnels by simple exposure of sepiolite to pyridine vapors. The incorporated pyridine molecules were found to H-bond to the structural water molecules coordinated to the edge Mg(II) cations. In a second step, upon heating to 140°C, approximately 50% of the pyridine was lost, together with most of the structural water coordinated to Mg(II). This was accompanied by direct coordination of the remaining pyridine molecules in the tunnels to the edge Mg(II) ions of the octahedral sheets, resulting in a material with a structure similar to the parent sepiolite, but with pyridine molecules coordinated to the Mg(II) edge cations. This material was found to be stable up to 450°C. At this temperature, the coordinated pyridine molecules escape from the tunnels, resulting in a collapsed sepiolite structure. Co-intercalation of pyridine with deuterated benzene was performed in order to see whether pyridine molecules block the benzene inside the sepiolite as the MCH molecules do.

Figure 4.9 shows the ^{13}C MAS NMR spectra for d_6-benzene:pyridine co-intercalation into sepiolite. At room temperature (Figure 4.9a) there are three peaks belonging to pyridine (151.1, 136.9 and 124.3 ppm) and one peak belonging to benzene at 127.4 ppm. As the d_6-benzene:pyridine sepiolite sample is heated, d_6-benzene is completely evaporated from the sepiolite already after having heated the sample at 60°C for 20 hours, the pyridine molecule is resistant to heating even at 120°C for 20 hours. Figure 4.10 shows the ^{29}Si CP/MAS NMR spectra for the d_6-benzene:pyridine co-

intercalated sample, which shows the characteristic three peaks, indicating that sepiolite is always filled with some organics.

Figure 4.11 shows the ^{2}H NMR for the d_6-benzene:pyridine co-intercalated sample at room temperature. The spectrum consists of a Lorentzian central line (much smaller compared to the one in Figure 4.7) superposed on a much broader powder pattern. The central peak is attributed to benzene molecules adsorbed on the external surfaces undergoing rapid isotropic motion, while the broad powder pattern is predominantly attributed to benzene molecules trapped inside the tunnels as well as some rigid structural HDO molecules from any isotopic exchange that may have occurred. Therefore, there is more benzene trapped inside the tunnels of sepiolite when it is co-intercalated with pyridine than when it is just intercalated by itself. However, pyridine does not block benzene molecules in sepiolite as they could be removed with heating quite easily.

The spectrum (Figure 4.11) predominantly shows the powder pattern, a quadrupolar coupling constant of $\chi = 93.0$ kHz and an asymmetry parameter of $\eta = 0.003$.

Table 4.1 Comparison of the ^{2}H NMR spectral parameters for polycrystalline benzene to benzene that is undergoing 6-fold rotation and to samples prepared at room temperature: deuterated benzene intercalated into preheated sepiolite, and deuterated benzene and pyridine co-intercalated into preheated sepiolite.

	d_6-benzene sepiolite (Figure 4.7)	**d_6-benzene:pyridine sepiolite (Figure 4.11)**	**^{2}H d_6-benzene 6-fold rotation (Albunia *et al.*, 2005)**	**Polycrystalline ^{2}H d_6-benzene at 200 K (Boden *et al.*, 1978)**
χ	**89.0**	**93.0**	**88.5**	**177.0**
$\Delta\nu_{xx}$ (kHz)	**61.6**	**69.5**	**63.7**	**127.3**
$\Delta\nu_{yy}$ (kHz)	**71.9**	**70.0**	**69.1**	**138.2**
$\Delta\nu_{zz}$ (kHz)	**133.5**	**139.5**	**132.8**	**265.5**
η	**0.077**	**0.003**	**0.041**	**0.041**

The observed splitting is slightly lower than half the value of the expected quadrupolar coupling of aromatic systems, indicating that the benzene-d_6 molecules are mainly involved in a fast rotation about their C_6 symmetry axis, perpendicular to the aromatic ring (Figure 4.12), with some additional out-of-plane tumbling of the molecules (Albunia *et al*., 2005). Also, in the paper by Nishikiori and others (1991), it was indicated that for benzene that undergoes an n-fold ($n \geq 3$) reorientation or rotational diffusion about its 6-fold axis, a quadrupolar coupling constant varies between 90.7-95.4 kHz and an asymmetry parameter of $\eta = 0$.

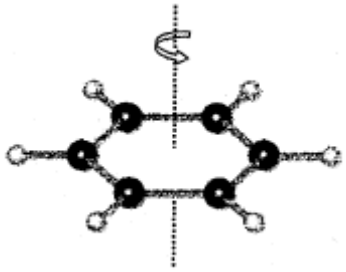

Figure 4.12 Benzene fast rotation about its C_6 symmetry axis, perpendicular to the aromatic ring. Obtained from Trezza and Grassi (2002), *part of Figure 1.

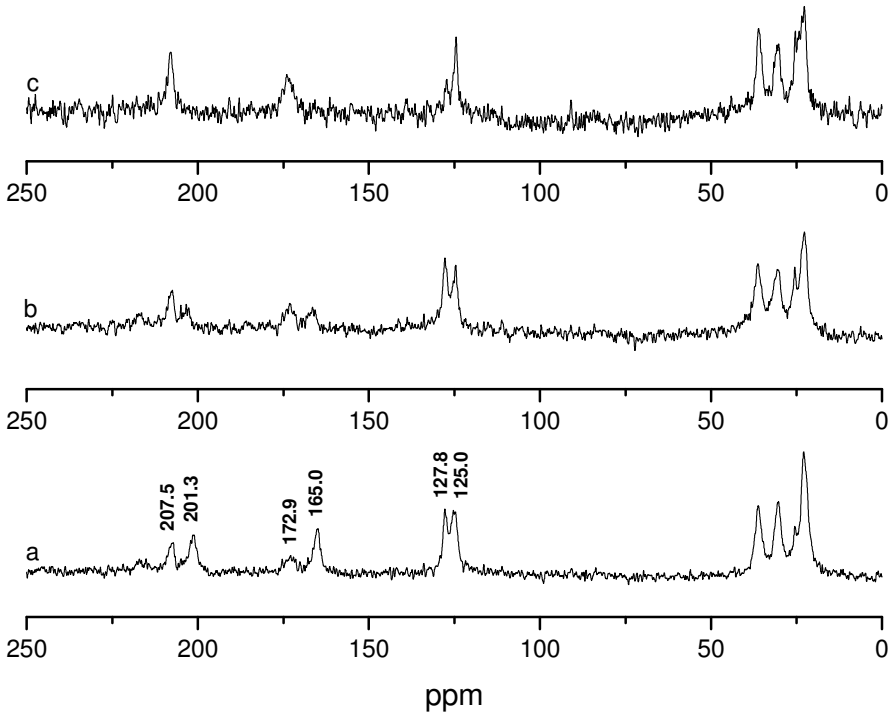

Figure 4.13 Preheated sepiolite was co-intercalated with d_6-benzene:MCH 50:50 by mass mixture and then analyzed. ^{13}C MAS NMR spectra of: (a) sample at room temperature; (b) sample (a) heated at 60°C for 20 hours; and (c) sample (b) heated at 120°C for 20 hours.

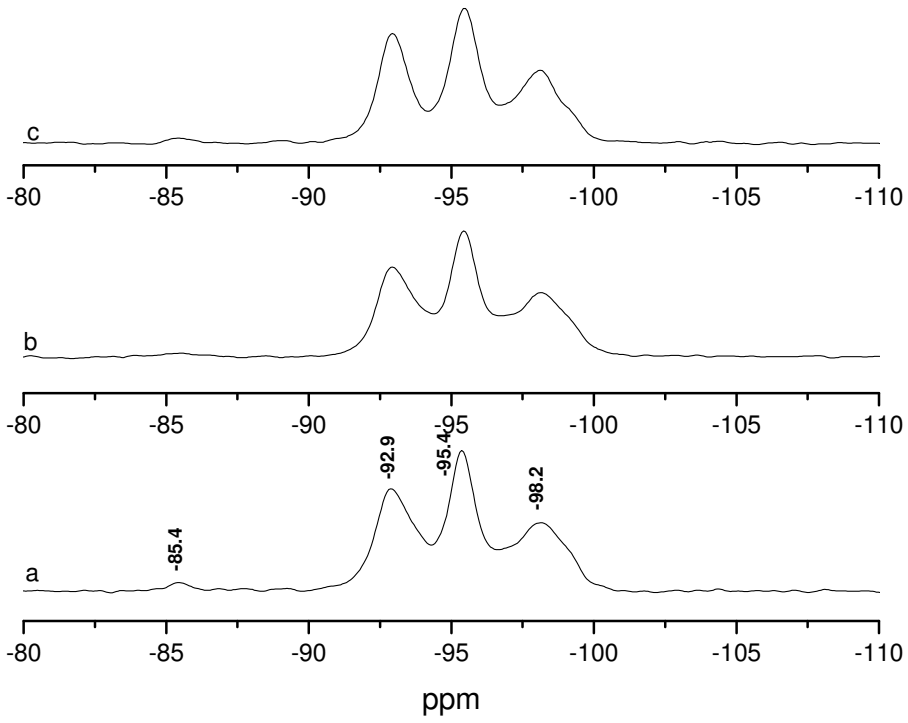

Figure 4.14 Preheated sepiolite was co-intercalated with d_6-benzene:MCH 50:50 by mass mixture and then analyzed. ^{29}Si CP/MAS NMR spectra of: (a) sample at room temperature; (b) sample (a) heated at 60°C for 20 hours; and (c) sample (b) heated at 120°C for 20 hours.

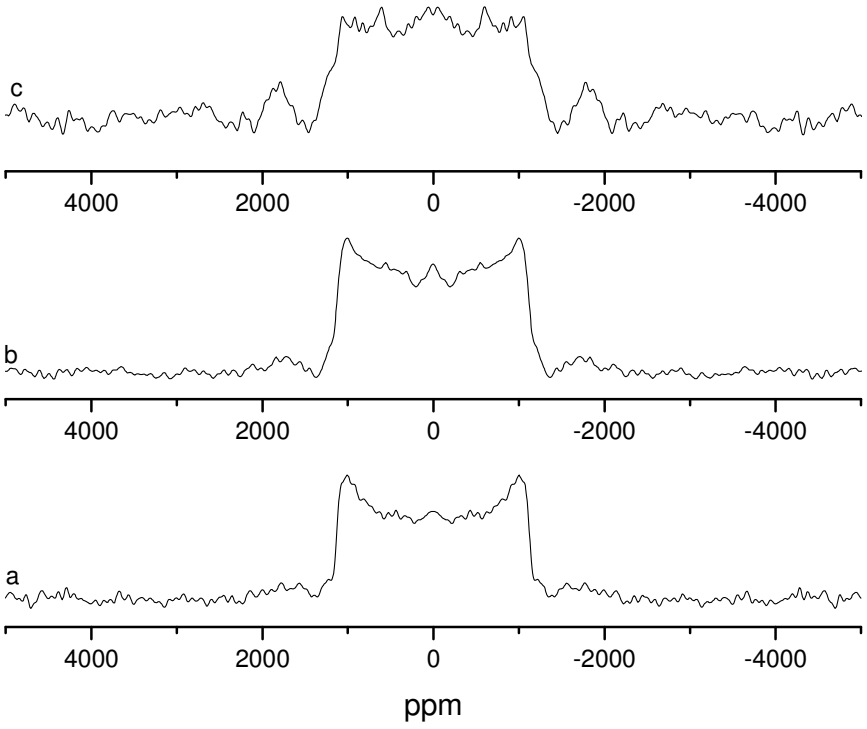

Figure 4.15 Preheated sepiolite was co-intercalated with d_6-benzene:MCH 50:50 by mass mixture and then analyzed. ^{2}H NMR spectra of: (a) sample at room temperature; (b) sample (a) heated at 60°C for 20 hours; and (c) sample (b) heated at 120°C for 20 hours.

Figure 4.13 is basically exactly the same as Figure 4.4; the only difference is that deuterated benzene is used this time. Also, it seems like the amount of benzene is reduced after prolonged heating of the d_6-benzene:MCH sepiolite sample at 120°C; this feature was not really observed in Figure 4.4. This could perhaps be explained by some random experimental difference (two experiments were carried out quite a few months apart). It would be good to do both co-intercalations: deuterated benzene with MCH as well as benzene with MCH simultaneously and see if those two samples are identical as expected. However, the purpose of co-intercalation of deuterated benzene with MCH into sepiolite was done mainly with the purpose of studying molecular motions of benzene molecule inside the sepiolite. Figure 4.14 shows the ^{29}Si CP/MAS NMR spectra for the d_6-benzene:MCH co-intercalated sample, which shows the characteristic three peaks, indicating that sepiolite is always filled with some organics.

Figures 4.15a – 4.15c show the ^{2}H NMR for the d_6-benzene:MCH co-intercalated sample at room temperature, the sample heated at 60°C for 20 hours, and then further heated at 120°C for 20 hours, respectively. The spectra consist of broad powder patterns, which are attributed to benzene molecules trapped inside the tunnels as well as some rigid structural HDO molecules from any isotopic exchange that may have occurred. MCH molecules seem to be at least partially blocking benzene molecules from leaving sepiolite when heated.

Table 4.2 Comparison of the ^{2}H NMR spectral parameters for polycrystalline benzene to benzene that is undergoing 6-fold rotation, and to deuterated benzene and pyridine co-intercalated into preheated sepiolite at room temperature, after heating at 60°C and after heating at 120°C.

	d_6-benzene: MCH sepiolite (room temp.)	**d_6-benzene: MCH sepiolite (60°C)**	**d_6-benzene: MCH sepiolite (120°C)**	**^{2}H d_6-benzene 6-fold rotation (Albunia *et al*., 2005)**	**Polycrystalline ^{2}H d_6-benzene at 200 K (Boden *et al*., 1978)**
χ	**86.0**	**85.0**	**89.7**	**88.5**	**177.0**
$\Delta\nu_{xx}$ (kHz)	**59.5**	**59.3**	**62.6**	**63.7**	**127.3**
$\Delta\nu_{yy}$ (kHz)	**69.5**	**68.2**	**72.0**	**69.1**	**138.2**
$\Delta\nu_{zz}$ (kHz)	**129.0**	**127.5**	**134.6**	**132.8**	**265.5**
η	**0.078**	**0.070**	**0.070**	**0.041**	**0.041**

The observed splitting is slightly lower than half the value of the expected quadrupolar coupling of aromatic systems, indicating that the benzene-d_6 molecules are mainly involved in a fast rotation about their C_6 symmetry axis, perpendicular to the aromatic ring (Figure 4.12), with some additional out-of-plane tumbling of the molecules (Albunia *et al*., 2005).

Heating co-intercalated methanol:MCH or ethanol:MCH sepiolite samples for periods of time

Co-intercalation of MCH molecules with various organic molecules did not yield any noticeable release of MCH molecules from the sepiolite tunnels. To find out the percentage of organic matter that is lost from sepiolite with heating, co-intercalated samples of methanol:MCH and ethanol:MCH sepiolite were heated quickly (in 5 minutes) to 100°C with the TGA instrument and allowed to stand at that temperature for

24 hours. The weight loss percentage patterns for two samples can be observed in Figures 4.16 and 4.17.

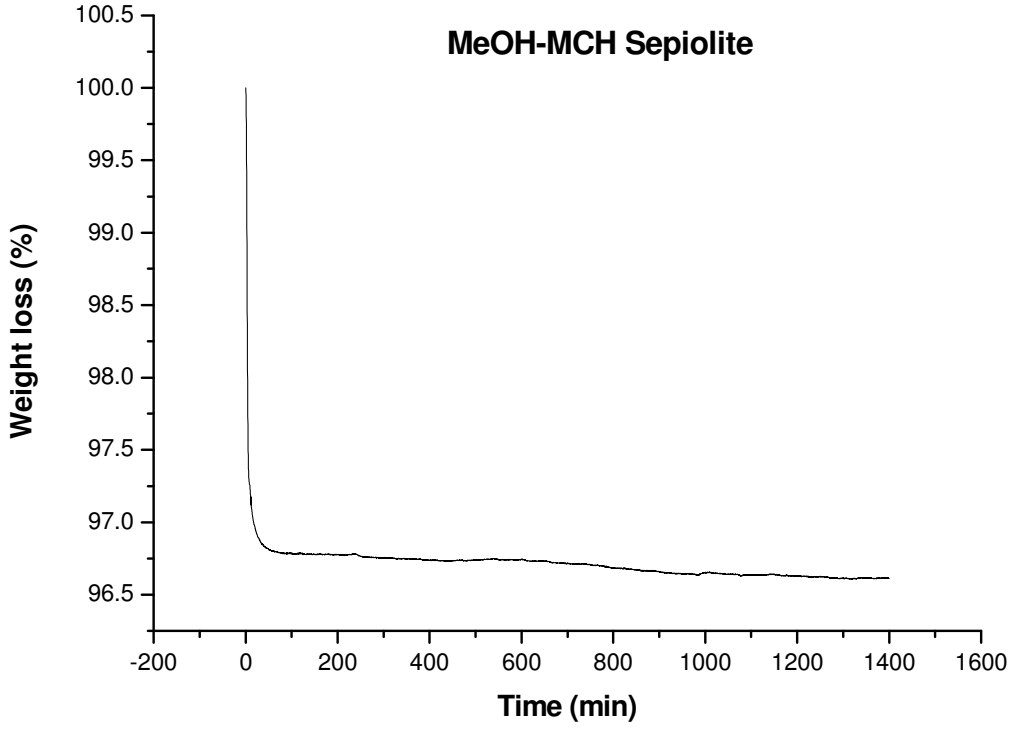

Figure 4.16 Weight loss curve for methanol:MCH sepiolite co-intercalated sample. Sample was heated to 100°C in 5 minutes and then allowed to stand at that temperature for 24 hours.

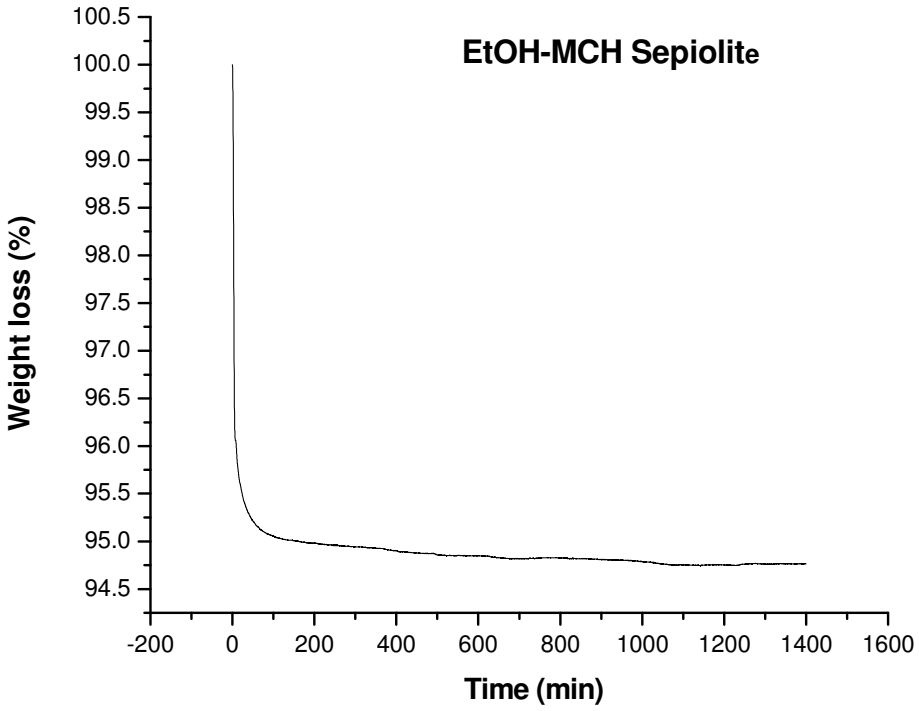

Figure 4.17 Weight loss curve for ethanol:MCH sepiolite co-intercalated sample. Sample was heated to 100°C in 5 minutes and then allowed to stand at that temperature for 24 hours

For the methanol:MCH sepiolite co-intercalated sample, after heating to 100°C in 5 minutes the weight loss percentage is 2.3%. After heating the sample at 100°C for 24 hours, about an additional 1.1% of weight loss is obtained. Most of the weight loss occurs during the initial fast heating, however. At that point, most of the methanol and some external MCH molecules are evaporated. For the ethanol:MCH sepiolite co-intercalated sample, after heating to 100°C in 5 minutes the weight loss percentage is 3.5%. After heating the sample at 100°C for 24 hours, about an additional 1.7% of weight loss is obtained. Most of the weight loss occurs during the initial fast heating, like in the methanol:MCH sepiolite co-intercalated sample. At that point, most of the ethanol and some external MCH molecules are evaporated. Both samples (methanol:MCH and ethanol:MCH sepiolite co-intercalated samples) lose about the same amount of organic material; the higher weight percent value in the ethanol:MCH sepiolite can be attributed to the higher molecular weight of ethanol compared to methanol. In both samples, the MCH molecule release obtained is really insignificant.

(Ross *et al*. (1996) showed that MCH applied at rates 20 g/ha (50 bubble capsules per hectare) can reduce the probability that high-risk Douglas-fir will become infested.)

Acidic treatment of MCH-sepiolite samples

It is known that HCl would attack magnesium atoms of the sepiolite from the purification studies of the sepiolite. It was hoped that by partial dissolution of magnesium atoms the tunnel size of sepiolite would increase, so that MCH would have more room to escape the sepiolite. With the aim of obtaining slow and controlled release of MCH molecules from sepiolite tunnels, it was hoped that by treating MCH-sepiolite samples

with an acid solution, some of the MCH could be taken out from the sepiolite. However, it was also desired that the sepiolite structure would not be destroyed by acidic treatment. It was previously found by a member of our group (Gervais, 2008) that by treating sepiolite with 0.5 M HCl, sepiolite structure is relatively unaffected; it keeps its fibrous morphology. The ^{29}Si CP/MAS spectrum of a 0.5 M HCl treated sepiolite is identical to the ^{29}Si CP/MAS spectrum of a pure sepiolite. However, the literature search indicated that treating sepiolite with a 0.5 M HCl solution for 24 hours will result in partial dissolution of both octahedral and tetrahedral sheets (Yebra-Rodriguez *et al*., 2003). A mild acid attack at boiling temperature under reflux for 1 hour is sufficient to remove most of the octahedral cations in the sepiolite; after treatment with 3 M HCl, sepiolite is completely destroyed. It was also indicated that in spite of the partial dissolution of sepiolite with mild acidic treatment, its fibrous morphology is preserved; acid penetrates into the channels all over the surface. Upon treating sepiolite with 0.5 M HCl, its surface area increased from 213 m^2/g in untreated sepiolite to 294 m^2/g (Myriam *et al*., 1998).

0.5 M HCl was used to treat MCH-sepiolite samples. All the samples were treated with 20 ml of 0.5 M HCl at room temperature on the stirring plate. The only variables that were changed were either stirring time or the MCH-sepiolite sample mass. After stirring samples were filtered, filtrates were collected, diluted and analyzed for their MCH concentrations with a UV-Vis spectrophotometer. First of all, the calibration curve was constructed:

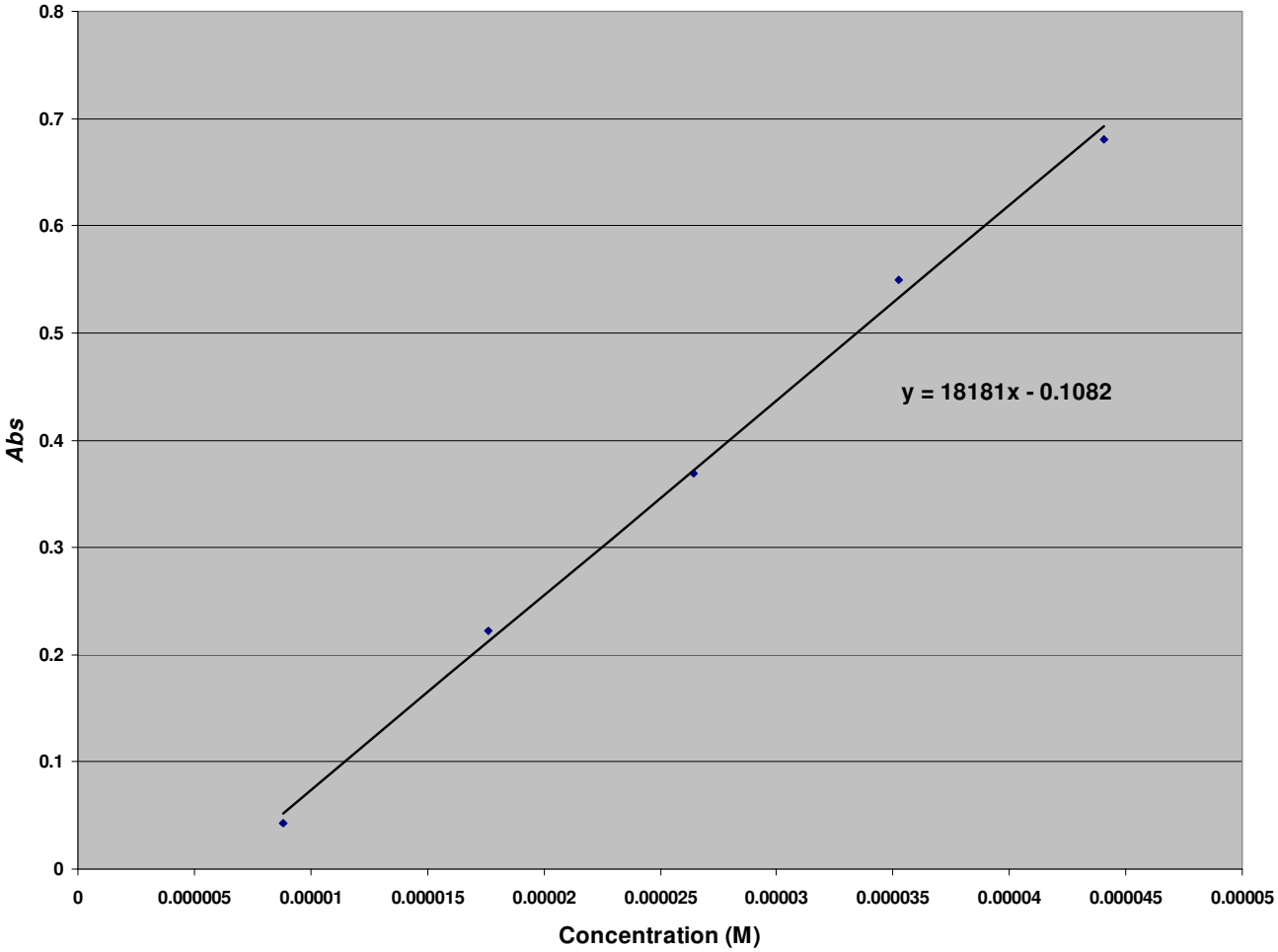

Figure 4.18 Calibration curve. MCH concentration in moles per litre versus MCH absorbance. MCH was found to absorb at 241 nanometres in the UV-Vis spectrometer.

Before really investigating how much MCH could be released by acidic treatment, it was important to find out how much MCH was absorbed into sepiolite when MCH was allowed to intercalate into preheated sepiolite in a vapour phase. This was done in various ways just to look for consistency in the results. Data obtained from TGA analysis is shown in Table 4.3.

Table 4.3 Data obtained from TGA analysis for pure sepiolite, heated sepiolite and MCH-sepiolite. Data shows the initial mass sample used for analysis, sample weight percentage that remains after analysis, weight percent that is lost during the analysis and the molecules that are lost.

	Pure Sepiolite	Heated Sepiolite	MCH-Sepiolite
Sample used for analysis (mg)	**13.1938**	**13.2774**	**12.0355**
Sample weight (%) after analysis	**78.59525**	**85.70202**	**74.68692**
Weight loss (%)	**21.40475**	**14.29798**	**25.21208**
Molecules lost	**H_2O**	**H_2O**	**H_2O & MCH**

In the pure sepiolite the total weight loss is due to the zeolitic and structural water molecules (21.40475%). In the preheated sample most of the zeolitic water is already evaporated and the total weight loss in Table 4.3 is mainly due to structural water (14.29798%): that is why it is smaller value than in pure sepiolite. Preheated sepiolite was used to intercalate MCH molecules into the sepiolite. It was hoped that MCH molecules filled all the empty tunnels of the sepiolite and the amount of water absorbed back into sepiolite was much smaller compared to pure sepiolite sample. The total weight loss in the MCH-sepiolite sample is mainly due to structural water and any MCH molecules absorbed into the sepiolite (25.21208%). To find out the weight loss due to MCH, the following calculation was done:

25.21208% - 14.29798% = 10.9141% (weight loss due to the MCH)

1.3136 mg of MCH in 12.0355 mg sample

This means that **~109.1 mg** of MCH is in a 1 g sample.

The TGA instrument has some uncertainties, like any other instrument. To verify the above 109.1 mg of MCH in 1 g of MCH-sepiolite sample, the calculation of the absorbed amount of MCH into sepiolite was done from the sepiolite parameters:

- Each tunnel is ~ 10.6 x 3.7 Å
- Micropore volume of sepiolite is 77 mm^3/g
- Need to calculate the total depth of the sepiolite tunnels in 1 gram of sepiolite

$$X\ Å \times 10.6\ Å \times 3.7\ Å = X39.22\ Å^3$$

$$(1\ Å^3 = 1.0 \times 10^{-21}\ mm^3)$$

$$77\ mm^3 = X3.922 \times 10^{-20}\ mm^3$$

$$X = 1.96328 \times 10^{21}\ Å$$

$$X = 1.96328 \times 10^{11}\ m$$

(This is the sum of all the tunnel lengths combined in 1 gram of sepiolite).

For comparison, the distance from the sun to the earth is 1.496×10^{11} m (Kuang et. al., 2003).

$$S_{Sepiolite} = (1.96328 \times 10^{11}\ m)(10.6 \times 10^{-10}\ m) = 208\ m^2$$

$$S_{MCH} = (3.8 \times 10^{-10}\ m)(8.0 \times 10^{-10}\ m) = 3.04 \times 10^{-19}\ m^2$$

$$\#\ \text{of molecules of MCH} = S_{Sepiolite} / S_{MCH} = 6.84 \times 10^{20}$$

$$\text{Moles of MCH} = (6.84 \times 10^{20}) / (6.022 \times 10^{23}\ mol^{-1}) = 0.00114\ mol$$

$$\text{Mass of MCH} = (0.00114\ mol)(110.1537\ g/mol) = 0.125\ g = 125\ mg$$

125 mg of MCH in 1.125 g of MCH-sepiolite sample.

111 mg of MCH in 1 g of MCH-sepiolite sample.

This 111 mg of MCH in 1 g of the MCH-sepiolite sample compares really well with the value obtained from the TGA data. Now that the amount of MCH in sepiolite is known, it is interesting to see how much of it can be removed with 0.5 M HCl treatment.

Table 4.4 MCH-sepiolite samples of different mass were treated with 20 ml of 0.5 M HCl for 1 hour. Samples were then filtered; filtrates were collected, diluted and analyzed for their MCH concentrations with UV-Vis spectrophotometer. *Value is calculated.

MCH-sepiolite (g)	Absorbance	MCH released (mg)
0.2035	**0.14434**	**15.3**
0.3973	**0.25330**	**21.9**
0.6009	**0.33430**	**26.8**
0.8080	**0.43488**	**32.9**
1	—	***38.4**

If 1 gram of the MCH-sepiolite was stirred for one hour in 20 ml of 0.5 M HCl solution, then about 38.4 mg of MCH would be released from 1 gram of the MCH-sepiolite sample. About 35% of the MCH that was absorbed in 1 gram of MCH-sepiolite would be released. All the absorbance values were obtained from the UV-Vis spectrophotometer and these values were then plugged into the equation of a best fit straight line in the calibration curve obtained earlier. In this way, the amount of MCH released from the MCH-sepiolite samples was calculated. MCH released in milligrams could be plotted against the MCH-sepiolite in grams used initially; this gives a straight line. From there, it was calculated what amount of MCH would be released if the MCH-sepiolite mass would have been 1 gram.

The limitation of this technique is that it is not really applicable in a real-life situation in which acid is not always present. A lot of modifications and experiments still

need to be done to investigate this matter further. The acid experiment carried out was just a preliminary route to see how acid could potentially affect MCH-sepiolite samples.

The MCH-sepiolite sample and the MCH-sepiolite sample after acidic treatment and after drying in the air were submitted for C, H, N analysis. Samples were stored in a vial prior to the analysis. This was another way to verify the amount of MCH molecules in the sepiolite before and after acidic treatment. The results obtained are given in Table 4.5.

Table 4.5 C, H, N analysis for the MCH-sepiolite and acid-treated MCH-sepiolite. Samples were not analyzed for hydrogen as there is also hydrogen in sepiolite; this would give total amount of hydrogen in MCH and sepiolite.

Sample ID	Weight (mg) entered	%N	%C	%H	%S
MCH-sep	4.343	0.00	7.81	0.00	0.00
MCH-sep(H+)	4.257	0.00	4.52	0.00	0.00

After the calculations were carried out using the data in Table 4.5, it was found that there is 102 mg of MCH in 1 gram of the MCH-sepiolite sample. A bit of a lower value compared to the TGA analysis value (109 mg) and to the value obtained from the sepiolite parameters calculations (111 mg), this could be explained by the fact that the sample was stored in a vial prior to the C, H, N analysis for about a month. So, it is possible that some of the MCH did find its way out of the sepiolite prior to the C, H, N analysis. However, all the instruments have errors, so all those values obtained from the various techniques are pretty comparable. The amount of MCH released from the sepiolite due to the acidic treatment was found to be 43.1 mg using the data in table 4.5; this is a bit higher value then the one found through the UV-Vis spectrophotometer studies (38.4 mg). But again, these values are pretty comparable taking into consideration the instrumentation errors.

A kinetics study of the MCH release from the sepiolite was another subject of interest. For that, the MCH-sepiolite samples were stirred in 20 ml of 0.5 M HCl solution for different amounts of time, then filtrates were collected, diluted and analyzed for their MCH concentrations with a UV-Vis spectrophotometer. The set of experiments carried out is shown in Table 4.6.

Table 4.6 MCH-sepiolite samples were treated with 20 ml of 0.5 M HCl for different lengths of time. Samples were then filtered; filtrates were collected, diluted and analyzed for their MCH concentrations with UV-Vis spectrophotometer.

MCH-sepiolite sample stirring time in acid solution (min)	MCH-sepiolite (g)	Absorbance	MCH released (mg)
15	**0.2024**	**0.11316**	**13.4**
30	**0.2028**	**0.12114**	**13.9**
45	**0.2032**	**0.14834**	**15.5**
60	**0.2028**	**0.11913**	**13.8**
75	**0.2046**	**0.14899**	**15.6**
90	**0.2048**	**0.12485**	**14.1**
105	**0.2050**	**0.12353**	**14.0**
120	**0.2039**	**0.11180**	**13.3**
180	**0.2057**	**0.10834**	**13.1**

It could be concluded from the last column of Table 4.6 that the release of MCH from sepiolite is really independent of the length of time used to stir the MCH-sepiolite samples in 20 ml of 0.5 M HCl solution. The amount of MCH that was obtained from the sepiolite with the acidic treatment of MCH-sepiolite samples that were around 0.2 grams varies between 13.1 – 15.6 mg.

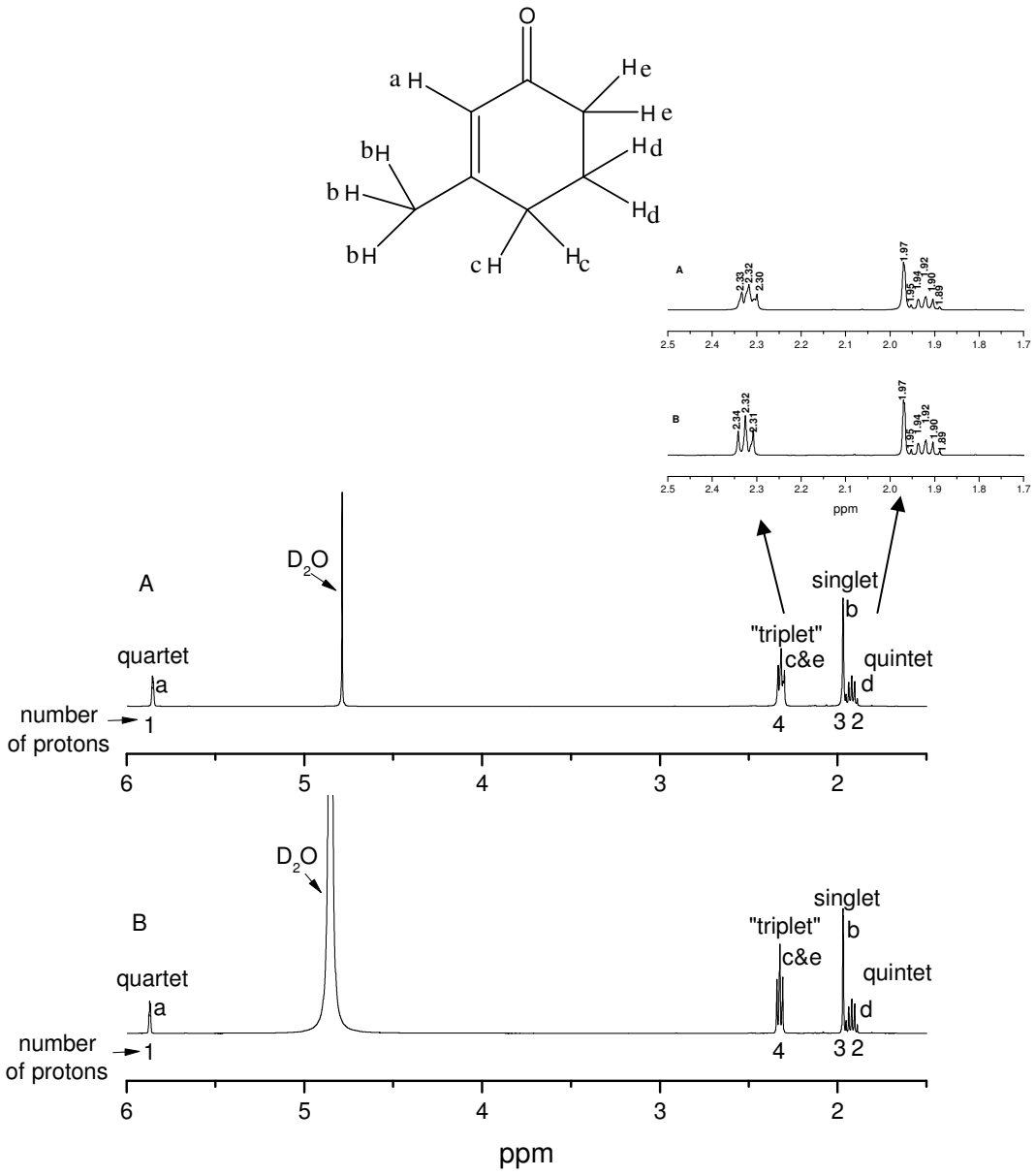

Figure 4.19 ^{1}H NMR for (A) 3-methyl cyclohexen-1-one (MCH) and for (B) MCH in 0.5 M HCl solution. D_2O was used as NMR solvent.

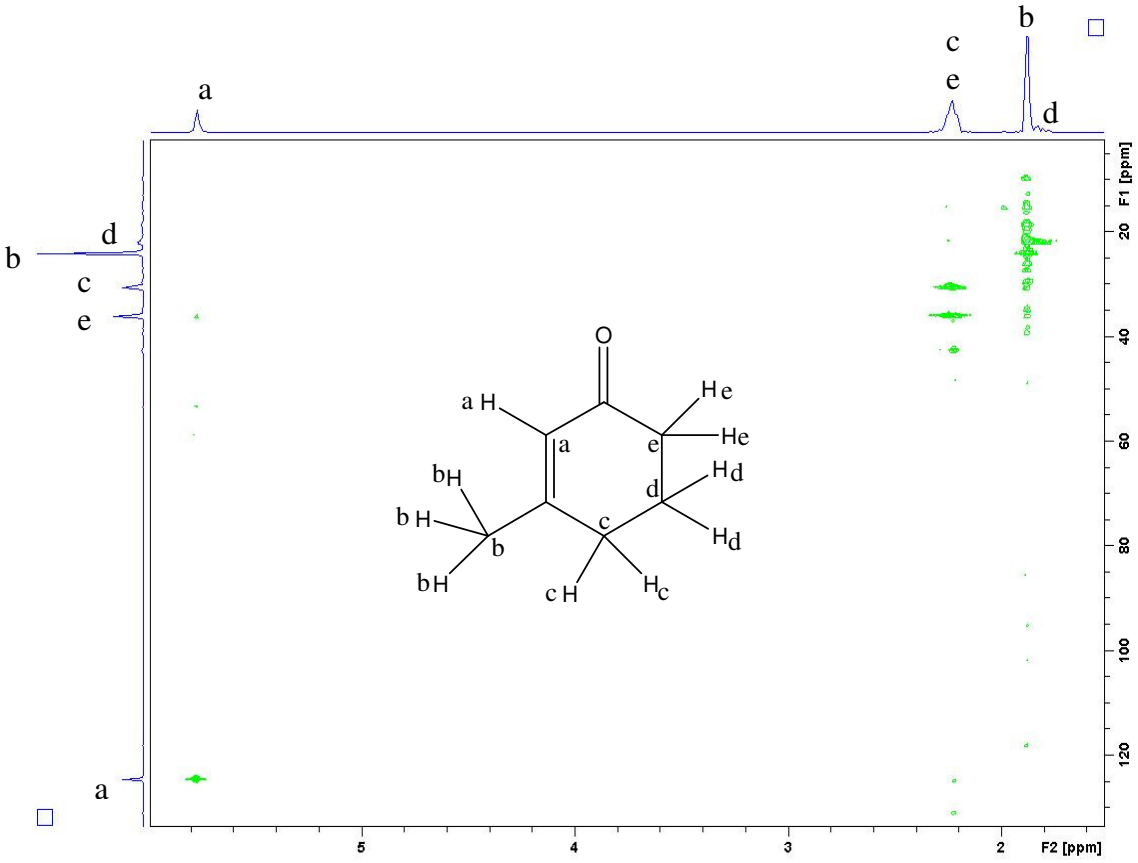

Figure 4.20 HETCOR spectrum for 3-methyl cyclohexen-1-one (MCH).

To see if 0.5 M HCl changes the structure of the MCH molecule, ^{1}H NMR was performed on pure MCH and MCH in a 0.5 M HCl solution; the NMR solvent in both cases was D_2O. The NMR spectra for those two are shown in Figure 4.19. MCH has 5 unique hydrogens, which are marked as H_a, H_b, H_c, H_d and H_e in Figure 4.19. There is one H_a hydrogen; it couples to three H_b hydrogens and appears as a quartet peak at about 5.87 ppm. Three H_b hydrogens do not couple to anything; they appear as a singlet peak at 1.97 ppm. H_d hydrogens couple to two H_c and two H_e hydrogens, and give a quintet signal at about 1.92 ppm. H_c and H_e hydrogens both couple to two H_d hydrogens and each of them should appear as a triplet signal. Instead, H_c and H_e both occur at the same ppm value of 2.32 and give one triplet signal. A similar spectrum was obtained for MCH in acidic solution, which means that the 0.5 M HCl solution does not alter the original structure of MCH.

Proton and carbon atoms interact in two very important ways. First, they both have magnetic properties, and they can induce relaxation in one another. Second, the two types of nuclei can be spin-coupled to each other. This latter interaction can be very useful, since directly bonded protons and carbons have a coupling constant value that is at least a power of 10 larger than nuclei related by two-bond or three-bond couplings. This marked distinction between orders of couplings provides with a sensitive way of identifying carbons and protons that are directly bonded to one another.

The correlation between carbons and attached protons is given in two-dimensional axis by HETCOR experiment. The chemical shifts of the ^{13}C atoms are plotted along one axis ant the chemical shifts of the protons along the other axis. A spot of intensity in this type of two-dimensional spectrum would indicate the existence of a C-H bond.

To investigate H_c and H_e hydrogens, a HETCOR spectrum was performed and is shown in Figure 4.20. The correlation between unique hydrogens and unique carbons is indicated with alphabetical letters (a-e) in Figure 4.20. Hydrogens H_c and H_e, though, appear at the same ppm value on the ^{1}H NMR, each has its own carbon location on the ^{13}C NMR spectrum. Carbon for H_e hydrogens appears at 36.0 ppm on the ^{13}C NMR spectrum. Carbon for H_c hydrogens appears at 30.5 ppm on the ^{13}C NMR spectrum. Carbon for H_b hydrogens appears at 24.0 ppm on the ^{13}C NMR spectrum. Carbon for H_d hydrogens appears at 21.9 ppm on the ^{13}C NMR spectrum. And carbon for H_a hydrogen appears at 124.6 ppm on the ^{13}C NMR spectrum.

Conclusion

This chapter investigated the possibilities of obtaining the slow and controlled release of MCH from the sepiolite tunnels. First of all, co-intercalations of the MCH molecule with organic solvents were performed. The ^{13}C MAS NMR showed that at room temperature there are two different MCH molecules: one MCH inside the tunnels and the other one outside the tunnels of the sepiolite. After heating nanohybrid materials at 60˚C for 20 hours, ^{13}C MAS NMR showed only the MCH molecules that are inside the tunnels. Further heating of nanohybrid materials at 120˚C for 20 hours showed that methanol, ethanol or acetone peaks are greatly reduced on the ^{13}C MAS NMR spectrum; however, the benzene peak was not reduced. MCH molecules were observed to be in the tunnels of sepiolite even after prolonged heating of nanohybrid materials. The slow

release of MCH molecules from the sepiolite tunnels has not been obtained with co-intercalation with organic molecules and heating.

Acidic treatment of MCH-sepiolite samples was also performed to see how the weak acid treatment affects the release of MCH from the sepiolite. When 1 gram of the MCH-sepiolite sample was stirred with 20 ml of 0.5 M HCl at room temperature, about 35% of intercalated MCH was removed from the sepiolite. However, more studies need to be done in this area to obtain the controlled release of MCH. Also, more studies need to be done to see how this could be applied in real-life situation in which acid is not always present.

References

Albunia, A.R., Graf, R., Guerra, G. and Spiess, H.W. (2005) ^{2}H NMR study of aromatic guest dynamics in clathrate phases of syndiotactic polystyrene macromol. *Chem. Phys.*, **206**, 715-724.

Boden, N., Clark, L.D., Hanlon, S.M. and Mortimer, M. (1978) Deuterium nuclear magnetic resonance spin echo spectroscopy in molecular crystals. *Faraday Symposia*, **13**, 109-123.

Eckman, R.R. and Vega, A.J. (1986) Deuterium Solid-State NMR Study of the Dynamics of Molecules Sorbed by Zeolites. *J. Phys. Chem.*, ***90***(19), 4679-4683.

Facey, G.A., Kuang, W. and Detellier, C. (2005) Multinuclear Spectroscopy studies of the structuration of the tunnels of sepiolite in the presence of intracrystalline pyridine molecules. *J. of Phys. Chem.*, **109**, 22359-22365.

Facey, G.A., Ratcliffe, C.I. and Ripmeester, J.A. (1995) Solid state NMR studies of the molecular motion of pyridine in its tri-o-thymotide clathrate. *J. Phys. Chem.*, **99**, 12249-12256.

Gervais, F. (2008) Functionalization of sepiolite fibres. *Honours Thesis: research supervisor: Dr. Christian Detellier.* 29 pp.

Kuang, W., Facey, G.A., Detellier, C., Casal, B., Serratosa, J.M. and Ruiz-Hitzky, E. (2003) Nanostructured hybrid materials formed by sequestration of pyridine molecules in the tunnels of sepiolite. *Chemistry of Materials*, **15**(26), 4956-4967.

Myriam M., Suarez, M. and Martin-Pozas, J.M. (1998) Structural and textural modifications of palygorskite and sepiolite under acid treatment. *Clays and Clay Minerals*, **46**, 225-231.

Nishikiori, S., Ratcliffe, C.I. and Ripmeester, J.A. (1991) Solid-state ^{2}H and ^{1}H NMR of guest and host motions in the Hofmann-type and related benzene clathrates. *The Journal of Physical Chemistry*, **95**(4), 1589-1596.

Ross, D.W., Gibson, K.E., Their, R.W. and Munson, S.A. (1996) Optimal Dose of an Anti-aggregation Pheromone (3-Methylcyclohex-2-en-1-one) for Protecting Live Douglas-Fir from Attack by Dendroctonus pseudotsugae (Coleopera: Scolytidae). *Journal of Economic Entomology*, **89**(5), 1204-1207.

Trezza, E. and Grassi, A. (2002) Dynamics of Aromatic Molecules Clathrated in Crystalline Syndiotactic Polystyrene: A Solid State ^{2}H NMR Investigation of the Host/Guest Complexes. *Macromol. Rapid Commun.*, **23**(4), 260-263.

Weir, M.R., Rutinduka, E., Detellier, C., Feng, C.Y., Wang, Q., Matsuura, T. and Le Van Mao, R. (2001) Fabrication, characterization and preliminary testing of all-inorganic ultrafiltration membranes composed entirely of a naturally occurring sepiolite clay mineral. *Journal of Membrane Sci.*, **182**, 41-50.

Wyatt, T.D. (2003) Pheromones and animal behaviour: communication by smell and taste. Cambridge University Press, New York, 391 pp.

Yebra-Rodrígues, A., Martín-Ramos, J.D., del Rey, F., Viseras, C. and López-Galindo, A. (2003) Effect of acid treatment on the structure of sepiolite. *Clay Minerals*, **38**, 353-360.

Chapter 5

Structural studies of synthetic Maya-Blue

Introduction

The Maya Civilization is the general name that archaeologists have given to several loosely affiliated, independent city states that shared a cultural heritage. This civilization was especially noted for the only known fully developed written language of the pre-Columbian Americas, as well as for its architecture, art, astronomical and mathematical systems. Initially established during the Pre-Classic period (c. 2000 BC to 250 AD), according to Mesoamerican chronology, many Maya cities reached their highest state of development during the Classic period (c. 250 AD to 900 AD) and continued throughout the Post-Classic period until the arrival of the Spanish. The Maya Civilization occupied the Central American continent, including the southern Yucatan peninsula of Mexico and what are now Guatemala, Belize, Honduras and El Salvador, an approximate area of 150 000 square miles.

Among many technological wonders from that era is a pigment known as Maya Blue. This very unusual, turquoise-like colour was used extensively by the Maya for many purposes. The Maya used the pigment for paint that was applied to wall murals, sculpture and pottery, among other objects. They also used the pigment to colour the bodies of sacrificial victims before they were thrown into sacred wells or had their hearts cut out at the temple altars (Price and Burton, 2010).

The pigment is a mixture of organic and inorganic compounds bonded by hydrogen that, in addition to its very impressive colour, has exceptional durability. The colour still remains on a variety of Mayan artifacts and architecture to this day. It is resistant to natural acids, alkalis, solvents, heat and vegetation. Maya Blue is resistant to

colour loss after centuries in the tropical rainforest of the Maya heartland (Price and Burton, 2010).

The existence of the pigment was first discovered by Merwin (1931). Gettens and Stout (1946) were the first ones who employed the term "Mayan Blue," which was subsequently renamed "Maya Blue." Palygorskite and sepiolite were identified as the predominant chemical constituents of Maya Blue (Gettens, 1962). Initially, it was hypothesized by Gettens (1962) that the pigment was purely of an inorganic nature, composed just of a blue palygorskite mineral. However, Shepard (1962) then introduced the idea of Maya Blue being a complex consisting of an inorganic carrier and an organic dye. There is no existing record of the original method of Maya Blue preparation. Van Olphen (1966) was the first to synthesize a complex analogous to Maya Blue. He wrote that there are two ways of preparing a complex of attapulgite (palygorskite) and indigo: (1) by heating palygorskite and indigo, then remove any excess indigo by an acetone wash; (2) by reducing indigo with a solution of $Na_2S_2O_4$, bring palygorskite into contact with this solution and exposing them to air; heating is still a necessary final step to achieve acid stability. In a comparative study by Kleber *et al.* (1967), it was found that the Fourier transform infrared (FTIR) and powder X-ray diffraction (PXRD) spectra of the synthetic palygorskite-indigo complex were roughly equivalent to the corresponding spectra obtained from authentic Maya Blue samples (Hubbard *et al*., 2003).

The principal constituents of Maya Blue are palygorskite and sepiolite. It is proposed that the pigment is an adsorption complex of palygorskite and natural indigo (Van Olphen, 1966). Historically, indigo was extracted from plants. Nearly all indigo produced nowadays (several thousand tons per year) is synthetic. Indigo (or indigotin,

3*H*-indol-3-one, 2-(1,3-dihydro-3-oxo-2H-indol-2-ylidene)-1,2-dihydro), is constituted by quasi-planar molecules with approximate dimensions of 4.8 x 12 Å (Sánchez del Rio *et al*., 2005). Indigo, with the chemical formula $C_{16}H_{10}N_2O_2$ (Figure 5.1), has a slightly elongated central C=C bond and an elongated C=O bond.

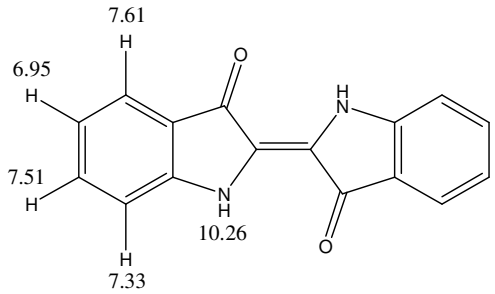

Figure 5.1 Structure of indigo. This figure also shows ^{1}H NMR chemical shifts in ppm for the unique hydrogens of the indigo molecule. Chemical shifts were obtained from McClay *et al.* (2005).

Hydrogen attractions between adjacent molecules cause structural bending of the molecule, as well as solid-state aggregation in which one indigo molecule is linked to four others (Hubbard *et al*., 2003). The aggregates are durable and it was noted that diminished intermolecular attractions between neighbouring indigo molecules remain even in the vapour phase (Gordon and Gregory, 1983).

There is much confusion with regard to understanding the structure of synthetic Maya Blue. The characterization and comparison of pure and synthetic Maya Blue, as well as the structure of synthetic indigo-palygorskite and indigo-sepiolite complexes, are being questioned (Raya *et al*., 2010). It has been proposed that the complex is situated at the surface of the fibres and at the entrance of tunnels (Hubbard *et al*., 2003), (Sanchez *et al*., 2009), inside the external channels exclusively (Chiari *et al*., 2008), or inside both internal and external channels (Fois *et al*., 2003), (Giustetto *et al*., 2005), (Giustetto *et al*., 2006). Thus, the interactions between indigo and both palygorskite and sepiolite are not

clearly known. Interactions of indigo carbonyl groups with water coordinated to magnesium (H-bond) (Giustetto *et al*., 2005), (Giustetto *et al*., 2006), (Polette *et al*., 2002), (Chiari *et al*., 2003) or directly with clay structural octahedral cations (magnesium or aluminum) were suggested (Tilocca and Fois, 2009*)*. Direct bonding between indigo carbonyl and Al^{3+} replacing Si in the surface tetrahedral lattice was also described (Polette-Niewold *et al*., 2007), (Chianelli *et al*., 2005), (Fuentes *et al*., 2008). Interactions of both indigo carbonyl and amino groups with palygorskite edge silanol groups (H-bond) (Hubbard *et al*., 2003), (Sanchez del Rio *et al*., 2009) were proposed. Even van der Waals interactions between indigo and Si tetrahedral site (Fois *et al*., 2003), and change in the indigo planarity were also considered (Polette-Niewold *et al*., 2007), (Witke *et al*., 2003).

The fibrous structures of palygorskite and sepiolite may be destroyed through extended treatment with strong acid. Sepiolite is especially sensitive to strong acid due to its high magnesium component and the large size of its structural micropores (Myriam *et al.*, 1998). Indigo by itself is also not stable, for example, when treated with nitric acid or acetone. When pure indigo or an unheated heterogeneous mixture of palygorskite and indigo is immersed in a concentrated solution of nitric acid, the dye is very quickly transformed into a yellow-red water-soluble indigoid derivative, isatin (van Olphen, 1966), (Hubbard *et al*., 2003). However, the indigo present in heated palygorskite-indigo complexes does not react with nitric acid. The secret in obtaining stable indigo-clay complexes is that indigo-clay samples must be heated. A heated sepiolite-indigo sample prepared by our group was found to be stable to organic solvents (acetone, chloroform,

methanol), acids (hydrochloric acid, sulphuric acid, nitric acid) and bases (sodium hydroxide, potassium hydroxide).

It was also interesting to find out whether other types of clay minerals could form comparable stable complexes with indigo the way palygorskite and sepiolite can. Van Olphen prepared indigo samples with kaolinite, nontronite, Wyoming bentonite (all clays with plate like structures) and mordenite (a zeolite with a cage-type structure); our group also prepared samples with montmorillonite, silica and sand. All of these complexes did not show any resistance to nitric acid before or after heating. So, it seems like a channel structure (palygorskite or sepiolite) is essential to achieve acid stability in clay-indigo complexes.

In this work, the preparation and properties of sepiolite-indigo complexes were studied. The characterization of this complex was done through TGA, DTA (derivative thermogravimetric analysis), DTG and solid-state multinuclear magnetic resonance. Textural analysis of sepiolite-indigo adducts was also performed, yielding quantitative data on the internal micropores of the samples. The results seem to indicate the presence of a strong interaction between indigo molecules and the surface bordering the clay mineral nanotunnels.

Experimental

Materials

Crude sepiolite was obtained from the University of Missouri's Source Clay Mineral Repository. It was then purified according to already established procedures

involving crushing, centrifuging and weak acid treatment to eliminate carbonates (Weir *et al*., 2001). Synthetic indigo (2-(1,3-dihydro-3-oxo-2H-indol-2-ylid-ene)-1,2- dihydro-3H-indol-3-one; ~95%) was obtained from the Aldrich Chemical Company and used as received.

Preparation of the indigo adducts

Sepiolite-indigo complexes were prepared using a procedure adapted from one of van Olphen's experiments (van Olphen, 1966). Synthetic indigo was mixed in a mortar and pestle with a fixed proportion of purified sepiolite. Using a pestle, the heterogeneous mixture was crushed vigorously for several minutes at room temperature until it became a fine, consistent, light blue powder. Fractions of the mixture were removed and analyzed using several spectroscopic techniques. The powder was then transferred into a ceramic crucible and heated by means of a Thermoline 48000 furnace at 120ºC for 20 hours. Samples were heated for 20 hours to ensure complete reaction of the dye with the clay mineral. A separate sample was prepared in which sepiolite was preheated at 120ºC for 20 hours and then crushed with indigo.

Similar sample preparation was also done in the air-free environment, where samples were heated under vacuum in the vacuum line, and crushed or packed into the NMR rotor in the vacuum bag under nitrogen gas.

Thermal analysis

The TGA, DTA and DTG analyses were performed using a SDT 2960 Simultaneous DSC-TGA instrument. Approximately 12 mg of sample was placed in the

instrument's platinum crucible. The furnace chamber was flooded with helium gas throughout the analysis operation. Although several different heating strategies were used to analyze samples, a uniform ramp rate of 10ºC/min was used.

Textural analysis

BET surface area and micropore measurements were taken using a Micromeritics ASAP-2010 instrument, with N_2 being used as an adsorbent gas at 77K. Samples were degassed according to thermal gravimetric results (120˚C) to eliminate surface and zeolitic water; degassing was done at 10^{-2} Torr. The molecular cross-section of nitrogen used in the data analysis was 0.1620 nm^2. T-plot measurements were made using a standard thickness range of 3.5-5 Å.

Multinuclear magnetic resonance

Cross-polarization magic-angle spinning nuclear magnetic resonance (CP/MAS-NMR) characterization was performed on sepiolite-indigo adducts. Samples were analyzed on a Bruker AVANCE 200 spectrometer. ^{29}Si spectra were acquired at 39.75 MHz, whereas ^{13}C spectra were acquired at 50.31 MHz. A ramped CP pulse was used in all ^{29}Si and ^{13}C cross-polarization experiments. Recycle delay time was set to 2 seconds, and the proton 90° pulse was 4.25 μs for ^{29}Si and 4 μs for ^{13}C. The contact time to allow magnetization transfer between proton and ^{13}C nuclei was 2 ms, whereas for ^{29}Si it was 10 ms. Spinning rates were 4.5 kHz and 4.0 kHz for ^{13}C nuclei and ^{29}Si nuclei, respectively. The ^{29}Si NMR signals were externally referenced to the $-Si(CH_3)_3$ group, the resonance of Tetrakis(trimethylsilyl)silane at -9.9 ppm, corresponding to

tetramethylsilane (TMS) at 0ppm. ^{13}C signals were externally referenced to the high frequency signal of glycine at 176.41 ppm.

Results and discussion

Sepiolite-indigo samples were prepared and studied in the hope of better understanding the mysterious structure of Maya Blue. Samples prepared were as follows: Sample 1 (crushed sepiolite-indigo [2 wt.% indigo]), Sample 2 (Sample 1 heated at 120°C for 20 hours) and Sample 3 (preheated sepiolite crushed with indigo [2 wt.% indigo]). First of all, micropore analysis of sepiolite-indigo samples was looked at; all the data is presented in Table 5.1 below.

Table 5.1 Micropore analysis of sepiolite-indigo samples. Sample 1 (crushed sepiolite-indigo [2 wt.% indigo]), Sample 2 (Sample 1 heated at 120°C for 20 hours) and Sample 3 (preheated sepiolite crushed with indigo [2 wt.% indigo]).

Sample description	T-plot		Horvath-Kawazoe	
	Micropore area (m^2/g)	Micropore volume (mm^3/g)	Maximum pore volume (mm^3/g)	Median pore diameter (Å)
Unheated pure sepiolite	163	84	141	6.3
Pure sepiolite heated at 120°C for 20 hours	158	80	132	6.3
Sample 1	129	56	111	7.3
Sample 2	109	48	106	7.5
Sample 3	75	34	92	7.9

Note that the microporous structure of sepiolite is preserved upon heating to 120ºC. The micropore area before heating was recorded as 163 m^2/g; the area after heating was 158 m^2/g (Table 5.1). However, it is also important to point out that prior to running microporosity experiments all the samples are degassed on the porosimeter

instrument as part of the procedure. Most of the zeolitic water would be expected to be degassed out at this step. So, in principle, samples of pure and heated sepiolite would be expected to have similar results (which they do). It is apparent that when sepiolite is crushed with indigo a significant decline in microporosity results. The micropore area decreased from 163 m^2/g in the pure sepiolite sample to 129 m^2/g in the unheated, crushed, sepiolite-indigo sample. Also, while the heated sepiolite sample was observed to have a micropore area of 158 m^2/g, the thermally treated sepiolite-indigo complex was shown to have microporosity of 109 m^2/g. The sample in which preheated sepiolite was crushed with indigo proved to have the smallest value for microporosity: 75 m^2/g. Consequently, the micropore volume of unheated sepiolite (84 mm^3/g) was larger than that of the unheated sepiolite-indigo complex (56 mm^3/g); the volume of the thermally treated samples decreased from 80 mm^3/g to 48 mm^3/g when indigo was present. Again, the sample in which preheated sepiolite was crushed with indigo proved to have the smallest value for micropore volume: 34 mm^3/g (Table 5.1). Similar trends were observed in a Horvath-Kawazoe (HK) analysis for cumulative pore volume (Table 5.1). The HK showed median pore diameters in the range of 6.3 – 7.9 Å for the five sepiolite-based (unheated sepiolite, heated sepiolite, unheated sepiolite-indigo, heated sepiolite-indigo and preheated sepiolite crushed with indigo) samples. These values are consistent with the theoretical dimensions of the rectangular tunnels found in the clay mineral (Jones and Galán, 1998). The data in Table 5.1 offer strong evidence that the micropores of sepiolite are partially blocked upon formation of the sepiolite-indigo adduct. Also, it seems like the sepiolite pores that remain accessible after interaction with indigo keep their primary structure.

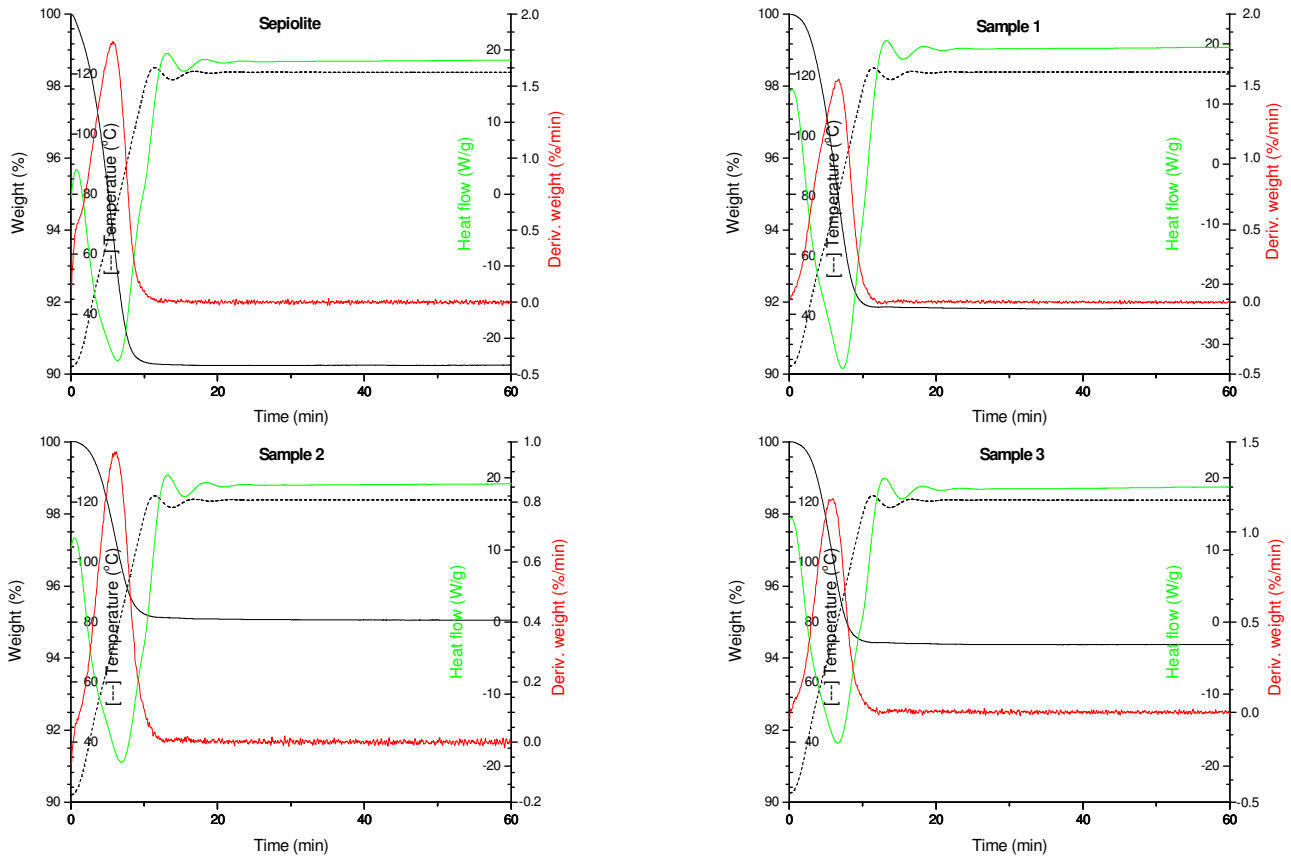

Figure 5.2 Thermal analyses (TGA, DTG, DTA) of pure sepiolite: Sample 1 (crushed sepiolite-indigo [2 wt.% indigo]), Sample 2 (Sample 1 heated at 120°C for 20 hours) and Sample 3 (preheated sepiolite crushed with indigo [2 wt.% indigo]). All samples were ramped to 120°C and heated at this temperature for 2 hours (only the first hour is shown); the temperature curve is illustrated with a broken line.

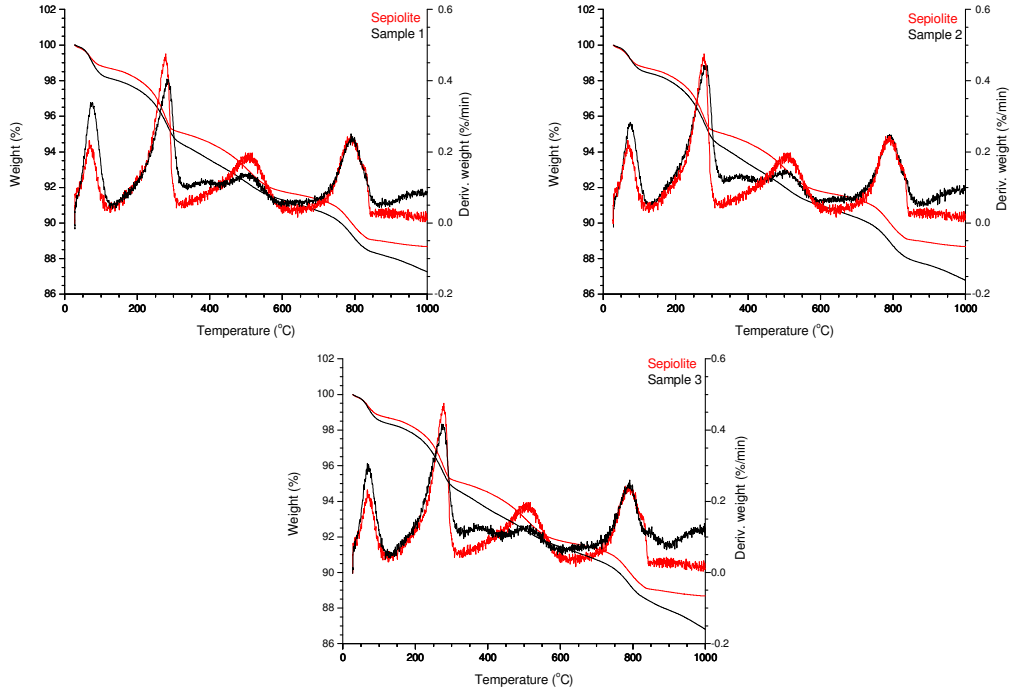

Figure 5.3 Thermal comparison (TGA, DTG) between Sample 1 (crushed sepiolite-indigo [2 wt.% indigo]), Sample 2 (Sample 1 heated at 120°C for 20 hours) or Sample 3 (preheated sepiolite crushed with indigo [2 wt.% indigo]) and pure sepiolite, both preheated at 120°C for 2 hours and cooled to room temperature under air flow prior to analysis.

It is known that the structural stability of sepiolite-indigo adducts is very dependent on heating, so it was interesting to see a TGA study of these adducts. In the first series of thermal experiments, sepiolite and sepiolite-indigo samples (2 wt.% indigo) were ramped to 120ºC and maintained at this temperature for 2 hours. The findings of this investigation are described in Figure 5.2. In the DTG curve, the weight loss is apparent during the thermal escalation to the plateau temperature. The weight loss of ~9.7% in sepiolite, ~8.1% in Sample 1 (crushed sepiolite-indigo [2 wt.% indigo]), ~4.9% in sample 2 (Sample 1 heated at 120°C for 20 hours) and ~5.6% in Sample 3 (preheated sepiolite crushed with indigo [2 wt.% indigo]) is attributed to the loss of externally bound and zeolitic water. Endothermic peaks on the DTA plots confirm this water loss. When the plateau temperature was reached after 15 min, no further major mass loss was observed. It may be assumed that all of the loosely bound water was lost at this point.

After the first series of thermal experiments, the four described samples were cooled under air to room temperature over a period of 1 hour. A standard TGA analysis to 1000ºC was then performed on the same samples using Ne gas. The results of these experiments are shown in Figure 5.3. In all four cases, four major weight loss stages may be seen on the TGA and DTG curves. For sepiolite, the first weight loss of 1.2% occurs from room temperature to 100ºC and is attributed to loosely bound water; the second loss, of 3.5 wt.%, occurs between 100 and 300ºC and represents the first structural water. This is followed by a loss of 3.4% in the 300-600ºC ranges, corresponding to the loss of the second structural water, and a loss of ~2.8% in the high temperature region (600-900ºC) caused by dehydroxylation of the edge silanol and the structural Mg-OH groups. The TGA and DTG of the sepiolite-indigo complexes are nearly identical, with the exception

of an additional peak at ~360ºC. This peak is identified as the indigo peak due to the comparison with the TGA curve of pure synthetic indigo, which showed a weight loss of ~80% occurring at ~360ºC due to decomposition. It could be concluded from the TGA and DTG results that the overall structure of sepiolite is maintained after heating in the presence of the indigo molecule. It is also important to mention that the decomposition temperature of indigo in the complexes was nearly identical to that of the pure synthetic compound.

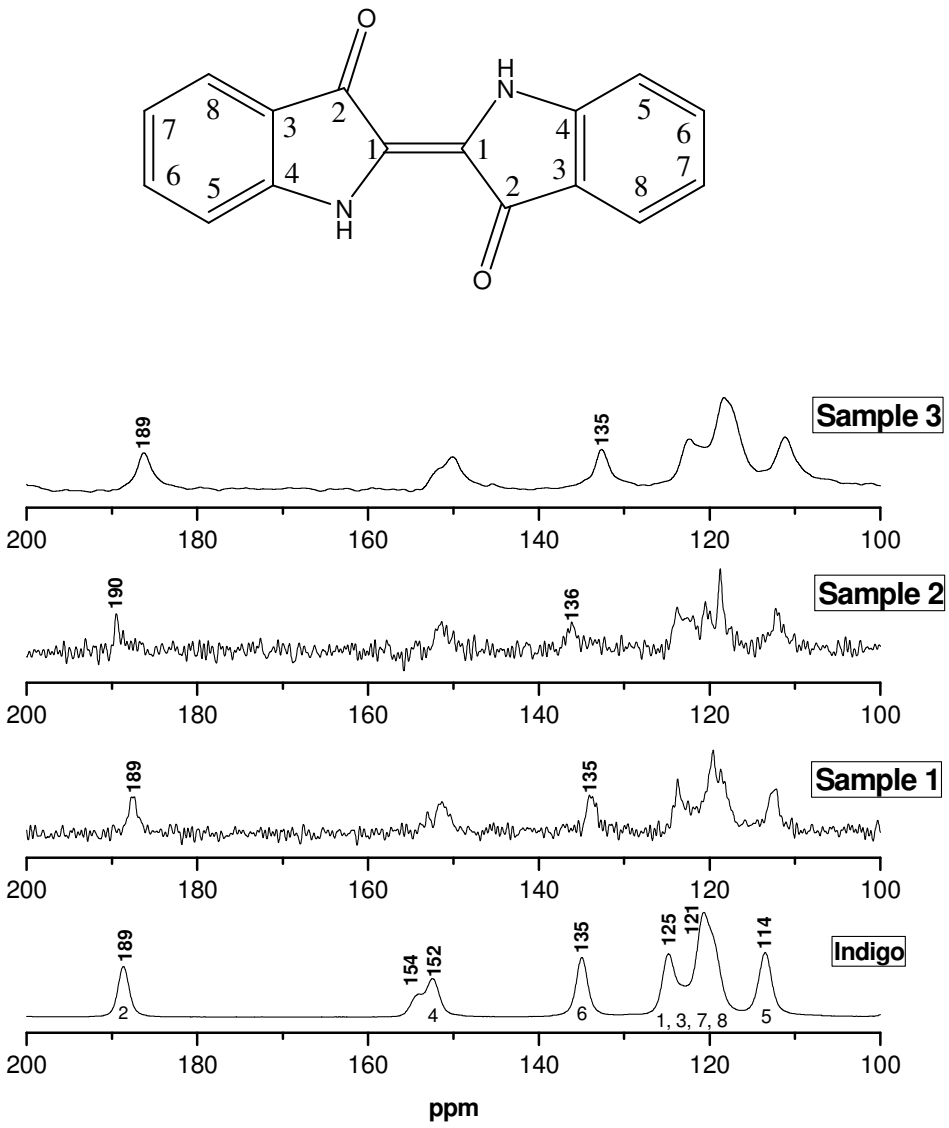

Figure 5.4 ^{13}C CP/MAS NMR spectra of synthetic indigo: Sample 1 (crushed sepiolite-indigo [2 wt.% indigo]), Sample 2 (Sample 1 heated at 120°C for 20 hours) and Sample 3 (preheated sepiolite crushed with indigo [2 wt.% indigo]).

Figure 5.4 displays the ^{13}C CP/MAS NMR spectrum of indigo: Sample 1 (crushed sepiolite-indigo [2 wt.% indigo]), Sample 2 (Sample 1 heated at 120°C for 20 hours) and Sample 3 (preheated sepiolite crushed with indigo [2 wt.% indigo]). The broadness of the peaks of synthetic indigo may be explained by the presence of multiple crystallographic sites for each carbon in the indigo molecule (Gribova, 1955). Molecular variance such as this arises due to strong intermolecular associations and aggregation between neighbouring indigo molecules (Hubbard *et al*., 2003). From the spectrum of Sample 1 (crushed sepiolite-indigo [2 wt.% indigo]), it could be noticed that peaks in the region between 115 – 130 ppm are a bit more resolved compared to pure synthetic indigo. Otherwise, the spectrum for Sample 1 looks pretty much identical to the spectrum of synthetic indigo. There are a couple of changes that could be seen in the spectrum for Sample 2 (Sample 1 heated at 120°C for 20 hours). The first change is that peaks in the region between 115 – 130 ppm are even more resolved compared to Sample 1; this spectrum is the closest in showing 8 unique carbons of the indigo molecule. The second change is that peaks for C_2 and C_6 are a bit (~1 ppm) shifted compared to pure synthetic indigo or Sample 1; this is a very small shift compared to, for example, an excess of 10 ppm shift (for carbonyl carbon) upon incorporation of acetone molecules into the nanotunnels of sepiolite (Kuang *et al*., 2002). The shift is an indication, however, that the same changes are occurring in the indigo molecule upon heating it with sepiolite. Two species of indigo may be distinguished in Figure 5.4, one being unaffected pure indigo and the other representing an altered state of the indigo molecules (Hubbard *et al*., 2003). The spectrum for Sample 3 (preheated sepiolite crushed with indigo [2 wt.% indigo]) is

identical to pure synthetic indigo, which indicates that heating must occur after crushing sepiolite and indigo - not before - to achieve stable structure of sepiolite-indigo adduct.

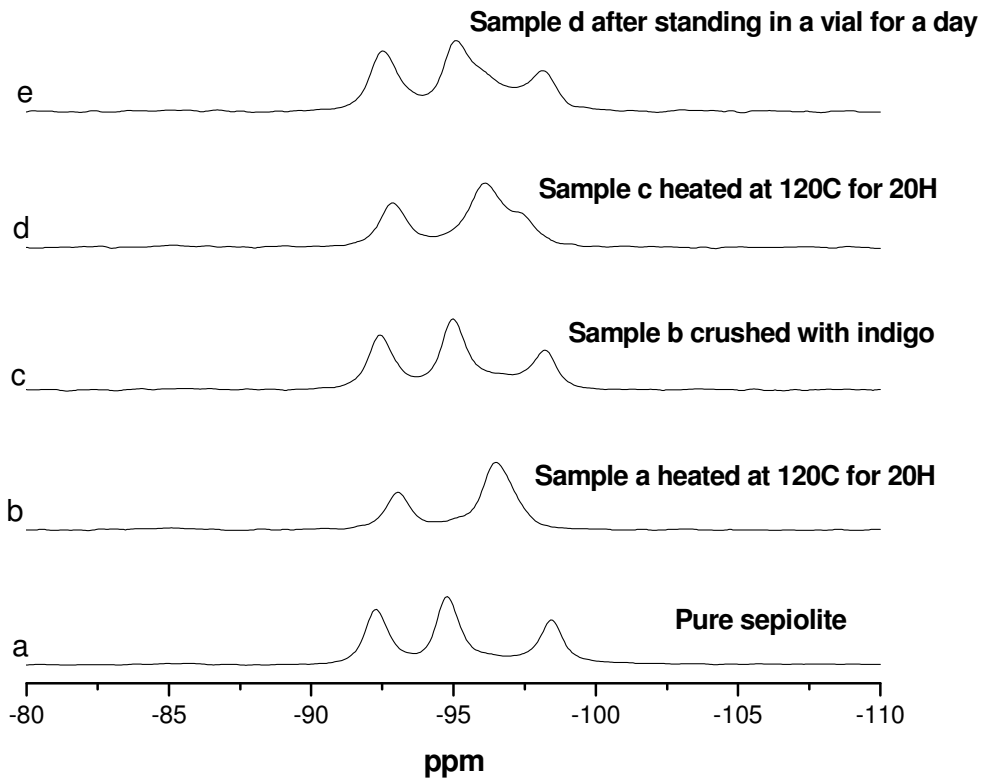

Figure 5.5 ^{29}Si CP/MAS NMR for (a) pure sepiolite, (b) sample (a) heated at 120°C for 20 hours, (c) sample (b) crushed with indigo (2 wt.% indigo), (d) sample (c) heated at 120°C for 20 hours and (e) sample (d) after standing in a vial for a day.

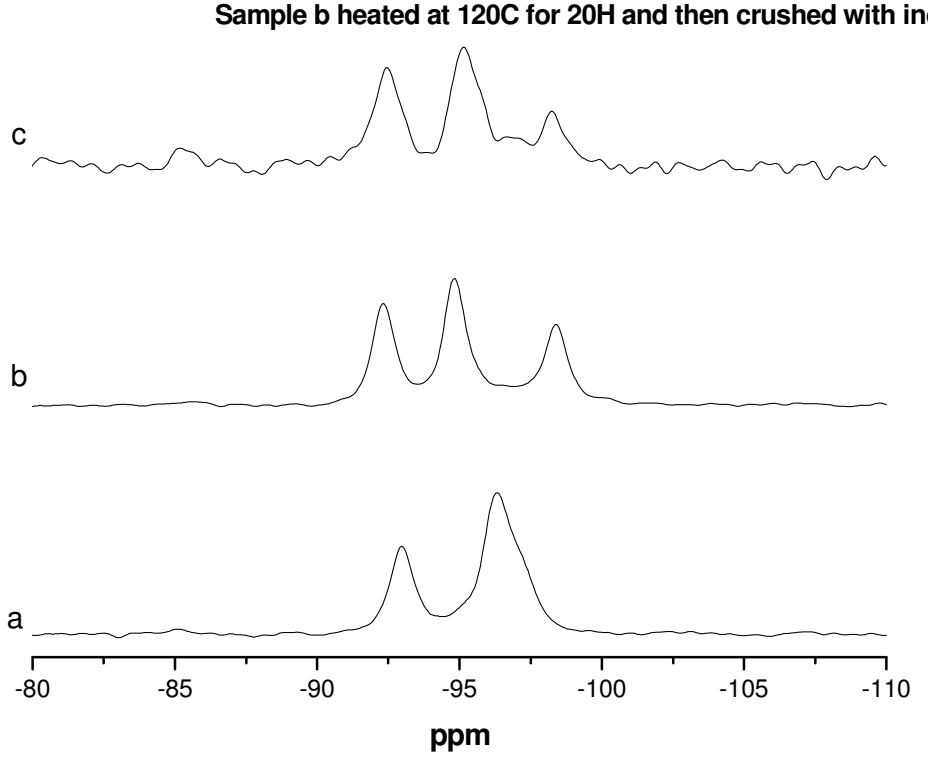

Figure 5.6 ^{29}Si CP/MAS NMR for (a) heated sepiolite at 120°C for 20 hours, (b) sample (a) after standing in open air for an hour and (c) sample (b) heated at 120°C for 20 hours and then crushed with indigo (2 wt.% indigo).

^{29}Si CP/MAS NMR studies were performed to better understand the interaction between sepiolite and indigo molecules. The results for those studies are shown in Figures 5.5 and 5.6. Figure 5.5 shows the following ^{29}Si CP/MAS NMR spectra: (a) pure sepiolite, (b) sample (a) heated at 120°C for 20 hours, (c) sample (b) crushed with indigo (2 wt.% indigo), (d) sample (c) heated at 120°C for 20 hours and (e) sample (d) after standing in a vial for a day. The pure sepiolite spectrum (Figure 5.5a) gives three characteristic Q^3 silicone signals, as expected. Pure sepiolite is filled with zeolitic water; this is the natural state of the sepiolite clay. In the heated sepiolite sample (Figure 5.5b), the ^{29}Si CP/ MAS NMR signals of the centre and the edge Si nuclei coincide at -97.0 ppm. The near-edge Si is represented by a chemical shift at -93.7 ppm. These two peaks are characteristic of the sepiolite that has its tunnels empty: dehydrated sepiolite. Once this heated sepiolite was crushed with indigo in the air environment, the ^{29}Si CP/MAS NMR spectrum gave three peaks, indicating that there was something in the tunnels of the sepiolite (Figure 5.5c). This sample was then heated at 120°C for 20 hours, then the ^{29}Si CP/MAS NMR spectrum gave two peaks, indicating that the tunnels were empty again (Figure 5.5d). However, it is known that the indigo molecule is still present in the sample. Lastly, this sample was allowed to stand in the vial for a day; the ^{29}Si CP/MAS NMR spectrum gave three peaks, indicating that there was something in the tunnels of the sepiolite (Figure 5.5e). Figure 5.6a is a spectrum for dehydrated sepiolite, as expected. Dehydrated sepiolite was allowed to stand in the air for one hour; the ^{29}Si CP/MAS NMR spectrum gave three peaks, indicating that water molecules filled the tunnels of the sepiolite in that time (Figure 5.6b). Figure 5.6c shows the ^{29}Si CP/MAS NMR spectrum for sepiolite that was dehydrated again and then crushed with indigo in

the air environment; three peaks are observed. From these ^{29}Si studies it seems like water molecules can move freely in and out of sepiolite from the sepiolite clay and from the sepiolite-indigo adducts. The ^{29}Si CP/MAS data indicates that indigo is not inserted into the nanotunnels of sepiolite in the same fashion as smaller organic molecules such as acetone (Weir *et al*., 2000), pyridine (Kuang *et al*., 2002) or MCH. To better understand how indigo interacts with sepiolite, it was desired to do experiments in which water molecules would not interfere. Sepiolite-indigo samples were prepared in the air-free environment, in which samples were heated under vacuum in the vacuum line and crushed or packed into the NMR rotor in the vacuum bag under nitrogen gas.

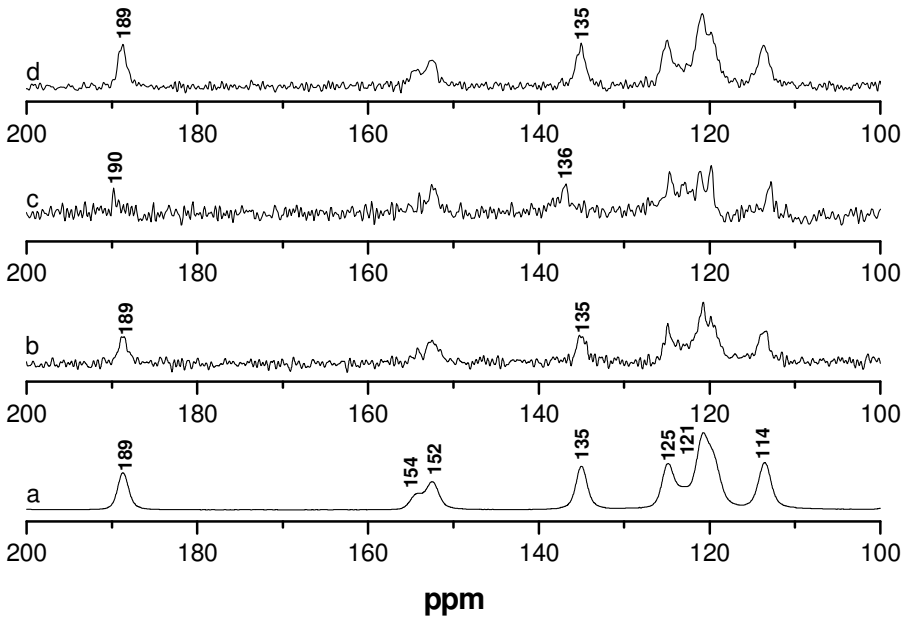

Figure 5.7 ^{13}C CP/MAS NMR spectra of (a) synthetic indigo, (b) sepiolite crushed with indigo in the air (2 wt.% indigo), (c) sample (b) heated at 120°C for 20 hours in the vacuum line and (d) sepiolite heated at 120°C for 20 hours in the vacuum line and then crushed with indigo (2 wt.% indigo) under nitrogen in the glove bag.

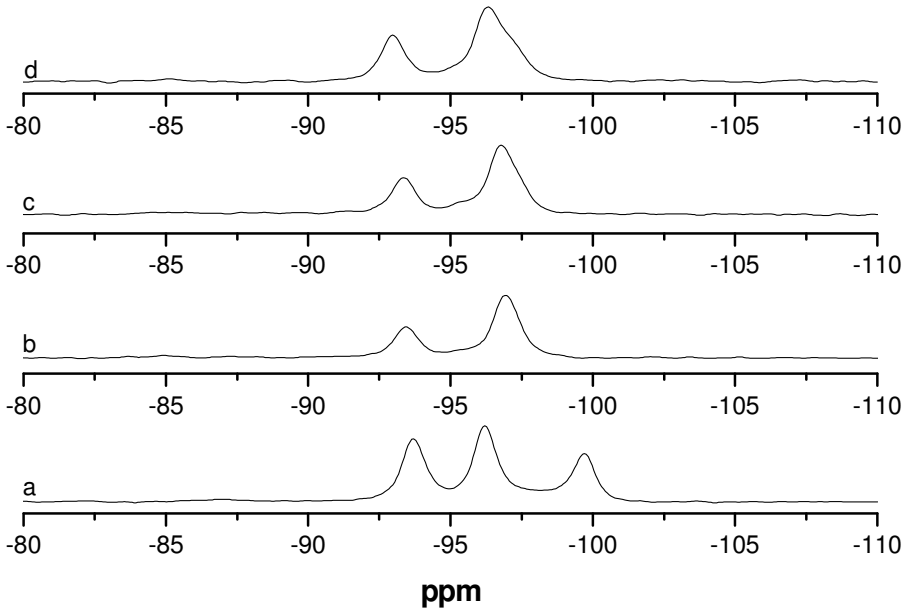

Figure 5.8 ^{29}Si CP/MAS NMR of (a) sepiolite crushed with indigo in the air (2 wt.% indigo), (b) sample (a) heated at 120°C for 20 hours in the vacuum line, (c) sepiolite heated at 120°C for 20 hours in the vacuum line and then crushed with indigo (2 wt.% indigo) under nitrogen in the glove bag and (d) pure heated sepiolite at 120°C for 20 hours.

Figure 5.7 shows ^{13}C CP/MAS NMR spectra for (a) synthetic indigo, (b) sepiolite crushed with indigo in the air (2 wt.% indigo), (c) sample (b) heated at 120°C for 20 hours in the vacuum line and (d) sepiolite heated at 120°C for 20 hours in the vacuum line and then crushed with indigo (2 wt.% indigo) under nitrogen in the glove bag. This figure is basically identical to Figure 5.4. It could be observed that after crushing sepiolite and indigo, and heating them (Figure 5.7c), the peaks for C_2 and C_6 are a bit (~1 ppm) shifted compared to the other spectra in Figure 5.7. Also, peaks in the region between 115 – 130 ppm are more resolved compared to other spectra; this spectrum is the closest in showing 8 unique carbons of the indigo molecule. The only difference that could be observed in Figure 5.7 compared to Figure 5.4 is in the Figure 5.7d spectrum. The Figure 5.7d spectrum looks identical to the Figure 5.7b spectrum, as opposed to the Figure 5.7a spectrum, as expected according to Figure 5.4. However, this difference is negligible.

Figure 5.8 shows ^{29}Si CP/MAS NMR for (a) sepiolite crushed with indigo in the air (2 wt.% indigo), (b) sample (a) heated at 120°C for 20 hours in the vacuum line, (c) sepiolite heated at 120°C for 20 hours in the vacuum line and then crushed with indigo (2 wt.% indigo) under nitrogen in the glove bag and (d) pure heated sepiolite at 120°C for 20 hours. The results obtained are as expected. When indigo is crushed with pure sepiolite, it is expected to see three Q^3 peaks on the ^{29}Si CP/MAS NMR, as the tunnels of the sepiolite are filled with zeolitic water; this is exactly the same result that would be obtained for pure sepiolite alone. It is interesting to point out that when working in the air-free environment with the sepiolite-indigo adducts, on the ^{29}Si CP/MAS NMR spectrum only two peaks are observed (Figure 5.8b and Figure 5.8c). This is exactly the same result that is obtained for dehydrated sepiolite in Figure 5.8d. That is why it is

believed that upon heating the indigo and sepiolite mixture, the indigo molecule is not intercalating into sepiolite, but rather is securing itself on the surface of the sepiolite. Sorption of molecules into the microporous tunnels is accomplished through hydrogen-bond interaction with the internal coordinated water of the clay mineral, after removal of zeolitic water (Serna and van Scoyoc, 1979). In the case of the sepiolite-indigo adducts, no hydrogen-bond interaction with the internal coordinated water of the sepiolite is observed (two peaks on the ^{29}Si CP/MAS MNR spectrum). As described earlier, the data in Table 5.1 gave strong evidence that the micropores of sepiolite are partially blocked upon formation of the sepiolite-indigo adduct. So, it is believed that indigo molecules are starting their entry into the tunnels of the sepiolite without really intercalating into it. Also, even after the sepiolite-indigo adduct is formed, water molecules are really easily transformed in and out of the sepiolite tunnels. The results from TGA analysis are also in agreement with this interpretation.

As a contradictory are the results obtained in the work done by Raya *et al.* (2010). In their work, they were also studying sepiolite-indigo adducts with solid state NMR. They did 2D ^{1}H-^{29}Si frequency-switched Lee-Goldburg (FSLG) HETCOR NMR for untreated sepiolite and for a sepiolite-indigo (11.5 wt.% indigo) complex heated for 10 minutes at 280°C. They also did a series of ^{13}C and ^{29}Si CP/MAS NMR studies for the following samples: sepiolite-indigo mixture unheated, sepiolite-indigo mixture heated for 10 minutes at 180°C, sepiolite-indigo mixture heated for 10 minutes at 280°C, sepiolite-indigo mixture heated for 10 minutes at 350°C, sepiolite-indigo mixture heated for 10 minutes at 400°C and sepiolite-indigo mixture heated for 10 minutes at 520°C. All the spectra of their results are shown next.

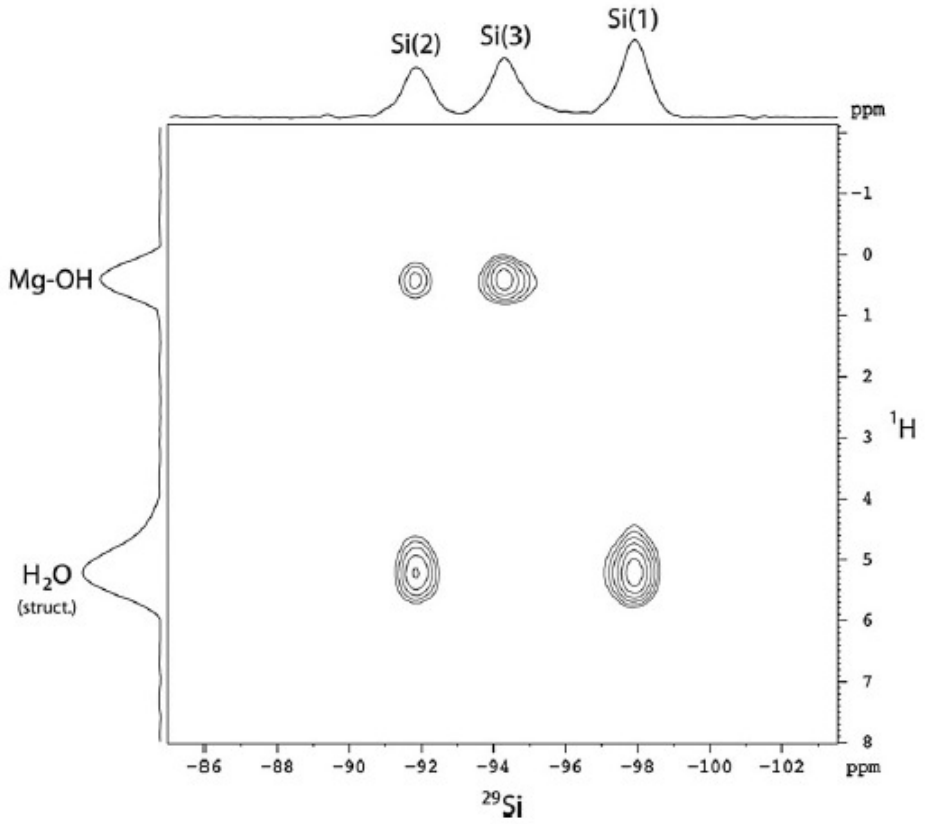

Figure 5.9 ^{1}H–^{29}Si FSLG-HETCOR spectrum of untreated sepiolite (mixing time of 2 ms). Figure obtained from Raya *et al.* (2010).

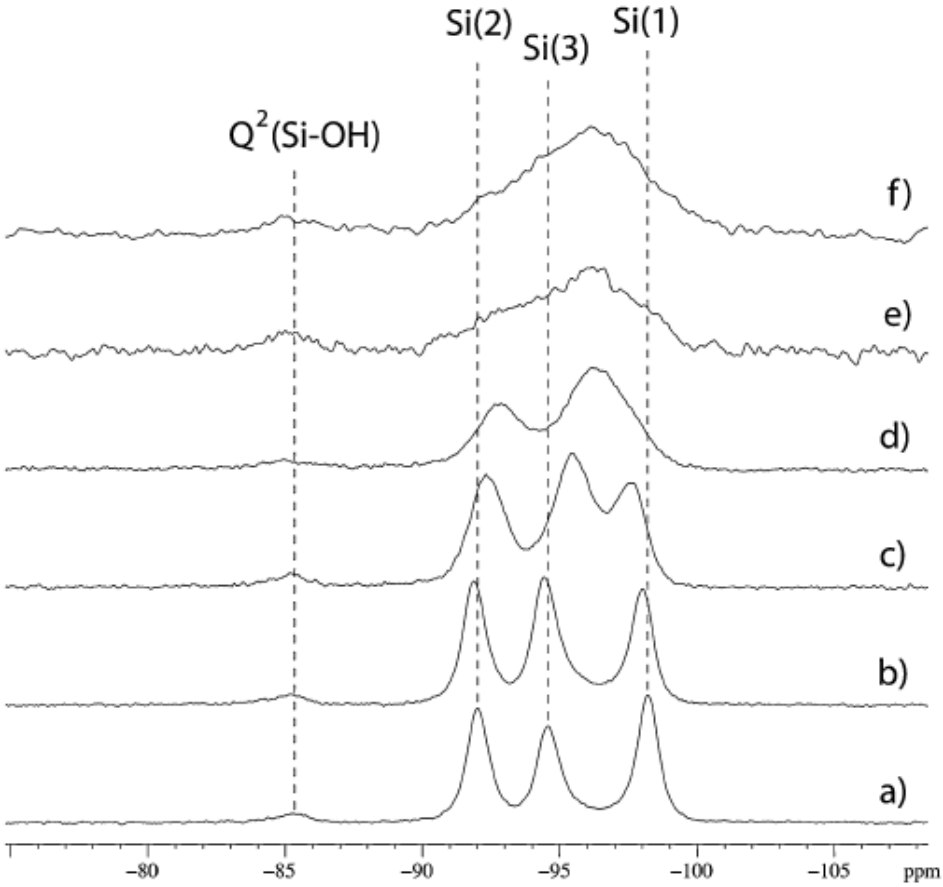

Figure 5.10 ^{29}Si CP/MAS spectra of the sepiolite-indigo (11.5 wt.% indigo) mixture. Thermal treatment: (a) unheated; heated for 10 min at (b) 180°C, (c) 280°C, (d) 350°C, (e) 400°C and (f) 520°C. Figure obtained from Raya *et al.* (2010).

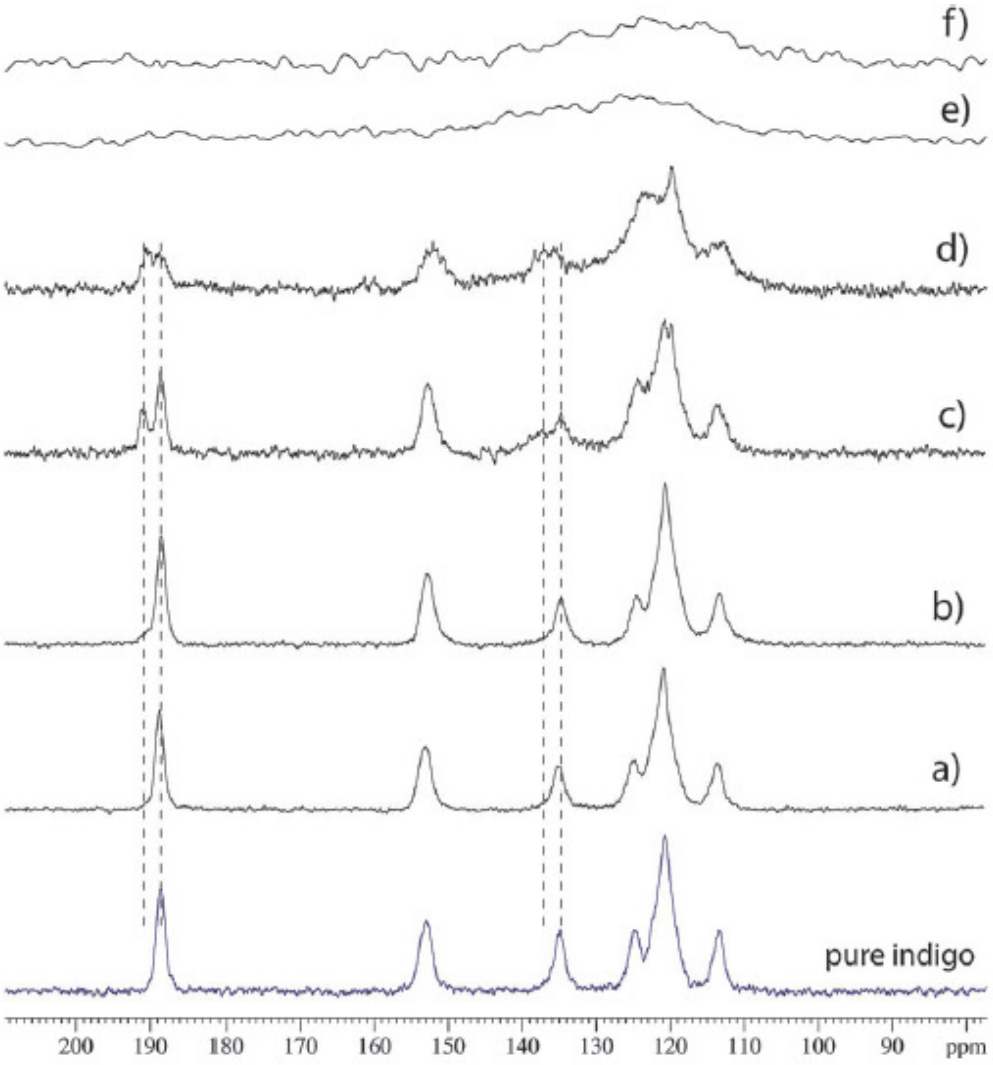

Figure 5.11 ^{13}C CP/MAS spectra of the sepiolite-indigo (11.5 wt.% indigo) mixture. Thermal treatment: (a) unheated; heated for 10 min at (b) 180°C, (c) 280°C, (d) 350°C, (e) 400°C and (f) 520°C. Figure obtained from Raya *et al.* (2010).

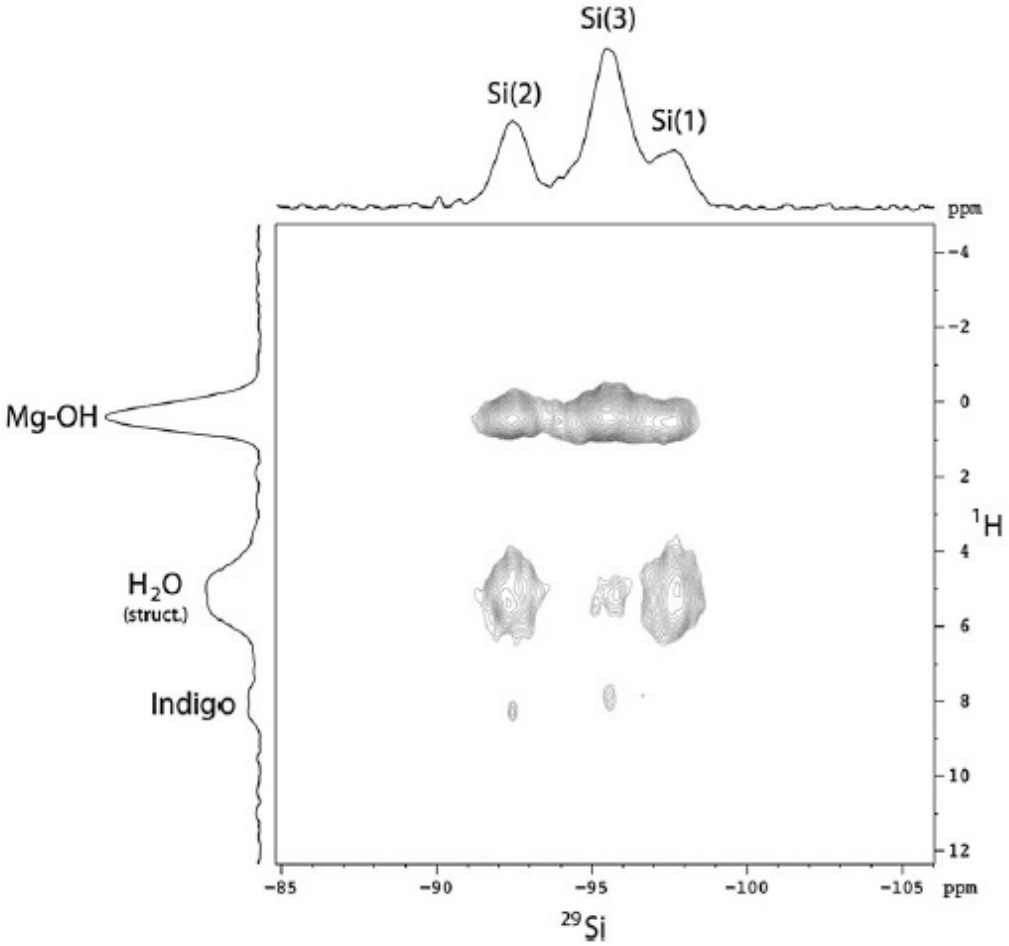

Figure 5.12 ^{1}H–^{29}Si FSLG-HETCOR spectrum of sepiolite-indigo (11.5 wt.% indigo) complex heated for 10 min at 280°C (mixing time of 6 ms). Figure obtained from Raya *et al.* (2010).

In Figure 5.9 the 2D ^{1}H–^{29}Si FSLG-HETCOR spectrum for untreated sepiolite with a mixing time of 2 ms can be seen. The ^{29}Si dimension demonstrates the expected three lines of roughly the same intensities, at -91.8, -94.3 and -97.9 ppm; two well-resolved resonances of comparable widths are observed in the ^{1}H dimension at 0.4 (for Mg-OH hydrogens) and 5.2 (H_2O_{struct} hydrogens) ppm. The lines at -94.3 and -97.9 ppm correlate exclusively with the Mg–OH groups and the coordinated water molecules, respectively, whereas the resonance at -91.8 ppm shows correlation to both types of ^{1}H nuclei. From the spectrum in Figure 5.9 the following conclusion can be made: the central lines are attributed to Type 3 (centre), the higher-field lines are attributed to Type 1 (edge) Si sites, and the lower-field resonance is consistent with the Type 2 (near edge) Si atoms, which occupy a position that is intermediate between the former two types of protons.

The ^{29}Si and ^{13}C CP/MAS spectra of the sepiolite-indigo (11.5 wt.% indigo) mixture both unheated, and heated between 180 and 520°C, are reported in Figures 5.10 and 5.11, respectively. It could be observed from Figure 5.10 that only after thermal treatment at 350°C for 10 minutes of the sepiolite-indigo mixture were the characteristic two peaks observed on the ^{29}Si CP/MAS NMR spectrum, indicating dehydrated tunnels of sepiolite. Featureless ^{29}Si CP/MAS NMR spectra were obtained for the higher heating temperatures, 400 and 520°C. Heating at higher temperatures causes some structural changes to occur in the sepiolite structure. According to Weir *et al.* (2000), folding of the sepiolite crystals occurs when approximately one half of the structural water has been removed, which allows the terminal Mg^{2+} to complete their coordination with the oxygen of the neighbouring silica surface. Structural folding is nearly completely reversible

provided that the treatment temperature does not exceed 250°C, but becomes irreversible once the true anhydride is formed. Raya *et al.* (2010) thermally treated their samples only for 10 minutes, so they required a temperature of 350°C to achieve the removal of the zeolitic water. Our group obtained the same results by heating at 120°C for 20 hours; this way, the possibility of changing the sepiolite structure by thermal treatment was avoided. Raya *et al.* (2010) also pointed out that the Q^2(Si–OH) signal is observed at -85 ppm for all the preheated samples, which they think suggests that there is no interaction between indigo and the external side surface.

In the ^{13}C CP/MAS NMR spectra of Figure 5.11, a signal with two shifted peaks at 138 (C_6 carbons) and 191 (carbonyl groups) ppm previously attributed to a complexed form of indigo is observed, in addition to that of pure indigo after thermal treatment of the sepiolite-indigo mixture at 280°C for 10 minutes. As in the ^{29}Si NMR (Figure 5.10), featureless ^{13}C NMR spectra are obtained with heating temperatures of 400 and 520°C (Figure 5.11e and Figure 5.11f). This is due to the decomposition of indigo.

In Figure 5.12 the 2D ^{1}H–^{29}Si FSLG-HETCOR spectrum of the sepiolite-indigo adduct (11.5 wt.% indigo), heated for 10 min at 280°C with a mixing time of 6 ms, can be seen. Apart from the strong correlations already detected in sepiolite (Figure 5.9), clear cross-peaks linking ^{29}Si resonances with new ^{1}H lines near 8 ppm are also observed. This is thought to be the region of the aromatic proton resonances of the synthetic indigo. Figure 5.1 shows the proton resonances of the synthetic indigo; the highest value for the aromatic region is at 7.61 ppm. The 2D spectrum is not perturbed by signals from indigo that are nonattached to the sepiolite. It can be seen in Figure 5.12 that the indigo ^{1}H signals correspond to the centre and near-edge Si nuclei; this indicates the existence of

relatively short internuclear distances between these Si sites and the indigo aromatic protons. The obtained NMR data tend to indicate that the indigo molecules interact with the internal surfaces of the external channels and of the tunnels of sepiolite. Raya *et al.* (2010) contend that the HETCOR spectrum of Figure 5.12 may be taken as an evidence of the insertion of indigo molecules in the sepiolite structure.

In terms of empty tunnels seen on the ^{29}Si spectra of sepiolite that are obtained by heating sepiolite-indigo samples, Raya *et al.* (2010) explains in the following matter: hydrogen bonds between the zeolitic and coordinated water molecules are numerous compared to the hydrogen bonds between coordinated water and a large molecule-like indigo. In fact, H-bond interactions are only possible between coordinated water and NH or CO groups for the indigo molecule; consequently, the chance of interaction decreases and then a large part of the coordinated water sees an empty channel.

Conclusion

Maya Blue is an organic/inorganic nanohybrid in which the indigo molecules are stabilized by natural clays (Gomez-Romero and Sanchez, 2005). Palygorskite and sepiolite are the major components of Maya Blue. There are still many difficulties encountered in understanding the palygorskite- and sepiolite-based Maya Blue. The complexity is related to unknown aspects of the Mayan process (and the possible existence of various processes), the indigo evolution and degradation, the difficulty of extracting and analyzing the organic matter, the presence of organic molecules added to

the original pigment, and the mixing of fibrous clays or adding of other minerals (clays, ochre, etc.) (Doménech *et al*., 2007), (Doménech *et al*., 2009).

The sepiolite-indigo adduct does display the characteristics of Maya Blue when sepiolite and indigo are mixed together with a mortar and pestle and then heated together at 120°C for 20 hours. Heating is necessary to achieve the characteristic stability of Maya Blue.

From the textural analysis it could be seen that microporosity of the sepiolite decreases after thermal treatment with indigo. Also, the TGA and DTG curves of the sepiolite-indigo are very much like pure sepiolite curves, except for an additional weight loss at ~360ºC, corresponding to indigo. The ^{29}Si CP/MAS NMR spectra of the heated sepiolite-indigo adduct is very similar to the one obtained for dehydrated sepiolite. From the ^{13}C CP/MAS NMR spectrum of the heated sepiolite-indigo adduct, it could be noted that the peaks in the 115 – 130 ppm range are the most resolved compared to the other spectra; also, two shifted peaks that correspond to the carbonyl and the C_6 carbons of the indigo molecule could be seen. The fact that the peaks in the 115 – 130 ppm range are more resolved is evidential of a transition from crystallographic symmetry to molecular symmetry (loss of aggregation). It is believed that indigo molecules start to enter the tunnels of the sepiolite without really intercalating into sepiolite. Also, even after the sepiolite-indigo adduct is formed, water molecules are really easily transformed in and out of the sepiolite tunnels.

References

Chianelli, R.R., de la Rosa, M.P., Meitzner, G., Siadati, M., Berhault, G., Mehta, A., Pople, J., Fuentes, S., Alonzo-Nunez, G. and Polette, L.A. (2005) Synchrotron and simulations techniques applied to problems in materials science: Catalysts and Azul Maya pigments. *J. Synchrotron Radiat.*, **12**, 129-134.

Chiari, G., Giustetto, R., Druzik, J., Doehne, E. and Ricchiardi, G. (2008) Pre-Columbian nanotechnology: Reconciling the mysteries of the Maya Blue pigment. *Appl. Phys. A: Mater. Sci. Process.*, **90**, 3-7.

Chiari, G., Giustetto, R. and Ricchiardi, G. (2003) Crystal structure refinements of palygorskite and Maya Blue from molecular modelling and powder synchrotron diffraction. *Eur. J. Mineral.*, **15**, 21-33.

Doménech, A., Doménech-Carbo M.T., and Vazquez de Agredos Pascual, M.L. (2007) Chemometric study of Maya Blue from the voltammetry of microparticles approach. *Anal. Chem.*, **79**, 2812-2821.

Doménech, A., Doménech-Carbo M.T., and Vazquez de Agredos Pascual, M.L. (2009) Correlation between spectral, SEM/EDX and electrochemical properties of Maya Blue: A chemometric study. *Archaeometry*, **51**, 1015-1034.

Fois, E., Gamba, A., and Tilocca, A. (2003) On the unusual stability of Maya blue paint: Molecular dynamics simulations. *Microporous Mesoporous Mater.*, **57**, 263-272.

Fuentes, M.E., Pena, B., Contreras, C., Montero, A.L., Chianelli, R., Alvarado, M., Olivas, R., Rodriguez, L.M., Camacho, H. and Montero-Cabrera, L.A. (2008) Quantum mechanical model for Maya Blue. *Int. J. Quantum Chem*, **108**, 1664-1673.

Gettens, R.J. (1962) Maya blue: an unsolved problem in ancient pigments. *American Antiquity*, **27**, 557-564.

Gettens, R.J. and Stout, G.L. (1946) Painting materials: a short encyclopedia. *D. Van Nostrand*, New York, pp. 130-131.

Giustetto, R., Levy, D. and Chiari, G. (2006) Crystal structure refinement of Maya Blue pigment prepared with deuterated indigo, using neutron powder diffraction. *Eur. J. Mineral.*, **18**, 629-640.

Giustetto, R., Llabrés i Xamena, F.X., Ricchiardi, G., Bordiga, S., Damin, A., Gobetto, R. and Chierotti, M.R. (2005) Maya blue: A computational and spectroscopic study. *J. Phys. Chem. B*, **109**, 19360-19368.

Gomez-Romero, P. and Sanchez, C. (2005) Hybrid materials. Functional properties. From Maya Blue to 21st century materials. *New J. Chem.*, 29, 57-58.

Gordon, P.F. and Gregory, P. (1983) Indigoid dyes. *Organic Chemistry in Colour*. Springer-Verlag, Berlin, pp. 208-211.

Gribova, E.A. (1955) X-ray study of indigo and thioindigo. *L. Ya. Karpov Physical Chemistry Institute: Doklady Akademii Nauk SSSR*, **102**, 279-281.

Hubbard, B., Kuang, W., Moser, A., Facey, G.A. and Detellier, C. (2003) Structural study of Maya Blue: textural, thermal and solid-state multinuclear magnetic resonance characterization of the palygorskite-indigo and sepiolite-indigo adducts. *Clay and Clay minerals*, **51**(3), 318-326.

Jones, B.F. and Galán, E. (1998) Sepiolite and palygorskite. *Hydrous Phyllosilicates* (S.W. Bailey, editor). Reviews in Mineralogy, **19**. Mineralogical Society of America, Washington, D.C., pp. 631-674.

Kleber, R., Masschelein-Kleiner, L. and Thissen, J. (1967) Study and identification of Maya blue. *Studies in Conservation*, **12**, 41-56.

Kuang, W., Hubbard, B., Moser, A., Facey, G.A. and Detellier, C. (2002) Organo-sepiolite and palygorskite nanocomposites. *Proceedings of the 5th International Conference on Solid State Chemistry*, Bratislava, Slovak Republic.

McClay, K., Boss, C., Keresztes, I. and Steffan, R.J. (2005) Mutations of toluene-4-monooxygenase that alter regiospecificity of indole oxidation and lead to production of novel indigoid pigments. *Appl. Environ. Microbiol.*, **71**, 5476-5483.

Merwin, H.E. (1931) In: *The Temple of the Warriors at Chichen Itza* (E.H. Morris, J. Charlot and A.A. Morris, editors). Carnegie Institution of Washington, Washington, D.C., publ. 406.

Myriam M., Suarez, M. and Martin-Pozas, J.M. (1998) Structural and textural modifications of palygorskite and sepiolite under acid treatment. *Clays and Clay Minerals*, **46**, 225-231.

Polette, L.A., Meitzner, G., Jose-Yacaman, M. and Chianelli, R.R. (2002) Maya blue: application of XAS and HRTEM to materials science in art and archaeology. *Microchemical Journal*, **71**, 167-174.

Polette-Niewold, L.A., Manciu, F.S., Torres, B., Alvarado Jr., M., Chianelli, R.R. (2007) Organic/inorganic complex pigments: Ancient colors Maya Blue. *J. Inorg. Biochem.*, **101**, 1958-1973.

Price, T.D. and Burton, J.H. (2010) An Introduction to Archaeological Chemistry. *Springer New York Dordrecht Heidelberg London*. pp. 311.

Raya, J., Hirschinger, J., Ovarlez, S., Giulieri, F., Chaze, A.-M. and Delamare, F. (2010) Insertion of indigo molecules in the sepiolite structure as evidenced by $^{1}H–^{29}Si$ heteronuclear correlation spectroscopy. *Phys. Chem. Chem. Phys.*, **12**, 14508-14514.

Sanchez del Rio, M., Boccaleri, E., Milanesio, M., Croce, G., van Beek, W., Tsiantos, C., Chyssikos, G.D., Gionis, V., Kacandes, G.H., Suarez, M. and Garcia-Romero, E. (2009) A combined synchrotron powder diffraction and vibrational study of the thermal treatment of palygorskite-indigo to produce Maya Blue. *J.Mater. Sci.*, **44**, 5524-5536.

Sanchez del Rio, M., Sodo, A., Eeckhout, S.G., Neisius, T., Martinetto, P., Dooryhée, E. and Reyes-Valerio, C. (2005) Fe K-edge XANES of Maya blue pigment. *Nuclear Instruments and Methods in Physics Research, Section B: Beam Interactions with Materials and Atoms*, **238**(1-4), 50-54.

Serna, C. and van Scoyoc, G.E. (1979) Infrared study of sepiolite and palygorskite surfaces. *Proceedings of the International Clay Conference, Oxford, 1978* (M.M. Mortland and V.C. Farmer, editors). Elsevier, Amsterdam, pp. 197-206.

Shepard, A. (1962) Maya blue: alternative hypotheses. *American Antiquity,* **27**, 565-566.

Tilocca, A. and Fois, E. (2009) The color and stability of Maya Blue: TDDFT calculations. *J. Phys. Chem. C*, **113**, 8683-8687.

Van Olphen, H. (1966) Maya Blue: a clay mineral-organic pigment? *Science*, **154**, 645-646.

Weir, M.R., Facey, G.A. and Detellier, C. (2000) ^{1}H, ^{2}H, and ^{29}Si solid state NMR study of guest acetone molecules occupying the zeolitic channels of partially dehydrated sepiolite clay. *Studies in Surface Science and Catalysis* (A. Sayari *et al.*, editors), **129**, 551-558.

Weir, M.R., Rutinduka, E., Detellier, C., Feng, C.Y., Wang, Q., Matsuura, T. and Le Van Mao, R. (2001) Fabrication, characterization and preliminary testing of all-inorganic ultrafiltration membranes composed entirely of a naturally occurring sepiolite clay mineral. *Journal of Membrane Sci.*, **182**, 41-50.

Witke, K., Brzezinka, K.W. and Lamprecht, I. (2003) Is the indigo molecule perturbed in planarity by matrices? *J. Mol. Struct.*, **661-662**(1-3), 235-238.

Chapter 6

General conclusions

Many new materials were prepared by the intercalation of organic molecules into the sepiolite tunnels. The two main objectives of this thesis were: (1) to obtain the slow and controlled release of the MCH molecule from the sepiolite tunnels so that the MCH-sepiolite nanohybrid could be potentially used to control Douglas-Fir beetle infestations in North American forests, (2) trying to identify the stability causes of the Maya-Blue through the preparation and investigation of the synthetic indigo-sepiolite adducts.

Chapter one gave general introduction into clay minerals and focused on specific characteristics of sepiolite clay. It is a non swelling, lightweight, porous clay with a large specific surface area. Chemically, sepiolite is a hydrous magnesium silicate whose individual particles have a needle-like morphology. The high surface area and porosity of sepiolite account for its outstanding absorption capacity for liquids. Sepiolite granules do not disintegrate even when saturated with liquids. Sepiolite has extensive usage. Sepiolite has numerous domestic applications such as moisture control, containment of accidental liquid spillages, and use in ashtrays to avoid smoke odor, control of liquid leakages and odors in dustbins, odor removal in refrigerators, etc. The popularity of sepiolite pet litters is due to its light weight, high liquid absorption and odor control characteristics.

Chapter two gave a little introduction of the characterization techniques used throughout this thesis, specifically: solid state nuclear magnetic resonance spectroscopy, thermal analysis (TGA, DTG, DTA) and porosimetry.

Chapter three investigated intercalation of the MCH molecule into the sepiolite. The focus of the chapter four was potential slow and controlled release studies of MCH from the sepiolite. Particularly investigated were co-intercalations of MCH with organic solvents as well as acidic treatment of MCH-sepiolite samples. Unfortunately, no release

of MCH was obtained from the co-intercalated MCH and organic solvents sepiolite samples.

In chapter five, Maya-Blue representative compound sepiolite-indigo was studied. This was done in the hope of understanding how exactly indigo and sepiolite interact with each other.

Much work still needs to be done in both of the main research areas mentioned above (MCH release and sepiolite-indigo compound). Though about 35% of the intercalated MCH was removed from the sepiolite with the acidic treatment of the MCH-sepiolite samples, more studies need to be done in this area to obtain the controlled release of MCH. Also, more studies need to be done to see how this could be applied in real-life situation in which acid is not always present. Maybe investigating MCH intercalation into acid pre-treated sepiolite. Also investigate, what is the best acid concentration to use in experiments.

Also, the stability causes of Maya-Blue are not yet understood, though, many efforts have been done to solve this mystery by various researchers. It is believed that in the synthetic indigo-sepiolite adducts indigo molecules start to enter the tunnels of the sepiolite without really intercalating into sepiolite. Also, even after the sepiolite-indigo adduct is formed, water molecules are really easily transformed in and out of the sepiolite tunnels.